

**Structural basis for a unique ATP
synthase core complex from
*Nanoarchaeum equitans***

SOUMYA MOHANTY

M.Sc

(Biomedical Sciences)

A THESIS SUBMITTED FOR THE DEGREE OF
DOCTOR OF PHILOSOPHY



Department of Biological Sciences

Faculty of Science

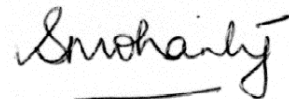
National University of Singapore

2015

Declaration

I hereby declare that this thesis is my original work and it has been written by me in its entirety. I have duly acknowledged all the sources of information which have been used in the thesis.

This thesis has also not been submitted for any degree in any university previously.

A handwritten signature in black ink, appearing to read 'Soumya Mohanty', with a horizontal line underneath the name.

Soumya Mohanty

Acknowledgements

“It always seems impossible until it’s done” – Nelson Mandela

This definitely sums up my PhD experience. This PhD would have been impossible without my supervisor, Prof. J. Sivaraman whose unflinching support, astute guidance, tremendous encouragement and above all, incredible patience is the sole reason for the successful completion of this PhD. Thank you for rekindling my love for science, Prof.

I would like to thank my ex-supervisor, Prof. Chris Hogue, for giving me the opportunity to work on this project. I thank my mentor, Prof. Low Boon Chuan for all the inspiration and the humor that has helped me get past some dark times. I would also like to thank Prof. G.V Sivasankar and Prof. K. Swaminathan for their kind words of advice. I would like to thank my collaborator, Prof. Adrian Velazquez-Campoy for his timely support. I would like to thank Priyanka for her amazing guidance and support. I have found an incredible friend and a mentor in you. I would also like to thank Dr. Jobichen Chacko for guiding me and teaching me most of what I know about X-ray crystallography. I would like to thank my labmates, Digant, Sarath, Apoorv, YC, Sunil, Pramila and Deepti for your unhesitant help. I will always cherish the times spent with all of you. May you all get all the best diffraction quality crystals. I would like to thank DBS and MBI for all the financial support. I would also like to thank the NSRRC Beamline at Hsinchu, Taiwan for providing me the opportunity to work with them.

I would like to thank my incredible buddies, Archna, Swati, Ashika, Vrunda, Andy, Spandu and Sudipto. Thank you for so many wonderful years of love and

laughter. The quest for a PhD in Singapore also led to meet some amazing people. I would like to thank the best friends one can ever as for, Shruthi, Rohith, Robert, Shelly, Aarthi, Aneesh, Shweta, Srinath, Sharvari, Shefali, Arun, Suhas, Asfa and Salma for giving me so much comic relief and a lifetime of happiness.

I would like to thank my Pa, for igniting in me the love for science and for your unbelievable sense of humor which never fails to make me laugh. Thank you, Ma for being the rock of my existence and for all your reality checks. I would like to thank my little sister, Shradha for being my comfort during troubled times and for being there for me through thick and thin. Thank you, the love of my life, my husband, Sheeladitya for 10 years of selfless love, support and inspiration. Thank you for believing in me, especially at times when I couldn't believe in myself. I thank all my family members, all the Mohantys and the Karmakars, for all the joy you have brought and continue to bring to my life. Last but not the least, I thank my grandparents, Jeje and Bou, who left me during this PhD journey. Both of you are the reason I am what I am today and you will always be in my heart. I dedicate this work to you.

Table of contents

| | |
|-----------------------------------|-------------|
| Acknowledgements..... | III |
| Table of contents..... | V |
| List of tables..... | VIII |
| List of figures..... | XI |
| List of abbreviations..... | XII |
| List of publications..... | XV |

| | |
|----------------------------|----------|
| <u>Summary.....</u> | 1 |
|----------------------------|----------|

Chapter 1: General introduction

| | |
|---|-----------|
| 1.1 Bioenergetics – an overview..... | 2 |
| 1.2 Adenosine triphosphate (ATP)..... | 2 |
| 1.3 ATP synthases..... | 5 |
| 1.3.1. Types of ATP synthases..... | 7 |
| 1.3.1.1 F ₁ F ₀ ATP synthases..... | 7 |
| 1.2.1.1.1 Subunit architecture | |
| 1.3.1.2 V ₁ V ₀ ATPases..... | 9 |
| 1.3.1.2.1 Subunit architecture | |
| 1.3.1.3 A ₁ A ₀ ATPases..... | 12 |
| 1.2.1.3.1 Subunit architecture | |
| 1.3.2. Evolutionary relationship amongst ATP synthase..... | 16 |
| 1.3.3 Function of ATP synthases/ases | |
| 1.3.3.1. Reversibility of function..... | 21 |
| 1.3.3.2 Mechanism of rotary catalysis..... | 22 |
| 1.3.3.2.1 Binding change mechanism..... | |
| 1.3.3.2.2 Nucleotide binding to the β (or A) and α (or B) subunits..... | 26 |
| 1.3.3.2.3 Role of γ subunit in rotary catalysis..... | 27 |
| 1.4 Bioenergetics of <i>Nanoarcheuam equitans</i>..... | 31 |

| | |
|---------------------|----|
| 1.5 Objectives..... | 34 |
|---------------------|----|

Chapter 2: Crystallization of regulatory subunit, NeqB and hexameric core complex, NeqAB with and without nucleotides, ADP and AMP-PNP from *Nanoarchaeum equitans*

| | |
|---|----|
| 2.1 Introduction..... | 36 |
| 2.2 Materials and methods..... | 36 |
| 2.2.1 Cloning, expression and purification of recombinant NeqB and NeqAB complex..... | 36 |
| 2.2.2 Dynamic light scattering..... | 38 |
| 2.2.3 Crystallization..... | 39 |
| 2.2.4 Data collection..... | 40 |
| 2.3 Results..... | 40 |
| 2.3.1 Cloning, expression and purification results..... | 41 |
| 2.3.2 Analysis of homogeneity..... | 43 |
| 2.3.3 Crystal viewing, diffraction and data collection..... | 43 |
| 2.3.4 Preliminary analysis..... | 46 |
| 2.4 Discussion..... | 48 |

Chapter 3: Structural basis for an evolutionary intermediate form of ATP synthase hexameric core from *Nanoarchaeum equitans*

| | |
|--|----|
| 3.1 Introduction..... | 50 |
| 3.2 Materials and methods..... | 52 |
| 3.2.1 Sequence alignment and phylogenetic analysis..... | 52 |
| 3.2.2 Cloning, expression and purification of Neq ATP synthase subunits..... | 53 |

| | |
|---|------------|
| 3.2.3 Crystallization, data collection and structure determination..... | 53 |
| 3.2.4 Blue Native PAGE..... | 54 |
| 3.2.5 Isothermal titration calorimetry (ITC)..... | 54 |
| 3.2.6 Dynamic light scattering (DLS)..... | 55 |
| 3.2.7 Analytical ultracentrifugation (AUC)..... | 55 |
| 3.2.8. Reconstitution of NeqABD complex..... | 55 |
| 3.2.9 ATPase assay..... | 56 |
| 3.3 Results..... | 56 |
| 3.3.1 Sequence homology of Neq ATP synthase subunits..... | 56 |
| 3.3.2 Phylogenetic analysis..... | 60 |
| 3.3.3 Structure of regulatory subunit, NeqB..... | 62 |
| 3.3.4 Structure of nucleotide free NeqAB complex..... | 69 |
| 3.3.5 Structure of nucleotide bound NeqAB complex..... | 78 |
| 3.3.6 Structure of nucleotide bound NeqAB complex..... | 86 |
| 3.3.7 ATP hydrolysis assay..... | 89 |
| 3.4 Discussion..... | 90 |
| <u>Chapter 4: Conclusion and future directions.....</u> | 96 |
| 4.1 Conclusion..... | 97 |
| 4.2 Future directions..... | 98 |
| <u>References:.....</u> | 100 |

List of figures

Chapter 1

1. *Figure 1.1* Events taking place during oxidative phosphorylation in the mitochondria.....4

| | |
|---|----|
| 2. Figure 1.2 Schematic representation of a typical ATP synthase performing rotary catalysis..... | 6 |
| 3. Figure 1.3 Subunit architecture of eukaryotic V-type ATPases and F-type ATP synthases..... | 11 |
| 4. Figure 1.4 Structural organization of A ₁ A ₀ -type ATP synthase from <i>Methanococcus jannaschii</i> | 14 |
| 5. Figure 1.5 Evolution of early forms of H ⁺ ATPases and ATP synthases..... | 18 |
| 6. Figure 1.6 Evolution of the modern day ATP synthase/ATPase from helicases..... | 20 |
| 7. Figure 1.7 One motor – two functions..... | 22 |
| 8. Figure 1.8 Binding change mechanism of catalysis..... | 24 |
| 9. Figure 1.9 Stages of ATP hydrolysis in V-type ATPase from <i>E.hirae</i> | 25 |
| 10. Figure 1.10 Structural features of γ subunit and its association with $\alpha\beta$ hexamer..... | 28 |
| 11. Figure 1.11 Asymmetric association of γ subunit with the β subunit during catalysis..... | 29 |
| 12. Figure 1.12 A comparison of the genes coding for subunits of A ₁ A ₀ synthase in <i>M. jannaschii</i> and <i>Nanoarchaeum equitans</i> | 32 |
| 13. Figure 1.13 Schematic representation of the protein complexes present at the cell-cell boundary of <i>Nanoarchaeum equitans</i> and its host, <i>Ignicoccus hospitalis</i> | 33 |

Chapter 2

| | |
|--|----|
| 14. Figure 2.1 MALDI-TOF MS analysis of NeqB..... | 41 |
|--|----|

| | |
|---|-------|
| 15. Figure 2.2 SDS gel image of purified NeqB and NeqAB..... | 41-42 |
| 16. Figure 2.3 Neq A ₃ B ₃ complex is hexameric..... | 42 |
| 17. Figure 2.4 Crystals of NeqB and NeqAB..... | 43 |
| 18. Figure 2.5 Representative diffraction patterns of crystals of NeqB and NeqAB..... | 45 |

Chapter 3

| | |
|---|-------|
| 19. Figure 3.1 Conserved sequences on NeqA and NeqB..... | 59 |
| 20. Figure 3.2 Phylogenetic analysis of NeqA and NeqB..... | 60-61 |
| 21. Figure 3.3 Structure of NeqB subunit..... | 63 |
| 22. Figure 3.4 Interactions of NeqA and NeqB with nucleotides..... | 67 |
| 23. Figure 3.5 Oligomeric states of NeqA and NeqB..... | 68 |
| 24. Figure 3.6 Interactions between NeqA and NeqB..... | 69 |
| 25. Figure 3.7 C α trace representation of bulge region on NeqA..... | 71 |
| 26. Figure 3.8 Structure of NeqAB complex..... | 72 |
| 27. Figure 3.9 Superimposition of NeqB..... | 76 |
| 28. Figure 3.10 Superimposition of C α trace representation of independent NeqB (marine blue) with homologs..... | 77 |
| 29. Figure 3.11 Surface representation of nucleotide binding pocket on NeqA..... | 79 |
| 30. Figure 3.12 Interacting residues of the NeqA and NeqB with nucleotides..... | 81 |
| 31. Figure 3.13 Cartoon representation of “closed” conformation of NeqAB complexes..... | 85 |

| | |
|--|----|
| 32. Figure 3.14 Comparison of hexameric core complex (A ₃ B ₃ hexamer)..... | 87 |
| 33. Figure 3.15 ATP hydrolytic activity of NeqA ₃ B ₃ and NeqA ₃ B ₃ D complex..... | 90 |
| 34. Figure 3.16 Schematic model of the inactive mechanism of the Neq core complex system..... | 92 |
| 35. Figure 3.17 Representation of the putative partially formed Neq ATP synthase..... | 95 |

List of tables

| | |
|---|----|
| 1. Table 1.1. Subunit composition in the V-type and F-type ATP synthases..... | 15 |
| 2. Table 2.1. Data-collection statistics..... | 47 |
| 3. Table 3.1. Crystallographic refinement details..... | 64 |
| 4. Table 3.2. Comparison independent NeqB structure with its homologs..... | 65 |
| 5. Table 3.3. Comparison of NeqA with its homologs..... | 73 |
| 6. Table 3.4. Comparison of NeqAB_native with its nucleotide free and nucleotide bound homologs from V ₁ /F ₁ complexes..... | 75 |
| 7. Table 3.5. Hydrogen bonding contacts between ADP and NeqAB (<3.4Å)..... | 82 |
| 8. Table 3.6. Hydrogen bonding contacts between AMPPNP (ANP) and NeqAB (<3.4Å)..... | 84 |
| 9. Table 3.7. Comparison of Neq A ₃ B ₃ (hexamer) with its homologs..... | 88 |

List of abbreviations

| | |
|-------------------------------|--|
| Å | angstrom (10^{-10} m) |
| Aa | Amino acids |
| ADP | Adenosine diphosphate |
| AMP-PNP | Adenylyl-imidodiphosphate (non-hydrolysable analog of ATP) |
| A ₁ A ₀ | Archaeal ATP synthases |
| ATP | Adenosine triphosphate |
| AUC | Analytical ultracentrifugation |
| BisTris | 1,3bis(tris(hydroxymethyl)methylamino)propane |
| BLAST | Basic Local Alignment Search Algorithm |
| BME | 2-mercapto-ethanol |
| BN | Blue Native |
| CMC | Critical micelle concentration |
| Da | Dalton |
| DLS | Dynamic light scattering |
| DNA | Deoxyribonucleic acid |
| <i>E. coli</i> | <i>Escherichia coli</i> |
| <i>E.hirae</i> | <i>Enterococcus hirae</i> |
| EGTA | Ethylene glycol tetraacetic acid |
| EM | Electron microscopy |
| FASTA | FAST-all |

| | |
|-------------------------------|---|
| F ₁ F ₀ | ATP synthase found in mitochondria, chloroplast or bacterial plasma membrane |
| ΔG | Gibbs free energy change |
| ΔH | Enthalpy change |
| H-bond | Hydrogen bond |
| HEPES | 4-(2-hydroxyethyl)-1 piperazineethanesulfonic acid |
| IMAC | Immobilized metal affinity chromatography |
| IPTG | Isopropyl thio-galactoside |
| ITC | Isothermal Titration Calorimetry |
| K _a | Association constant |
| K _d | Dissociation constant |
| kDa | Kilodalton |
| LB | Luria-Bertani |
| <i>M. mazei</i> | <i>Methanosarcina mazei</i> |
| <i>M. janaschii</i> | <i>Methanocaldococcus janaschii</i> |
| MALDI-TOF | Matrix-assisted laser desorption ionisation – time of flight |
| MCS | Multiple cloning site |
| MS | Mass spectrometry |
| MES | 2-(N-morpholino)-ethanesulfonic acid |
| MUSCLE | Multiple Sequence Comparison by Log- Expectation |
| N | Number of binding sites |
| Neq | <i>Nanoarchaeum equitans</i> |

| | |
|---------------------------------------|---|
| Ni-NTA | Nickel-nitrilotriacetic acid |
| OD | Optical Density |
| OSCP | Oligomycin sensitivity conferring protein |
| PAGE | Polyacrylamide gel electrophoresis |
| PCR | Polymerase Chain Reaction |
| PEG | Polyethylene glycol |
| Pi | Phosphate ion |
| pI | Isoelectric point |
| PMF | Proton motive force |
| RNA | Ribonucleic acid |
| ΔS | Entropy change |
| SDS-PAGE | Sodium dodecyl sulfate – Polyacrylamide gel electrophoresis |
| SEC | Size exclusion chromatography |
| t-RNA | Transfer RNA |
| Tris HCl | Tris (hydroxymethyl) aminomethane hydrochloride |
| V ₁ V ₀ ATPases | Vacuolar ATPases |
| WT | Wild-type |

List of publications

1. **Mohanty, S.,** Chacko, J., Chichili, V. P. R., Velazquez-Campoy, A., B.C, Low., Hogue,C.W.V.H., Sivaraman,J. *Structural basis for a unique ATP synthase core complex from Nanoarchaeum equitans* Journal of Biological Chemistry, 2015. **290**(45): p. 27280-27296

Summary

Archaeal ATP synthases are the oldest yet least studied of the ATP synthases. *Nanoarchaeum equitans* (*Neq*) is a hyperthermophilic archaeal parasite that lacks genes for several of the major subunits of the ATP synthase. Thus, the *Neq* ATP synthase is either a primitive or partially constructed or has lost these genes due to its parasitic dependency. In this thesis, we report the crystal structure and biophysical studies of the regulatory B subunit (NeqB), the hexameric core NeqAB (A_3B_3) and its complexes with ADP and AMP-PNP (analogue of ATP) in an effort to understand the catalytic capabilities of the archaeal *Neq* ATP synthase. NeqB is shorter than its eukaryotic and prokaryotic counterparts; yet, it forms a similar hexameric core A_3B_3 when combined with NeqA. This hexameric core, however, appears to be in a rigid, closed conformation, irrespective of the presence or absence of the nucleotide, which differs to that of its homologues, which require changes in their conformation (closed/open) for catalytic activity. Moreover, the central cavity in the Neq A_3B_3 hexamer complex also appears to be closed, despite the presence of nucleotide or absence of the central stalk. Finally, ATPase assays indicated a lack of significant hydrolysis with this hexameric core NeqAB complex in the presence or absence of the subunit D, which is required for its function. These results show that, although *N. equitans* possesses a fully assembled hexameric hexameric core complex (A_3B_3), it does not function as a bona fide ATP synthase in vitro.

Chapter 1

General introduction

1.1 Bioenergetics

Life has been found to exist in all conditions. All living beings require energy to survive and they employ various ways of obtaining energy, aerobically as well as anaerobically. Some accomplish through photosynthesis while some others do it through break down of chemical substrates. Some require oxygen, some do not. There are even organisms such as the *Rhodospirallae* that can perform anaerobic photosynthesis [1, 2]. Thus, for all these organisms, irrespective of their source of nutrition, energy is required to fuel all cellular and metabolic processes. Therefore, living organisms need to possess a mechanism of energy production through the breakdown of its nutrient source. Like every efficient machine, cells require back up energy storage mechanism as well as they are constantly imperilled by environmental stress such as food shortage. Therefore, an energy rich compound is required which is complex enough to store energy and yet simple enough to be broken down to release that energy.

1.2 Adenosine triphosphate (ATP)

12 years after the discovery of adenosine triphosphate (ATP), it was found to be the energy rich intermediate resulting from cellular respiration [3, 4]. In 1941, Fritz Lipmann postulated that ATP is the universal energy rich compound utilized in living beings that is capable of storing energy in its phosphate bonds [5]. ATP is produced by a complex enzymatic machinery known as the ATP synthase. In most aerobically respiring eukaryotes, the bioenergetics process is quite straightforward. The respiratory or photosynthetic processes take place in the chloroplasts of plants or the mitochondria of animals and ultimately culminate in oxidative phosphorylation which takes place in the mitochondria

and is executed by a series of enzyme complexes which includes the ATP synthase in the final step [6] (Fig.1.1). However, bacteria and archaea have a much diverse range of respiratory and bioenergetics processes owing to their extreme habitats. They utilize nutrients through various unorthodox modes such as fermentation or anaerobic respiration, chemotrophic or lithotrophic modes such as methanogenesis [7]. However, even in these organisms, despite the diversity in metabolic processes, the general bioenergetics pathway is similar constituting of the electron transfer chain and the complexes involved in it such as the cytochrome c complex and ultimately ending in ATP generation by the ATP synthase machinery [8, 9]. Therefore, irrespective of the mode of bioenergetics, the ATP synthases are ubiquitous in all living organisms and form one of the most vital enzyme complexes required for survival.

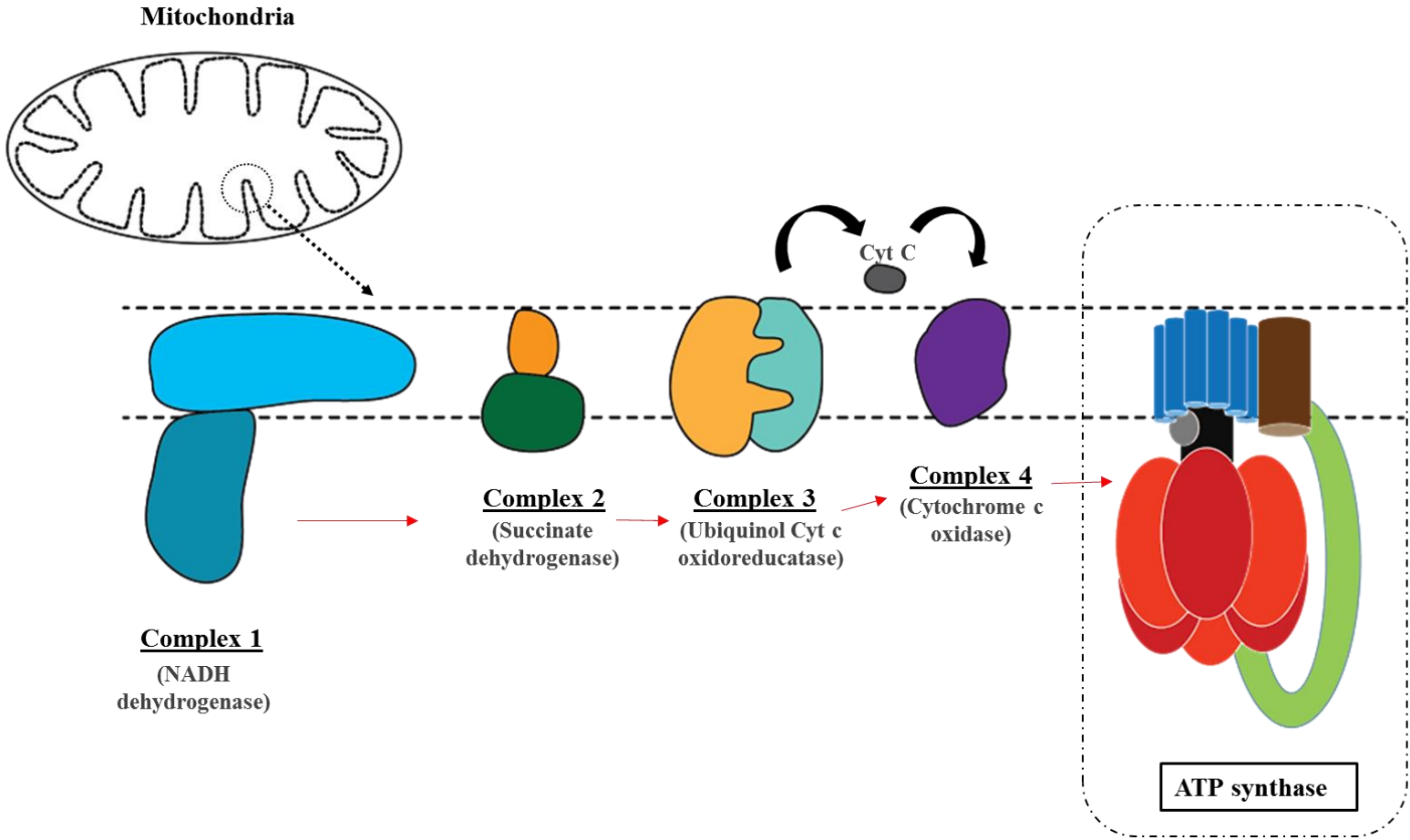


Fig1.1 *Events taking place during oxidative phosphorylation in the mitochondria* ATP synthesis is the final step in the respiratory chain and is powered by the protons generated by the processes of other respiratory enzymes across the membrane. The red arrows denote the sequence of the events.

1.3 ATP synthases

ATP synthases are a family of multi-subunit protein complexes which carry out the fundamental process of ATP generation [10-12]. This enzyme complex is an integral part of the electron transport chain and is made up of several subunits arranged in a typical fashion with a membrane embedded ion pump and a soluble hexameric catalytic head arranged in a typical “tennis racquet” like structure (Fig.1.2) [13, 14]. In eukaryotes, this hexameric catalytic head is present on the inner membrane of the mitochondria and the chloroplast and the genes coding for the ATP synthase complex is nuclear in origin. On the other hand, the ATP synthetic machinery in prokaryotes is mainly located on the cytoplasmic face of the plasma membrane and in bacteria and some archaea, the genes coding for this complex are found on operons such as the *unc* operon in *E.coli* [15, 16]. Besides the main synthetic machinery, there are variants of the ATP synthase complex that perform ATP hydrolysis and these are present in the organelles such as lysosomes and vacuoles. The ATP family of enzymes, therefore, is highly diverse and abundant.

The ATP synthase complex performs ATP synthesis by an interesting mechanism of “rotary catalysis”. In essence, this complex functions acts as a two part rotating machine. The catalytic head rotates around the central shaft forms the axis. This motion driven by simultaneous rotation of the membrane ring which in turn is energized by the influx of protons against the gradient that is present across the membranes [17] . Hence, the membrane ring or the rotor acts like a sort of “ion turbine” (Fig1.2). This rotary motion is one of its kind and the only other biological molecular machine that executes such kind of

movement is the bacterial flagella [18, 19]. Notably, the very same machine can also perform ATP hydrolysis in the absence of the proton flux in order to aid ion transport making it a highly versatile tool for biological functions [20]. This machine is also an interesting system to study from an evolutionary point of view as it is one of the earliest biological enzymes to arise [21].

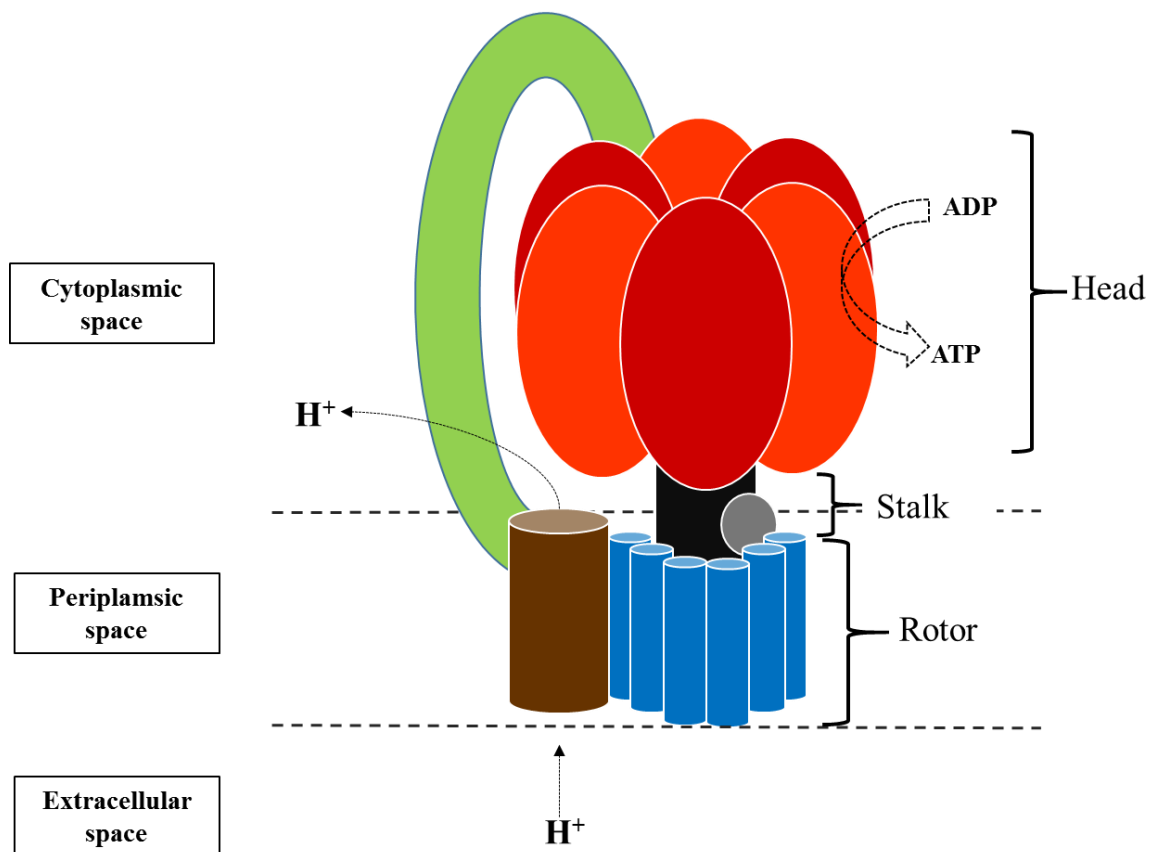


Fig1.2 Schematic representation of a typical ATP synthase performing rotary catalysis This figure shows a typical ATP synthase with the two modules, the rotor (head and stalk) and the stator. The rotational movement starts with the influx of the protons, followed by the rotation of the stalk and finally, the catalytic head or stator. This results in ATP generation. (This figure was adapted from Senior et al, 2012 [22]).

1.3.1 *Types of ATP synthases*

ATP synthases are a diverse class of enzymes which have diverged structurally as well as functionally into several different classes. There are three main

categories of ATP synthases. Each of these types is briefly discussed in the following sections.

1.3.1.1 *F₁F₀ATP synthases*

The F-ATP synthases, found in eukaryotes and prokaryotes, is the primary ATP synthesis machinery [23]. It is found in the inner membrane of the mitochondria of eukaryotes and forms an integral part of the respiratory enzyme complex and the electron transport chain (Fig 1.1) [24]. It synthesizes ATP by utilizing the proton gradient, otherwise known as the proton motive force (pmf) which is created during oxidative phosphorylation. It is also found in the chloroplast of plant cells and works in conjunction with the photosystems through a process called photophosphorylation [25, 26]. In prokaryotes, it is on the plasma membrane and functions in a way similar to the eukaryotic F₁F₀ ATP synthase [27]. Extensive work has been done to understand this motor in eukaryotes and prokaryotes. Most of our understanding of this machine comes from the bovine and yeast structures and the *E.coli*.

Subunit architecture

The F₁F₀ ATP synthase consist of a number of subunits that are arranged in a specific way. The F₁F₀ ATP synthases in prokaryotes and eukaryotes is made up of about eight to nine subunits [28, 29]. These subunits either have single or multiple copies (Table 1.1). In a typical F₁F₀ ATP synthase, 24 individual subunits come together to make up this complex machine (Fig1.3). In spite of these differences, the soluble catalytic part of the F₁F₀ ATP synthase or the F₁ sector is the portion where the catalysis takes place. This primarily consists of

a catalytic β subunit and the regulatory subunit α which forms a core hexameric complex. The β subunit has the conserved Walker motif region which binds to nucleotides. The γ subunit forms the central stalk that connects the hexameric head and the membrane ring. The γ subunit passes through the central cavity of the $\alpha_3\beta_3$ and is responsible for the rotation of the stator. The δ and ϵ subunits are accessory subunits of the central stalk. There are three copies of the α and β subunit and one each of γ , δ , ϵ subunits. The a and b subunits are parts of the F_0 complex which connect to the F_1 portion. This whole set up is collectively called the stator complex and its composition is $\alpha_3\beta_3\delta ab_2$. The membrane bound part or the F_0 sector prominently consists of the transmembrane ring composed of 12 c subunits (Fig1.3).

The first high resolution structure of the soluble or the F_1 complex of F-type ATP synthase was reported from bovine heart mitochondria in 1994 at 2.8 Å [30]. In this structure it was observed that the F_1 complex is made up of three α and three β subunits arranged alternately in a hexamer. The α and the β subunits are the largest of all the subunits of this complex and were found to be similar in size. These two subunits have similar folds. A part of the central stalk or γ subunit was also visualized. It was seen that both the N and the C terminus of the γ subunit enter the pore in which the γ subunit is a sort of twisted structure. The peripheral subunits, δ and ϵ were also present as a part of the F_1 domain even though they could not be properly resolved. The $\alpha\beta$ hexamer forms the core catalytic component and in the crystal structure, nucleotide binding was observed with both subunits. More interestingly, nucleotide binding to the β subunit found to be differential as in, only two out of the three β subunits were

bound to nucleotide while nucleotide was bound uniformly to all of the three sites on α subunit. It was shown later that the catalytic action is carried out by the catalytic sites on β (located at the interface of the $\alpha\beta$ subunits) while the other three nucleotide binding sites on β later known as the non-catalytic sites [31].

1.3.1.2 *V₁V₀ ATPases*

V-ATPases which are found in certain eukaryotic and prokaryotic organelles and vesicles such as vacuoles and lysosomes. Unlike the F-type ATP synthases, the function of the V-type is to transport protons upon ATP hydrolysis which is required for a number of cellular activities such as acidification of lysosomal compartments, endocytosis events, maintenance of the membrane potential and post translational modification [32-34].

Subunit architecture

The knowledge of the structure of eukaryotic V-type ATPases comes from the study of *Saccharomyces cerevisiae* while the prokaryotic V-type has been characterized in bacterial species such as *E.hirae* [35, 36]. It has also been observed that the prokaryotic V-types have a much simpler organization than the eukaryotes (Table 1.1) [34, 37]. While the overall structural organization of the V-type is similar to the F-type, there are some subunits that are unique to the V-type such as the D, C and H subunits (Fig.1.3).

The C and H subunits have been found in the eukaryotic V-type and not the prokaryotic ones. The subunit composition of eukaryotic V₁ complex is

A_3B_3DFEGH while that of prokaryotic one is A_3B_3DFECH . The A_3B_3 complex is homologous to $\alpha_3\beta_3$ complex of the F-type and has significant homology especially at the Walker motif region [38]. The D subunit is the central stalk component that is inserted in the central cavity of the A_3B_3 complex which is homologous to the γ subunit of the F-type. The stalk region of the V-type ATPases, especially the peripheral stalk subunits, has been observed to be much different and much more complex than that of the F-type ATP synthases (Fig. 1.3, Table 1.1).

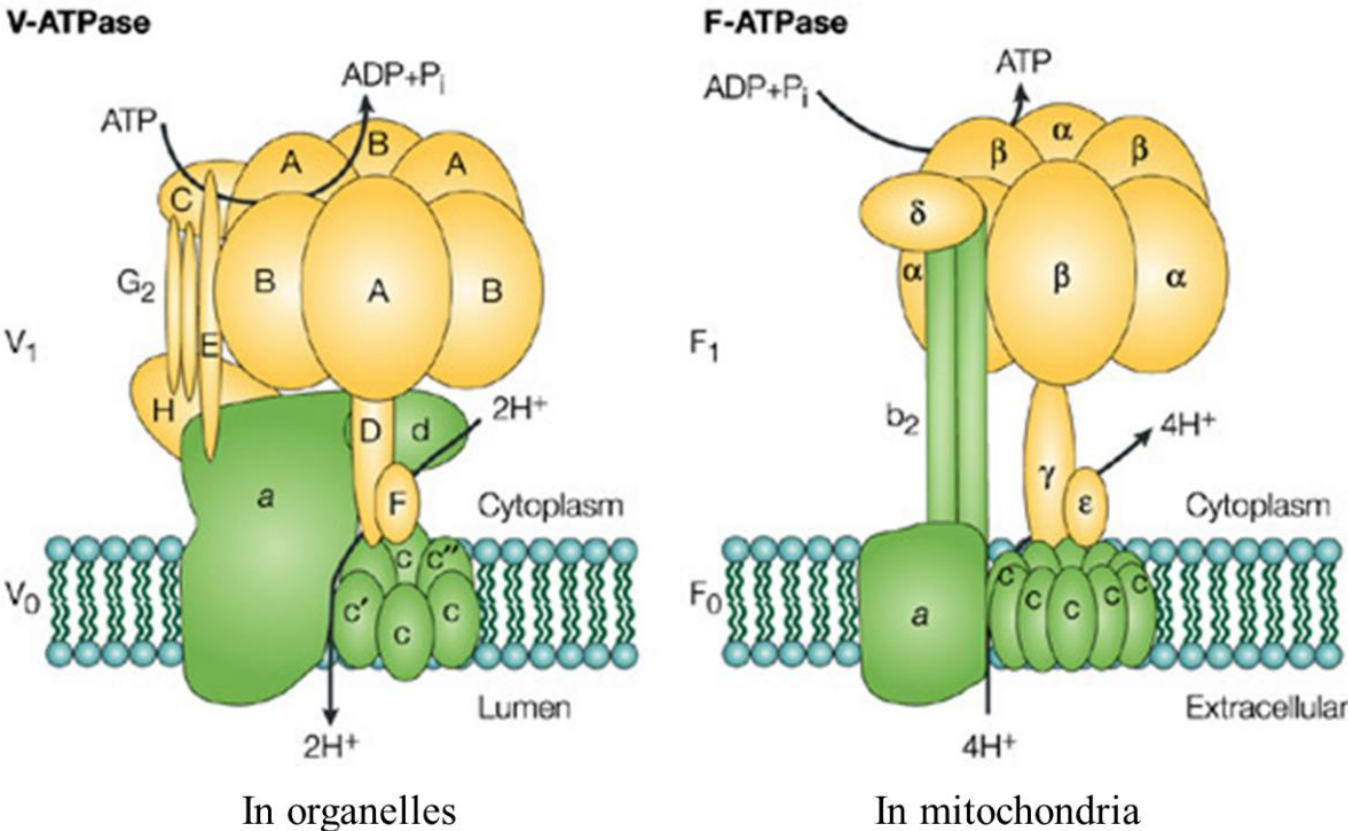


Fig1.3. *Subunit architecture of eukaryotic V-type ATPases and F-type ATP synthases:* The structural organization of the V-type and F-type ATP synthase are more or less similar however, they function in opposite ways. (The figure was adapted from Forgac et al, 2002 [39]).

1.3.1.3 A₁A₀ ATP synthases

Archaeal organisms are generally extremophilic in nature and are found in environmental conditions such as high temperature, high salt or anaerobic conditions [40, 41]. Based on this, archaeal organisms can be broadly classified as hyperthermophilic, halophilic or methanogenic. Depending on their ambient conditions, their energy demands also vary. However, the presence of ATP synthases is mandatory for these organisms. Genomic analysis of certain archaeal organisms such as *Methanosarcina mazei* shows a lack of F-type ATP synthases but the presence of genes similar to the V-type [42]. As these organisms are known to synthesize ATP, it was concluded that this V-type like ATP synthase representative might also perform ATP synthesis. This gave rise to a third class of ATP synthases known as the archeal or the A₁A₀ ATP synthases. The A-type ATP synthases have been found to be structurally similar to the V-type ATPases while functioning as ATP generators like the F-type and hence are thought to be chimera of the F and the V-type. The structural model of the ATP synthases from methanogenic bacteria such as *Methanosarcina mazei*, *Methanococcus janaschii* are quite well characterized and are considered as models for the A₁A₀ ATP synthases.

Subunit architecture

The cryo EM studies of *M.mazei* and *M.janaschii* showed that the structure of A₁ complex is quite similar to that of the prokaryotic V1 complex (Fig1.4). It consists of at least 9 subunits [43, 44]. The stator complex is made up of A₃B₃CDEF subunits. The A₀ rotor, on the other hand, has been found to be composed of the H, I and G subunits and K subunit. Multiple copies of the K

subunit form the membrane ring. The E and H subunits and the I subunit forms two separate peripheral stalks. The stoichiometry of the K subunits in the membrane ring was found to be variable [45]. Similar to the c subunits of the F-type and V-type ATPases, the K subunits have conserved acidic residues (Glu/Asp) which can bind to protons and enable their translocation [46]. The K subunits are proton selective and most of them are specific for H⁺. However, the archaeal ATP synthase of some anaerobic archaea such as methanogens have rotor rings that can bind to Na⁺ as well [47-49]. This is considered to be an evolutionary adaption for conserving ATP as organisms that employ anaerobic modes of respiration produce proton carrying fermentation by-products and hence, the internal H⁺ concentration is not conducive for efficient ATP production [50]. Therefore, sodium bioenergetics are more favorable.

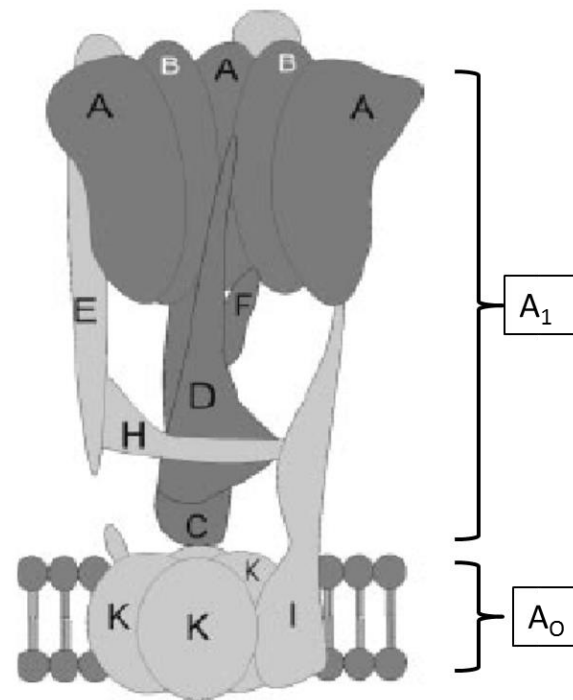


Fig1.4. **Structural organization of A₁A₀-type ATP synthase from *Methanococcus janaschii*:** Structural model for the representative A₁A₀ ATP synthase was derived from the cryo EM map of *M.janaschii* ATP synthase as well as structural models of individual subunits. All the subunits of A₁ and A₀ sector are labelled. (This figure was adapted from Gruber et al, 2004 [44]).

Table 1.1. Subunit composition in the V-type and F-type ATP synthases. This table summarizes the nomenclature and the known functions of the major subunits constituting the eukaryotic and prokaryotic F and V-type ATP synthases/ATPases emphasizing on the conservation of the catalytic portion and high variability in the rotor. The subunits highlighted in red are the most conserved ones throughout the ATP synthase family. [37, 44, 51-53]

| <u>Complex</u> | <u>Eukaryotic</u> | | <u>Prokaryotic</u> | | <u>Copies</u> | <u>Function</u> |
|--------------------------------|-------------------|---------------|--------------------|---------------|---------------|---|
| | <i>V-type</i> | <i>F-type</i> | <i>V/A-type</i> | <i>F-type</i> | | |
| F ₁ /V ₁ | A | β | A | β | 3 | ATP hydrolysis |
| | B | α | B | α | 3 | ATP binding |
| | C | - | - | - | 1 | Peripheral stalk |
| | D | γ/OSCP | D | γ | 1 | Central stalk or rotor |
| | E | - | E | - | 1 | Peripheral stalk |
| | F | ε | G | - | 1 | Central stalk or rotor |
| | G | - | F | - | 1 | Peripheral stalk |
| | H | - | - | - | 1 | Peripheral stalk |
| | - | δ | - | δ | 1 | Central stalk or rotor |
| F ₀ /V ₀ | a | a | I | a | 1-2 | Proton transport, stator |
| | d | b | C | b | 1-2 | Rotor |
| | e | - | - | - | 1 | Unknown |
| | c,c',c'' | c | K | c | 8-12 | H ⁺ /Na ⁺ transport, rotor ring |

1.3.2. Evolutionary relationship amongst ATP synthases

Owing to its indispensability for cellular growth and activity, ATP synthases are one of the earliest enzymes to have arisen and are believed to have appeared even before respiratory and photosynthetic enzymes. Since then, the enzyme complex has been evolving gradually into various sub types in order to introduce functional versatility suiting the needs of the organism.

The earliest organisms that existed were anaerobic and derived their energy mostly through processes like fermentation. Anaerobic processes lead to increase of protons inside the cell which would need to be extruded out in order to maintain the internal pH of the cell [54]. Hence, the need for a proton pump arose which could be powered by the ATP produced during nutrient breakdown giving rise to an early form of an ATPase [55]. Simultaneously, a possible loss of function mutation resulted in rendering three catalytic sites out of six as non-functional [56]. As catalysis is driven by the proton pumping through the multimeric membrane bound c-ring, the effort to maintain an optimal H^+/ATP ratio which will generate enough torque as well as not overuse protons played a role in shaping the formation of the catalytic β and the non-catalytic or regulatory α subunits [56, 57]. The experimental support for this proposal was obtained from the high resolution structure of the bovine heart mitochondria F_1F_0 ATP synthase where it was observed that the glutamate residue (E188) on the β subunit is responsible for the hydrolytic cleavage of the gamma phosphate of ATP [30]. The homologous residue on the α subunit is glutamine (Q208) which is not capable of this function [30]. The role of the H^+/ATP ratio in shaping the evolution of ATP synthase can also be deduced from the difference in the number of c-subunits that make up the ring [57].

It is postulated that the precursor ATP synthase arose before the divergence of eubacteria and archaeobacteria [21]. Subsequently, as the life forms evolved, more complex modes of bioenergetics came into the picture such as photosynthesis. Hence, in addition to the ATPase, the need arose for a system that can make ATP as well and thus, the precursor of the modern ATP synthase machinery arose, probably in an archaeal organism [58]. Later, as eukaryotes appeared, a second event led to the reversal of function giving rise to the V-type ATPases which still maintain high degree of structural similarity with the archaeal A-type ATP synthases. Finally, the F_1F_0 ATP synthase seems to have arisen from a third event where the changes appeared mostly in the stalk region and the c-ring (Fig1.5). Another theory which supports this is the endosymbiotic origin of mitochondria and chloroplasts in the eukaryotes [59]. According to this, mitochondria and chloroplast have originated from bacterial organism which was engulfed by a primordial eukaryote [60]. The protein complexes present on the membrane of the bacteria were also adopted and evolved with the organelles in the eukaryote and were shaped by the energetic demands of the eukaryotic cell thus forming the present day F_1F_0 ATP synthase [61].

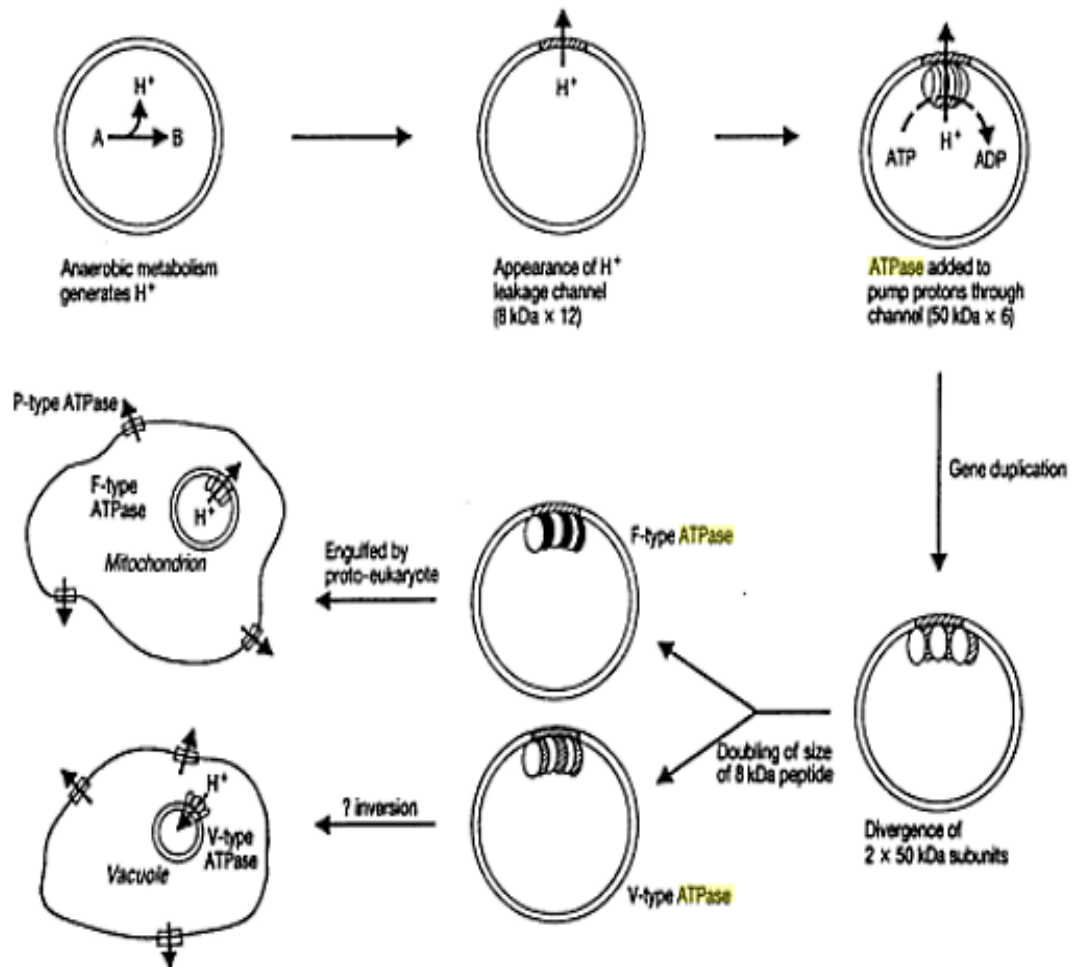


Fig.1.5 Evolution of early forms of H⁺ ATPases and ATP synthases This representation depicts the formation of the early F synthases and V-type ATPases according to the endosymbiotic theory (The copyrights for this figure has been obtained from Bioenergetics at a Glance: An Illustrated Introduction)

However, how the enzyme complex originated is quite a challenging question. Broadly classifying, the ATP synthase family of proteins consists of the F-type and the V-type. A closer look at the subunits of each of these types reveals that the β/A and the α/B subunits in F and V-type respectively which make up the hexameric catalytic complex are highly conserved especially in the nucleotide binding Walker motif or P-loop region [21]. However, the central stalk of the ATP synthase complex and the peripheral stalk subunits that connect the catalytic head to the membrane ring have been found to be much less conserved

(Table 1.1) [62]. Logically, the hexameric complex could be from a common ancestor. Therefore, it is believed that the hexameric catalytic portion of the ATP synthase might have been the first sub complexes to have arisen and the central and peripheral stalk components have evolved much later. This was supported by the evidence that the hexameric head of the ATP synthase family protein complexes bear significant resemblance to the hexameric helicases such as the RecA family proteins [63]. The helicases contain six identical subunits arranged in a hexameric fashion and they function by hydrolysing ATP. The P-loop sequence is present on these proteins as well. Based on the remarkable similarity between the helicases and the ATP synthase, it was proposed that the present day ATP synthases arose due to two separate gene duplication events [56, 64]. Another clue to the possible evolutionary mechanism of ATP synthases came from the discovery that the soluble catalytic head (F_1/V_1) is detachable from the membrane bound complex (F_0/V_0). This led to the speculation that the soluble and the membrane bound portions could have possibly evolved as separate entities [65]. This type of evolutionary model is called “modular evolution”. One such probable hypothesis was that perhaps membrane channels such as RNA/DNA or even protein translocases required ATP hydrolysis, which could be efficiently performed by the helicases, in order to translocate the biomolecules (Fig 1.6).

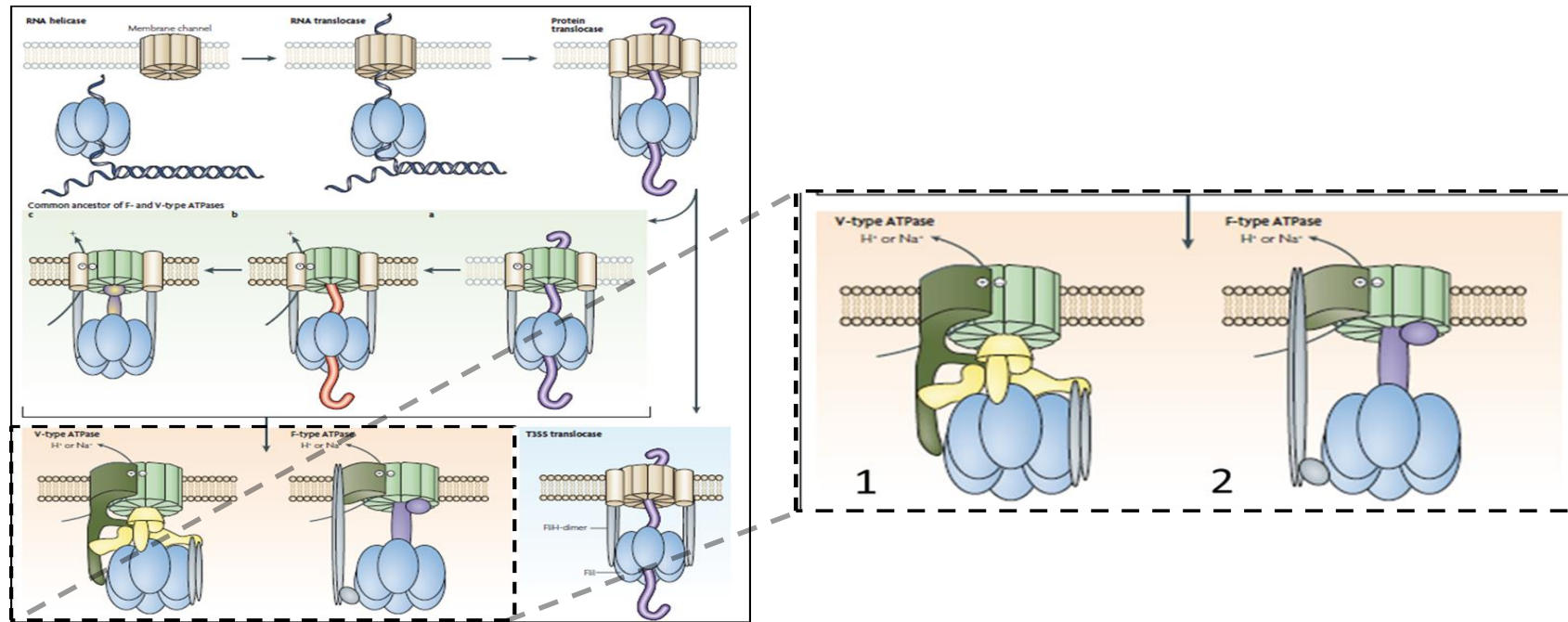


Fig1.6 ***Evolution of the modern day ATP synthase/ATPase from helicases*** These series of diagrams summarize how the F and the V-type ATPases came into existence by the amalgamation of an RNA helicase with a proton channel. The inset shows the modern day F-type and V-type emphasizing on the high degree of conservation of the catalytic hexamer and the difference in the stalk and rotor regions.(This figure was adapted from Koonin et al, 2007 [62]).

1.3.3. Function of ATP synthases/ATPases

As mentioned in the previous sections, ATP synthases can perform both ATP synthesis as well as ATP hydrolysis through the mechanism of rotary catalysis. Further details about the function will be discussed in the following sections.

1.3.3.1. *Reversibility of function*

The evolution of ATP synthases comprise of multiple events of inter conversion of ATP synthases into ATPases and vice versa. Therefore, it was not surprising that the F_1F_0 and the A_1A_0 ATP synthases are also capable of hydrolysis through the same binding change mechanism that is employed to synthesize ATP (Fig.1.7). Hence, the term ATP synthase and ATPases have been used interchangeably. The soluble F_1/A_1 complex is readily detached from the membrane ring and can independently hydrolyze ATP. In fact, experiments have shown that the hydrolysis of the F_1 portion can drive the rotation of the complex via the central stalk particularly the γ subunit [66]. It was reported that under high concentrations of Mg-ATP, the F_1 complex is capable of displaying ATP hydrolysis [31].

This dual functionality is evolutionary adaptation to utilize the same biological machine to perform multiple functions. However, the V-type ATPases cannot be utilized for ATP synthesis.

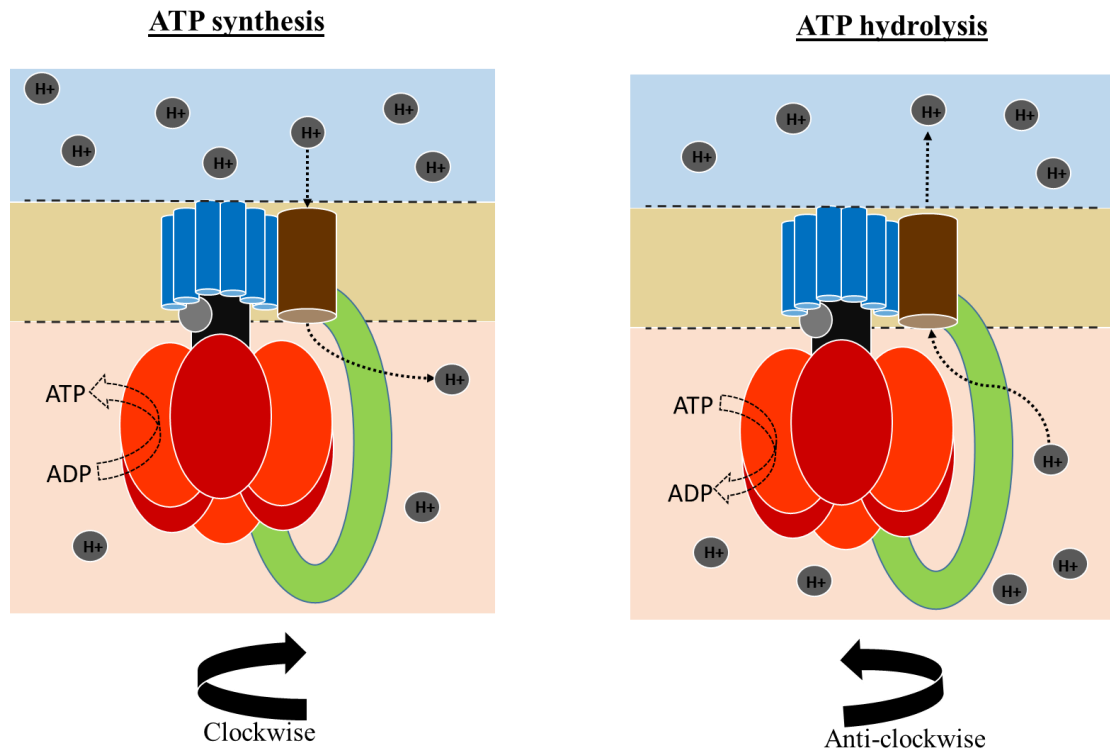


Fig1.7 *One motor – two functions* The direction of the rotary motion of the ATP synthetic machinery depends on the catalytic event taking place i.e. synthesis or hydrolysis.

1.3.3.2 Mechanism of rotary catalysis

The phenomenon of ATP production through oxidative phosphorylation has been known since the 1940-50s [67]. However, the exact mechanism and the complexes involved in ATP production was not known till the early 1960s. In 1961, Peter Mitchel coined the term “chemiosmosis” to explain how proton gradient leads to ATP synthesis by the ATP synthase. However, holistic information about the mechanism of ATP synthesis was not known till Paul Boyer’s postulated the “*binding change mechanism*” of action [10].

1.3.3.2.1 Binding change mechanism

According to the binding change mechanism theory, the ATP synthase complex

undergoes concerted global structural changes upon nucleotide binding leading to the production of ATP [68]. Further, to explain the binding change mechanism, Paul Boyer's group also introduced another important concept of "catalytic cooperativity" [69, 70]. This concept describes the cooperative action of the active sites on the catalytic or the β subunit according to which the release of the synthesized ATP only takes place when the next catalytic site is occupied with ADP and P_i . In order to explain this cooperative mode of action, it was proposed that each of the three catalytic sites alternately exist between three states; "open", "loose" and "tight". The production or hydrolysis of one ATP molecule takes place through a three-step process where the catalytic site alternates between the aforementioned states as the hexameric head rotates 120° (Fig.1.8). However, due to the lack of structural data, till the early 1970s, this concept was still merely theoretical and the exact mechanism by which ATP is generated was not known.

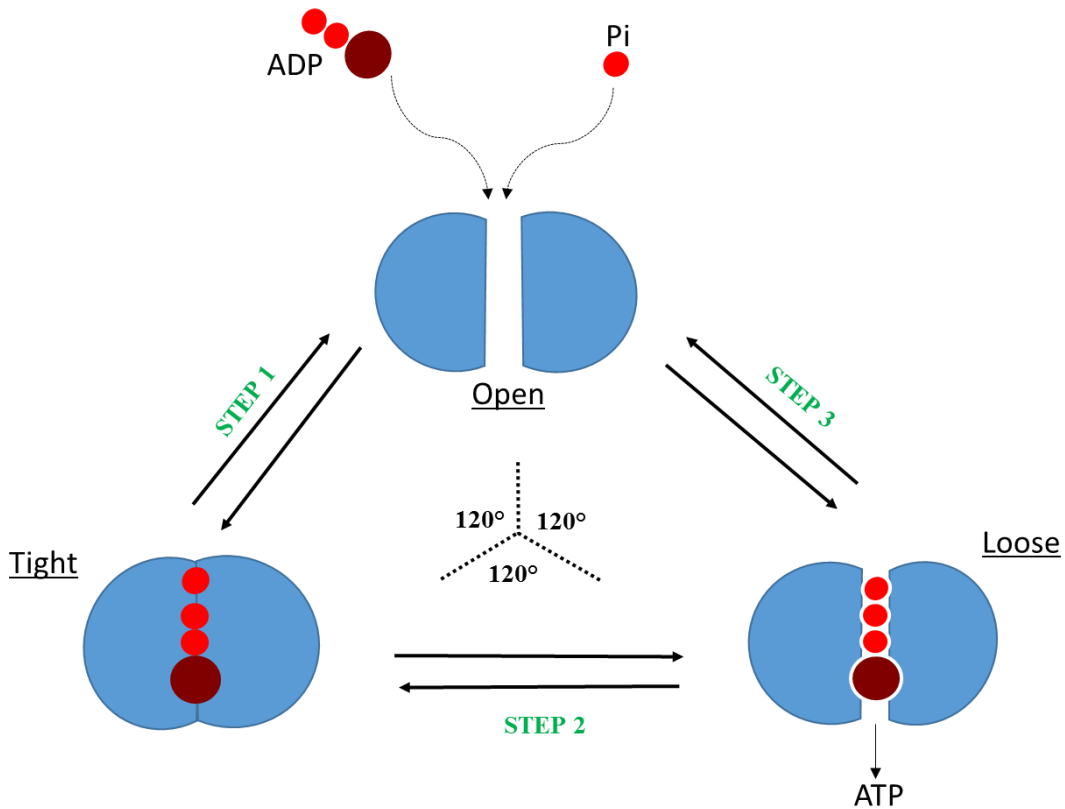


Fig1.8. **Binding change mechanism of catalysis:** This figure depicts the transitional states of a single catalytic site of the main catalytic subunit of the F_1F_0 ATP synthase, the β subunit during the 360° rotation. The catalytic site undergoes transition from the open (empty) \rightarrow tight (ADP+Pi bound) \rightarrow loose (ATP bound) form alternately leading up to ATP production and release and the process is in reverse for ATP hydrolysis.

The first structural information about the ATP synthase reported from John Walker's group in 1994 when they solved the structure of the F_1 complex of the F_1F_0 ATP synthase from the bovine heart mitochondria [30]. Remarkable structural changes occur in the catalytic head that lead to the ATP generation/hydrolysis. Putting together the high resolution structural data available for the F_1F_0 ATP synthases [30, 71], three different nucleotide binding, conformational states were observed in the catalytic hexamer. These structures also confirmed the catalytic co-operativity theory as nucleotides were bound to only two out of the three dimers with different binding affinity for each site [72]. Similar observations were later seen in the prokaryotic V-type ATPase

proving that the binding change mode of catalysis also applies in case of ATP hydrolysis (Fig 1.9) [35, 73].

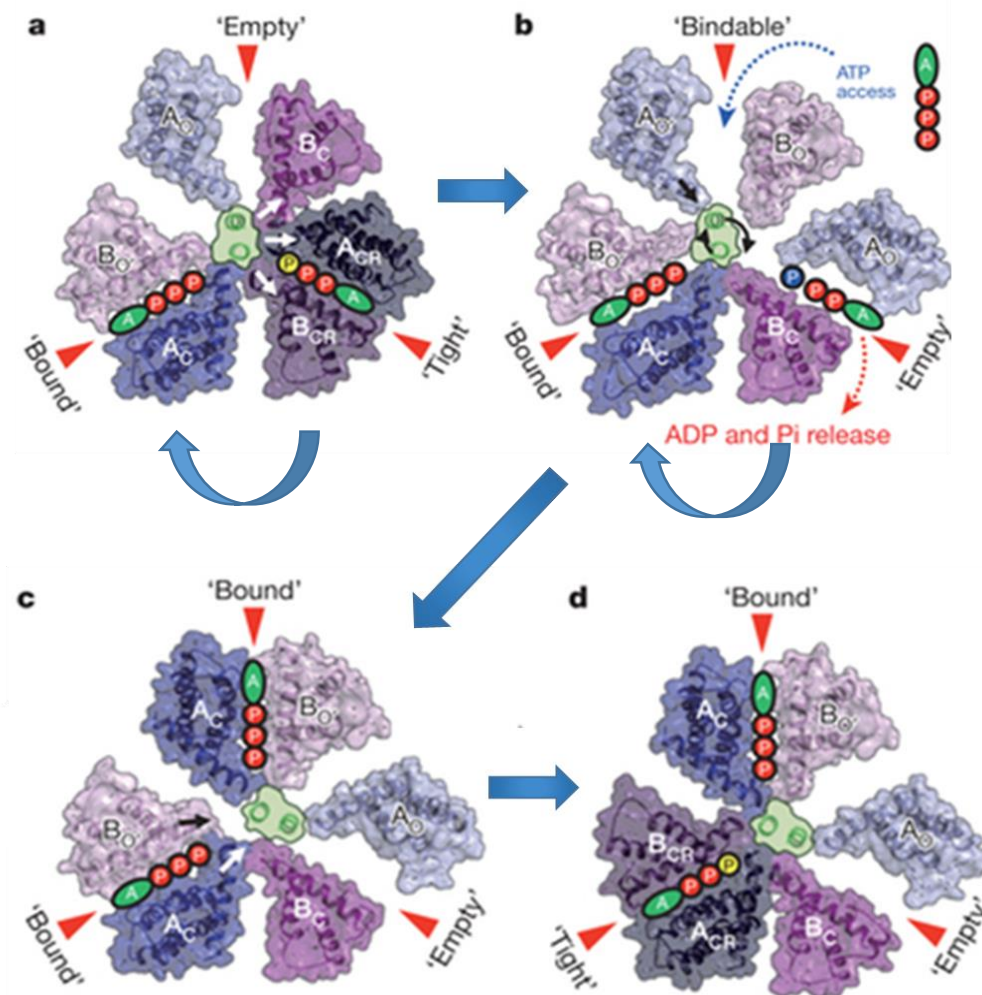


Fig1.9. *Stages of ATP hydrolysis in V-type ATPase from E.hirae*: The transition between the empty → bindable → bound → tight forms of the catalytic head were deduced based on the crystal structures of the asymmetric catalytic head. This asymmetry is crucial for ATP hydrolysis and forms the basis for the binding change mechanism. (This figure was adapted from Arai et al 2013 [35]).

The major torque generated for the rotation of the ATP synthase is by the membrane embedded component which is mainly composed of the multiple c subunits arranged in a ring fashion. Even though it is called a proton channel, it functions more like a proton translocase [74]. Each of the c-subunits have conserved negatively charged residues that can bind to H⁺ or Na⁺ and translocate

these ions. Each translocation step rotates the entire ring along with the catalytic head by $2\pi/3$ or 120° .

1.3.3.2.2 *Nucleotide binding to the β (or A) and α (or B) subunits*

The β (or A) subunits that are the main catalytic subunits contain a highly conserved motif known as the Walker motif (GXXXXGKT/S) that binds to nucleotides. This Walker motif is observed on many nucleotide binding proteins [75, 76]. This region is also known as the P-loop as it binds to the phosphate group on the ATP/GTP molecules. Nucleotide binding to the catalytic β subunit takes place through an interplay of three primary residues: (i) a positively charged residue that interacts with the oxygen moieties present on the phosphate group such as Lys (ii) a negatively charged residue that interacts with Mg^{2+} ion such as Asp or Glu and (iii) an aromatic residue that interacts with the adenine head group such as Tyr. These residues are found to be conserved on all the catalytic subunits known so far. The α or the regulatory subunit of F_1F_0 ATP synthase has been shown to bind to the nucleotides in the crystal structure of bovine heart mitochondria ATP synthase [77]. Sequence analysis shows that similar to the β subunit, the α subunit also contains the Walker motif region. However, similar Walker motif region was not observed on the B subunit of the V-type ATPases and A-type ATP synthases [21].

1.3.3.3.3 *Role of central stalk in rotary catalysis*

The first partial structure of ATP synthase reported by Abrahams et al in 1994 showed that the γ subunit makes up the major portion of the central stalk could be discerned [30]. This subunit was proposed to be the major “rotary shaft” of the ATP synthase machinery. The C-terminus of this large elongated coiled coil

α helical structure was found to be kinked. Experiments showed that chemical cross linking the C-terminus to the β subunit completely abrogated the ATP hydrolytic activity of the $\alpha_3\beta_3\gamma$ subcomplex showing that this part of the γ subunit needs to be free for the functioning of the complex [78]. Electron microscopy studies of several ATP synthase molecules revealed that the γ subunit was associated with a different $\alpha\beta$ pair at any given point of time concluding that like the $\alpha_3\beta_3$ hexamer, the γ subunit is also asymmetric in nature [79] (Fig.1.10). Efforts were made to understand how this motor shaft works. The first direct observation of rotation of the γ subunit was done by Noji et al in 1997 where they attached the $\alpha_3\beta_3\gamma$ subcomplex to a glass plate and studied the Mg-ATP hydrolysis induced rotation of the conjugated actin filament attached to the γ subunit using epifluorescent microscopy [66]. Notably, it was reported that all the actin filaments rotated in the same counter clockwise direction while ATP hydrolysis took place. No rotation was seen in the absence of ATP [80]. There were three 120° rotation steps during one hydrolysis cycle denoting the cyclical binding and release of nucleotides from the three catalytic sites (Fig.1.11) [81]. More recent single molecule studies on the rotational mechanism of the γ subunit revealed that each 120° has two sub steps, one at 90° and one at 30° corresponding to ATP binding and release respectively [82]. Similar work has been done very recently using the V-type ATPase from *Thermus thermophilus* where it was observed that the D subunit rotates in a manner similar to the F_1F_0 ATP synthase. This conclusively confirms that the rotary catalysis mechanism occurs in the V-type as well [83].

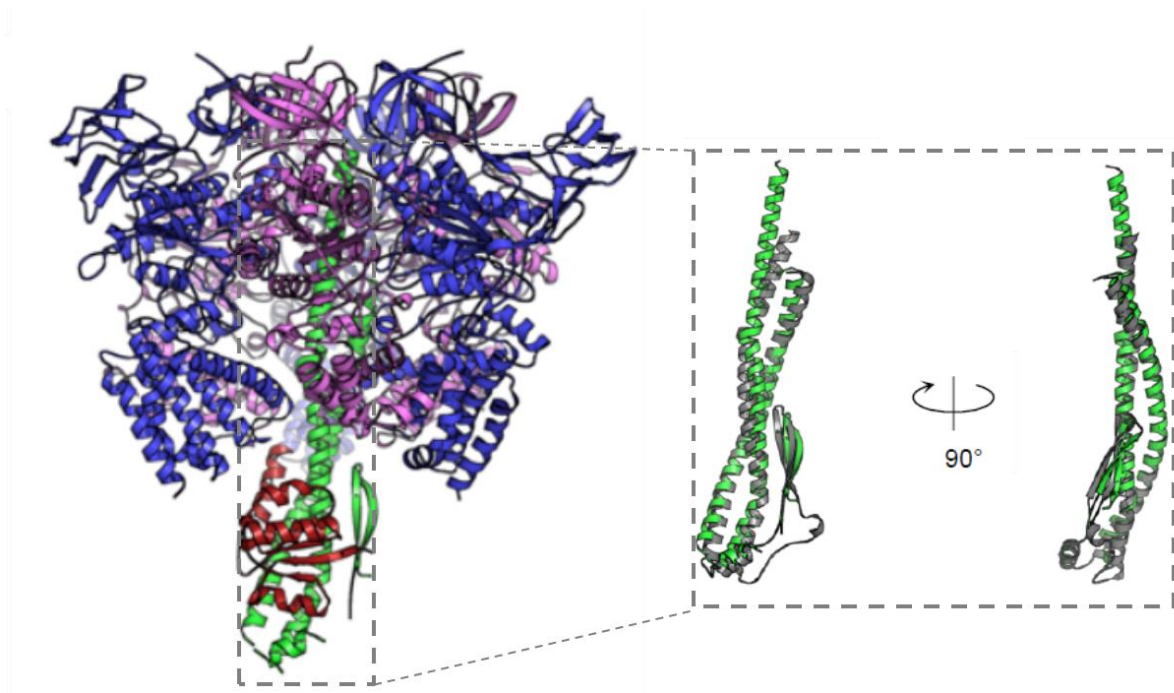


Fig1.10. Structural features of γ subunit and its association with $\alpha\beta$ hexamer: The two anti-parallel helices of the γ subunit (in green) enter the cavity of the $\alpha\beta$ hexamer (shown in blue and purple). The inset shows the twisted tertiary structure of γ subunit which enables it to associate with a single dimer at a time during rotation. (This figure is adapted from Murata et al 2013 [35]).

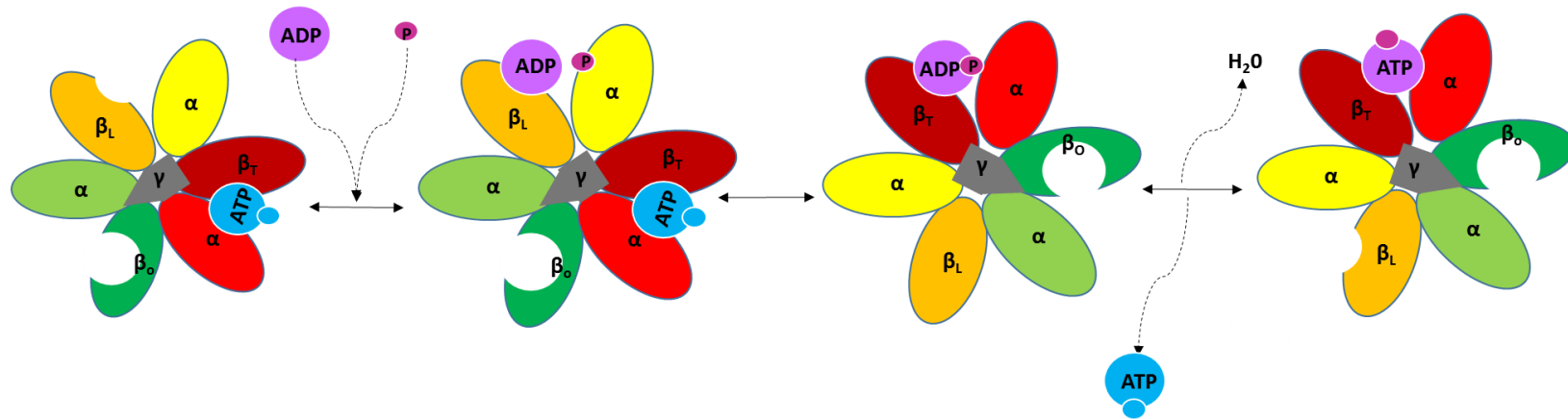


Fig1.11. Asymmetric association of γ subunit with the β subunit during catalysis Each of the three main catalytic subunits of the F_1F_0 ATP synthase, the β subunit, undergo transition from the tight (ATP bound) \rightarrow bindable \rightarrow open form alternately leading upto ATP production and release. The red, yellow and green pairs denote the tight, loose/bindable and the open forms respectively. The γ subunit (in grey) of the central stalk interacts with the β subunit in a similar sequential manner this driving the rotation of the catalytic head.

Chapter 1

So far, we have seen that ATP synthases are vital for the survival of living organisms and it has been observed that the architecture of this complex differs from organism to organism based on their nutrient source and habitat. Hence, to understand an organism's bioenergetics, it is crucial to understand the function of ATP synthase of that particular organism. Structural characterization inevitably elucidates the functionality of any protein complex. Extensive research is being carried out to structurally characterize ATP synthases from various organisms. The information gathered from these studies have enabled us to understand how the ATP synthases function and how they manage to adapt to meet the energetic demands of the particular organism. However, there are many organisms with interesting bioenergetics pathways in which this complex has not been explored yet. Hence, there is much scope to explore further into the details of what makes this complex a “marvellous molecular nano-machine”. In this regard, the next section provides details of a tiny hyperthermophilic, parasitic archaeal species *Nanoarchaeum equitans* and its fascinating bioenergetics.

1.4 Bioenergetics of *Nanoarchaeum equitans* (Neq)

Nanoarchaeum equitans is a tiny organism of size about 400nm which was serendipitously discovered in the hydrothermal vents [84]. This organism was found attached to another larger species of hyperthermophilic chrenoarcheon, *Ignicoccus hospitalis* and this kind of parasitic relationship has never been seen before in archaea. The genome of *Nanoarchaeum* was sequenced in 2003 and had a number of unusual characteristics [85]. The genomic size is about 490Kb and it is highly condensed. The genome lacks genes for most of the important metabolic pathways. Such a kind of highly reduced genome is characteristic of a parasitic organism. However, some of its features such as the presence of split reverse gyrase or tRNA genes indicate its possible placement as one of the ancestral living species. Detailed research about the interactions between *Nanoarchaeum equitans* and its host, *Ignicoccus hospitalis* has revealed a high amount of dependency of the parasite on its host for most of the major biochemical pathways such as lipid metabolism [86]. The host also harbors certain peculiarities characteristics particularly the structure of its plasma membrane which is one of its kind in the archeal family. This hints at a dynamic reliance of the parasite on its host.

One of the most interesting aspects of *Nanoarchaeum equitans* is its bioenergetics as it has been found to lack several of the ATP synthase subunits. Genes for only 5 subunits were found in the genome, in contrast that of its host and other archaeal species explored so far which have 9 genes (Fig1.12). These observations raise a question as to how the ATP generation in the organism

takes place. There are several possible explanations for this which are given below.

1. The organism might be capable of forming a functional yet minimalistic complex.
2. It could also have a rudimentary form of the complex which has lost its function.
3. It entirely depends on the host for its energy generation.

A recent development which solidifies the hypothesis of *Nanoarchaeum equitans* dependency on its host for bioenergetics was the experimental proof of the ATP synthase of *Ignicoccus hospitalis* being present on the outer layer of its plasma membrane (Fig.1.13) [87]. However, to understand which of these possibilities represents the actual scenario, in depth analysis of the structural and functional details of the *N.equitans* ATP synthase complex needs to be done.

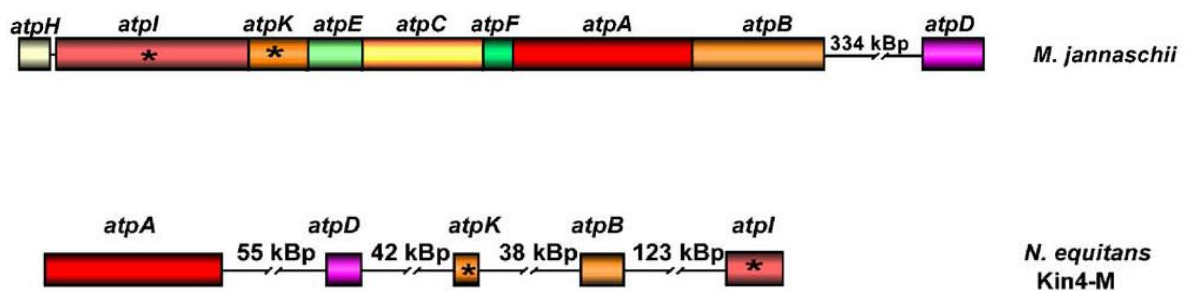


Fig 1.12: A comparison of the genes coding for subunits of A1A0 synthase in *M. jannaschii* and *Nanoarchaeum equitans*. This comparison highlights the lack of major subunits in *N.equitans* ATP synthase. (Genes marked with asterisks code for hydrophobic proteins [85]).

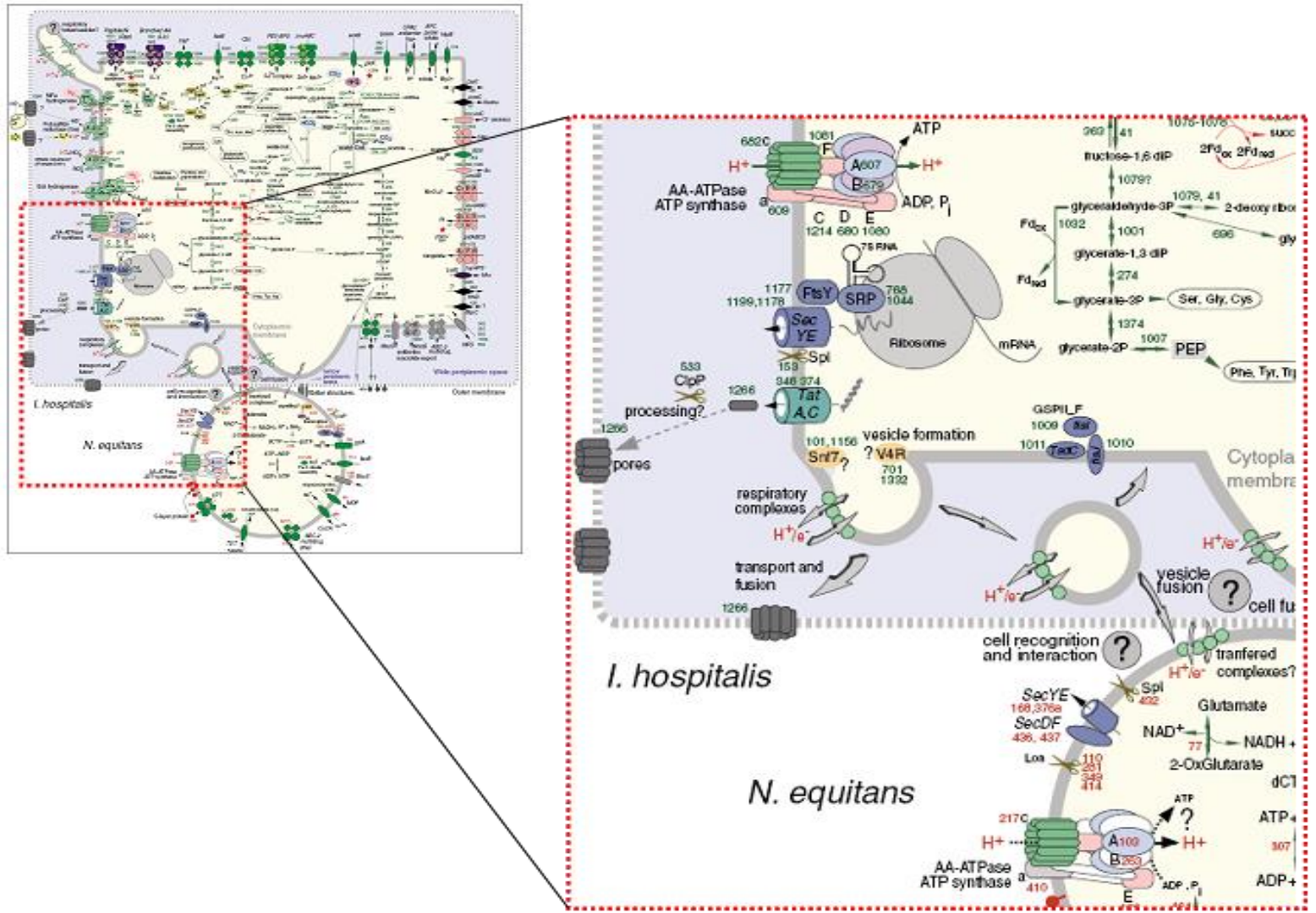


Fig 1.13. Schematic representation of the protein complexes present at the cell-cell boundary of *Nanoarchaeum equitans* and its host, *Ignicoccus hospitalis*. This figure shows all the putative protein complexes such as ion transporters present at the cell-cell interface of *N. equitans* and *I. hospitalis*. (This figure is adapted from Stetter et al, 2008 [88]).

1.5 Objectives

ATP synthases form a highly specialized enzymatic complex that functions through the unique mechanism of rotary catalysis. Every subunit of the ATP synthase complex has a role in its function. Most of the 8-16 subunits of F/V/A type ATP synthase complex have exclusive tasks to perform which makes them indispensable. *Nanoarchaeum equitans* ATP synthase possesses only five of these. The lack of these subunits has made this ATP synthase machinery the object of curiosity ever since its discovery in 2003. No other organism has been documented to have a functional ATP synthase with such a few subunits. It was also reported that the *Nanoarchaeum equitans* which are obligatory parasites on *Ignicoccus hospitalis* cannot survive when detached from the host. This raises intriguing questions about the architecture and the bioenergetics of this organism.

In an effort to understand the ATP synthesis machinery and in particular, the *Nanoarchaeum equitans* ATP synthase, the objective of this thesis is to decipher the structural features of this ATP synthase complex. As *Nanoarchaeum equitans* is an obligatory hyperthermophilic endosymbiote which requires hydrogen sulphide for its survival, isolating the ATP synthase proteins from the cultures was not a very promising approach. This led us to express the recombinant proteins of various subunits of the *Nanoarchaeum equitans* ATP synthase. Chapter 2 reports the cloning, purification, characterization and crystallization of regulatory subunit, NeqB and hexameric core complex, NeqAB with and without nucleotides ADP, AMP-PNP. The sequence and phylogenetic analysis, structural studies, biophysical interaction studies, ATPase assays and functional implications are presented in chapter 3.

Chapter 2

**Crystallization of regulatory subunit, NeqB
and hexameric core complex, NeqAB with
and without nucleotides ADP, AMP-PNP
from *Nanoarchaeum equitans***

2.1. Introduction

Of late, the study of archaeal ATP synthases has gained momentum as these complexes provide interesting insights into evolution of ATP synthase family. How a single complex has adapted to function in these extremophiles is another exciting area. The study of the soluble A₁ complex has been made the central focus as it is the main functional part of the enzyme. The structure of any protein complex holds key information about function. Therefore, recently, a lot of work has been done to structurally and biophysically characterize the various subunits as well as sub-complexes of the archaeal ATP synthases [44, 52, 89]. Isolation of the complete *M.mazei* ATP synthase showed that at least nine subunits are required to make up the entire A₁A₀ ATP synthase [90]. How *Nanoarchaeum equitans* manages to build an ATP synthase out of only five subunits became a long standing question. This question can only be answered through structural characterization of this complex. As a first step towards understanding the structure and function of *N.equitans* ATP core complex, in this chapter we report the expression, purification and crystallization the independent regulatory subunit, NeqB, and the hexameric core complex NeqAB (A₃B₃) hexamer from *N. equitans*.

2.2 Materials and methods

2.2.1 Cloning, expression and purification of recombinant NeqB and NeqAB complex

For the expression of full length, wild-type *Nanoarchaeum equitans* ATP synthase subunits, we created the genes coding for the 570 amino acid long, catalytic subunit A, NeqA(NEQ103) and 416 amino acid long, regulatory

subunit B, NeqB (NEQ263), through gene synthesis. These genes in pMK-RQ vector with a constitutively active glucose isomerase promoter and an C-terminal hexahistidine tag. For the co-expression of the NeqAB complex, genes coding for both NeqA and NeqB were subcloned into pET Duet vector. NeqA was cloned into MCS1 using BamHI and HindIII restriction sites, whereas the gene for NeqB was cloned into MCS2 using NdeI and XhoI restriction sites. These genes were expressed under the control of the inducible T7 promoter.

BL21 De3 cells were used for expressing the NeqB and the NeqAB complex. Cells transformed with NeqB construct were cultured in Terrific broth media containing 50 µg/ml kanamycin at 37°C for 24 h. NeqB was expressed constitutively and hence does not require induction. The AB_pET-Duet constructs were grown in TB media with 100 µg/ml ampicillin at 37°C until an OD₆₀₀ of 0.6 and then induced with 0.5 mM IPTG and grown at 16°C for 18 h. For both NeqB and NeqAB complex, cell lysis was done using Pierce BPER lysis buffer (Pierce Biotechnology, Rockford, IL, USA) containing lysozyme and DNase and were lysed enzymatically for 1 h. The lysates were heated at 75°C and spun down at 13,000 × g. Affinity purification was done using GE HiTrap columns (GE-Amersham, Buckinghamshire, UK) and 50 mM Tris HCL, 150 mM NaCl and 10 mM imidazole as binding buffer and 50 mM Tris HCL, 150 mM NaCl and 400 mM imidazole as elution buffer. The eluted fractions were desalted and exchanged into 50 mM Tris HCL pH 8.0 using GE PD10 desalting columns and loaded onto MonoQ columns (GE-Amersham). The eluted fractions were concentrated using Vivaspin concentrators (Viva Products, Littleton, MA, USA) and were applied to Superdex 200 GL 10/300 column (GE-Amersham). NeqB was found to be prone to precipitation in 50

mM Tris pH 8. Optisol solubility kit was employed to assess the optimum buffer conditions for NeqB (Dilyx Biotechnologies, Birmingham, AL). The gel filtration buffer was 50 mM Bis-Tris, 150 mM NaCl, 5 mM BME and 5% glycerol, pH 6.0, for NeqB, and 50 mM Tris, pH 8.0, for NeqA and NeqAB. The purified proteins were analysed using Novex 4–12% Bis-Tris gels from Invitrogen (Carlsbad, CA, USA) and quantified using a standard Bradford assay.

2.2.2 Dynamic light scattering (DLS)

DLS measurements were performed at room temperature on a DynaPro (Protein Solutions) DLS instrument (Wyatt Technology Corp., Santa Barbara, CA, USA). Fractions of individual NeqB and NeqAB from the gel-filtration chromatography were pooled separately and concentrated using Vivaspin concentrators (Sartorius AG, Germany). DLS was performed for NeqB at a concentration of 40 mg/ml in 50 mM Bis-Tris, pH 6.0, 150 mM NaCl, 5 mM BME, and 5% glycerol and for NeqAB are at a concentration of 20 mg/ml in a buffer consists of 50 mM Tris HCL pH 8.0. The homogeneity of each of the concentrated NeqB and NeqAB was verified by assessing the quality of the data represented in the sum of squares (SOS) error statistic reported for each sample acquisition (a single correlation curve). All samples were centrifuged at 10 000 g for 20 minutes prior to the experiments. The measurements were recorded at 298 K. The software provided by the manufacturer was used to calculate the hydrodynamic properties of NeqB and NeqAB complex.

2.2.3 Crystallization

NeqB

Initial crystallization screenings were carried out using the robotic (Mosquito system) with Crystal screen and Crystal screen-2 (Hampton Research), Index and Wizard screens 1, 2, 3 and 4 at room temperature (298K). A total of 336 conditions were set up using the 96 well plates with 200 μ l of crystallization solution in the reservoir. Each drop consists of 1 μ l of protein solution and 1 μ l of crystallization solution. The rod shaped crystals appeared in conditions with 100 mM Tris pH 8.5/ 100 mM HEPES pH 7.5, 200 mM $MgCl_2 \cdot 6H_2O$, 30% (v/v) PEG400. The identified initial conditions were further optimized by varying the precipitant concentration from 10 to 50 % to obtain large crystals. The diffraction quality crystals were obtained after 8 days from an optimized crystallization condition consisting of 100 mM HEPES pH 7.5, 200 mM $MgCl_2 \cdot 6H_2O$, 20% (v/v) PEG400 at 298K and crystals were grown to approximate dimensions of 0.2x0.3x0.2 mm within a week.

NeqAB complexes

Initial crystallization screening were carried out using the robotic (Mosquito system) with Crystal screen and Crystal screen-2 (Hampton Research) and Wizard screens 1, 2, 3 and 4 at room temperature (298K) with a total of 288 conditions. The cube shaped crystals appeared in several conditions with 1.26 M ammonium sulphate and the conditions with large, single crystals were further optimized by using additive screens. The diffraction quality crystals were obtained after 5 days from an optimized crystallization condition consisting of 0.1 M MES 6.5, 1.6 M ammonium sulphate and 10% dioxane at

298K and crystals grown to approximate dimensions of 0.1x0.2x0.2 mm. Similarly, NeqAB ADP and AMP-PNP crystals were obtained by incubating concentrated NeqAB complex with 10 mM Mg-ADP/AMPPNP and drops were set up using hanging drop vapor diffusion method. The dimensions of the crystals were similar to the native crystals.

2.2.4 Data collection

Crystals of NeqB and native NeqAB, its complexes with ADP and AMP-PNP were briefly soaked (10-20 secs) in a cryoprotectant solution consisting of crystallization condition supplemented with 50% glycerol and the crystals were picked up in a nylon loop and flash-cooled at 100 K in the nitrogen cold stream. The complete data sets for the NeqB and NeqAB native and nucleotide bound complexes were collected using the in-house Rigaku rotating anode generator (Microfocus rotating anode X-ray generator Rigaku MicroMax(tm)-007 HF (native NeqAB and NeqAB-AMPPP) and the NSRRC synchrotron beamline 13B (NeqB and NeqAB-ADP). The data collection statistics are provided in table 1.

2.3. Results

2.3.1 Cloning, expression and purification

The NeqB and NeqAB complex was expressed and purified (Fig.2.1; Fig.2.2). The optimized expression of NeqB and NeqAB resulted in approximately 5-6 mgs of protein per liter of culture. NeqB eluted at a volume corresponding to the monomer as compared with the molecular weight standards. The SDS-PAGE showed 99% purity of these proteins (Fig 2.2).

Gel filtration chromatography of NeqAB complex revealed that it elutes at a molecular weight of approximately 300-350kD in size which represents the hexameric molecular weight of the A₃B₃ complex (Fig 2.3). This hints at the formation of a possible hexamer.

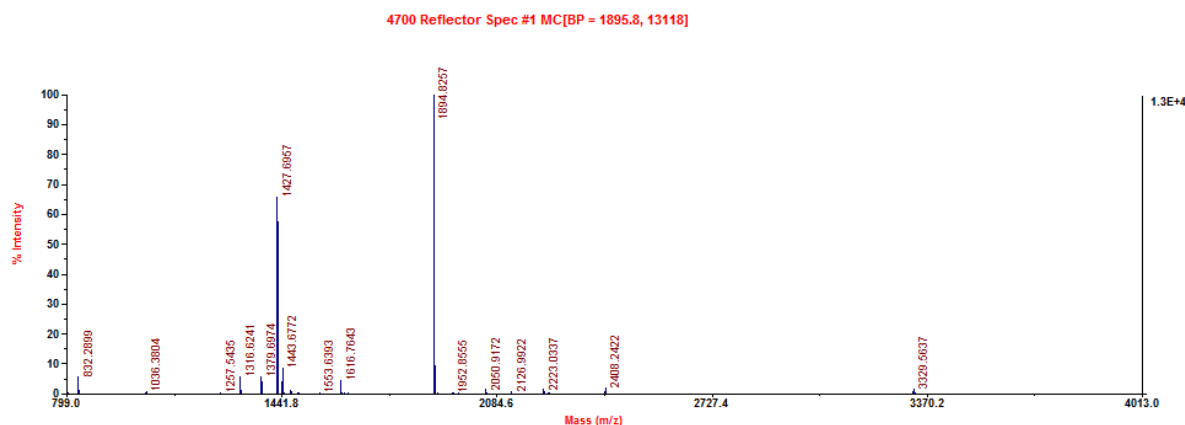


Figure 2.1. MALDI-TOF MS analysis of NeqB showing the mass of NeqB. The predominant peptides detected are from NeqB (NEQ263)

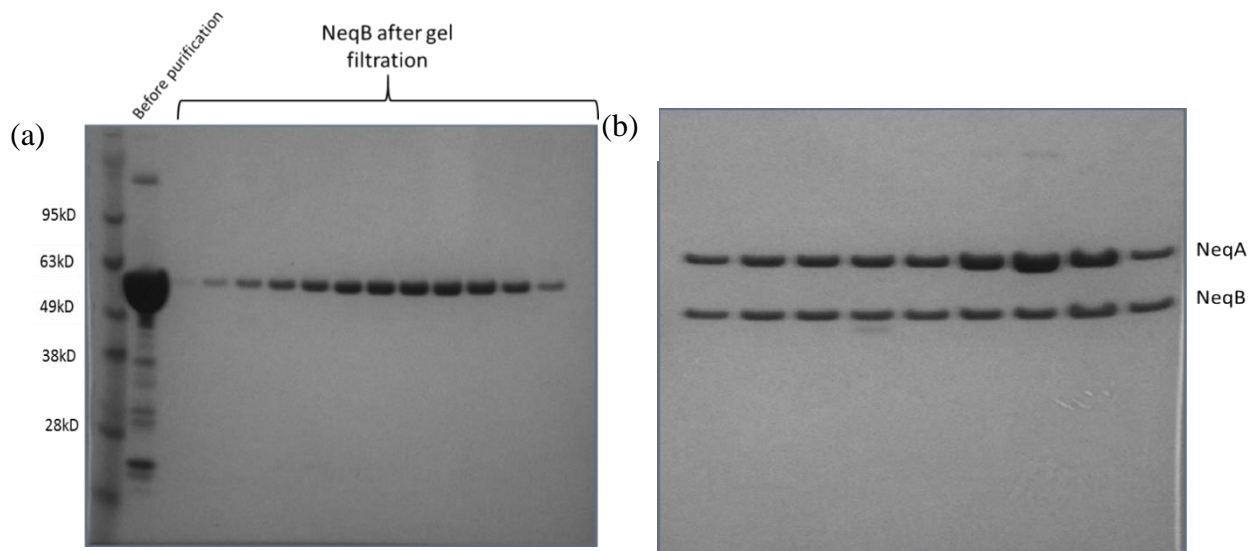


Figure 2.2 SDS gel image of purified NeqB and NeqAB shows the purity of a) NeqB (49kD) and b) NeqAB (62 and 49kD respectively). This analysis has been done using Invitrogen Novex pre-cast 4-12% SDS-PAGE gel followed by Coomassie dye based staining using Simply Blue safe stain.

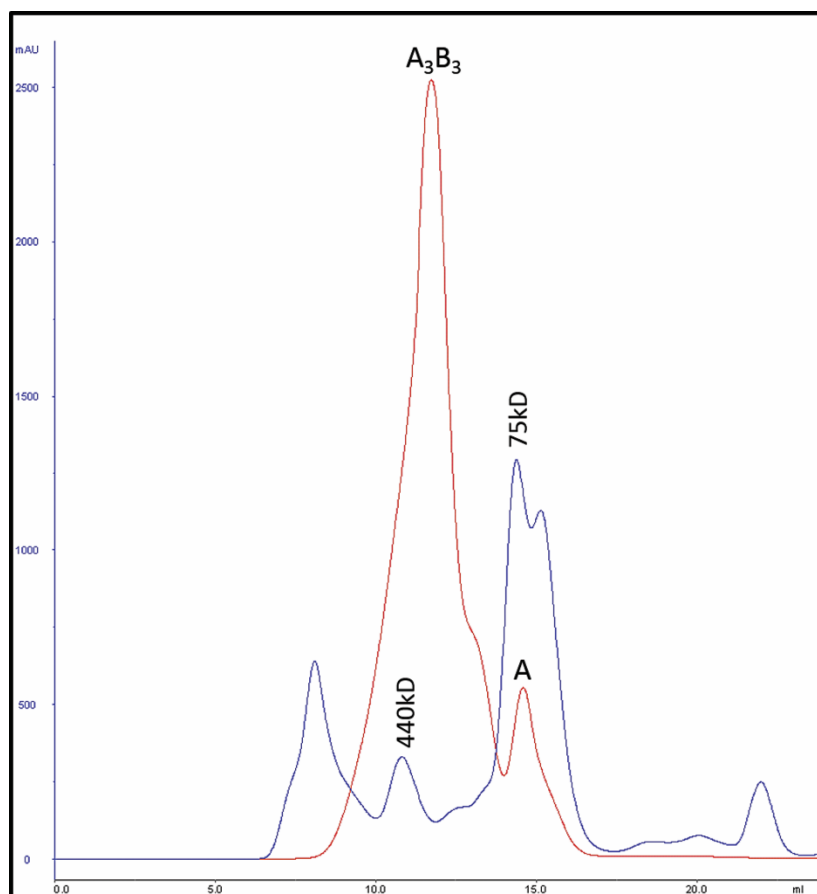


Figure 2.3 *Neq A₃B₃ complex is possibly hexameric* Gel-filtration chromatography elution profiles of NeqAB (red line) and standard proteins (Fe: 440kD, Con: 75kD). The gel-filtration profile shows that NeqAB elutes as hexamer with a molecular weight of approx.300kD.

2.3.2 Analysis of homogeneity of NeqB and NeqAB complex

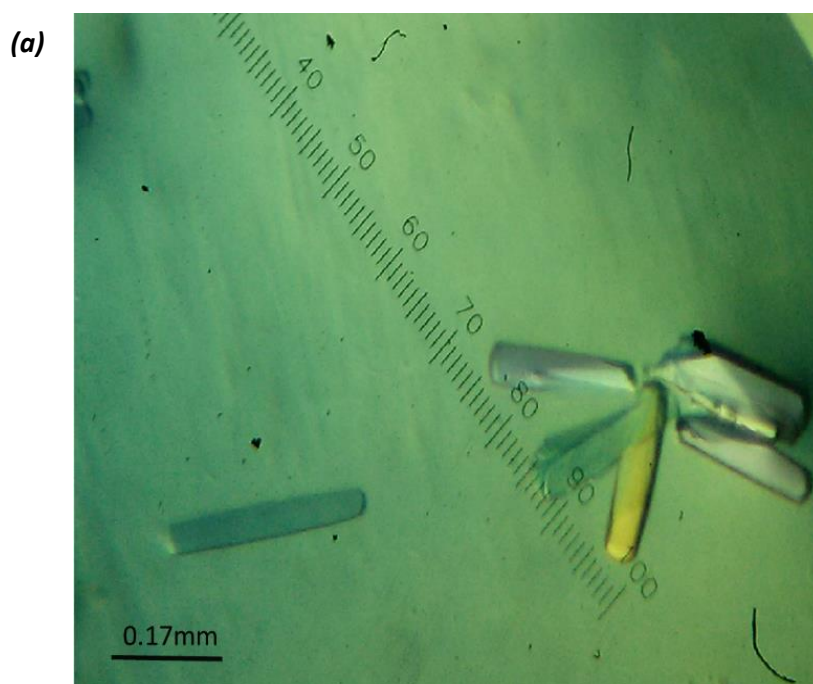
The purified NeqB and NeqAB complexes were concentrated upto 40 and 25 mg/ml respective and their homogeneity verified in the dynamic light scattering experiments during concentrations and prior to crystallization experiments. In case of NeqB, the DLS results showed the existence of monomer in solution and are consistent with the gel-filtration observation. DLS results show that NeqAB complex is monodisperse at 25 mg/ml. However, the oligomeric state of NeqAB was detected as a dimer in the DLS Pilot screens for NeqB and NeqAB complexes done using sitting drop method and after identifying the

optimum buffer condition, optimization was done using hanging drop method vapor diffusion method.

2.3.3 *Crystals, diffraction and data collection*

Initially, the crystallization of NeqB produced highly multi-nucleated needle like structures which were not suitable for diffraction. Significant number of optimization steps was employed to obtain diffraction quality crystals for NeqB. The crystals were rod shaped (Fig 2.4a). The crystals were frozen and diffracted at the NSSRC synchrotron facility to obtain a complete 2.8 Å resolution data set (Fig 2.5).

The NeqAB complex crystals formed more readily than NeqB. The initial screening conditions yielded in large single cubical crystals (Fig 2.4b). Most of these conditions were reproducible and many diffraction trials were done in the in-house X ray system. The best quality crystals were selected for diffraction at the NSSRC beamline. A representative diffraction image is given below (Fig 2.5). Details about data collection are given below in table 2.1.



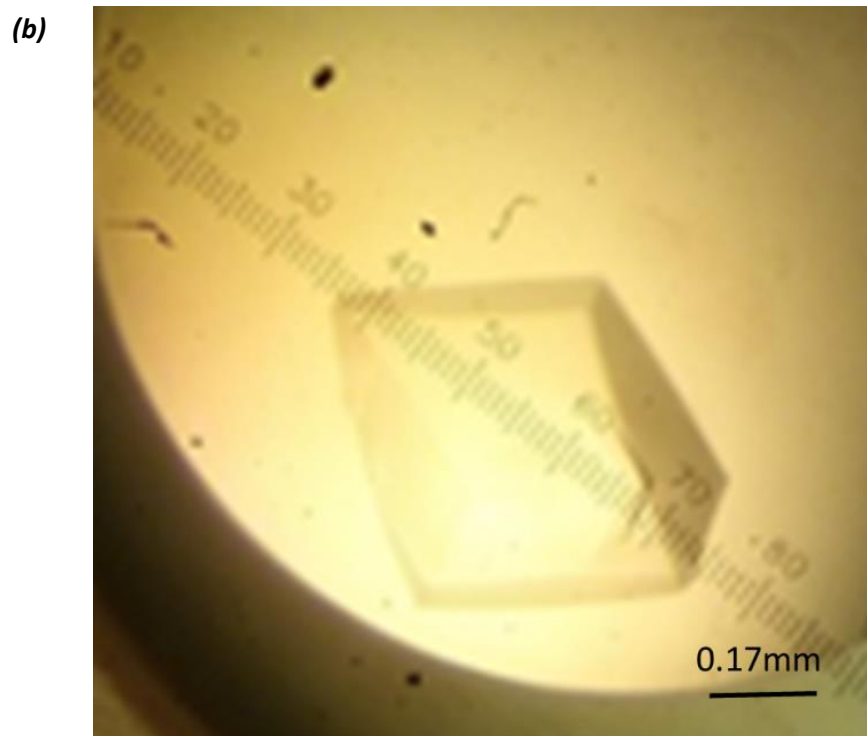
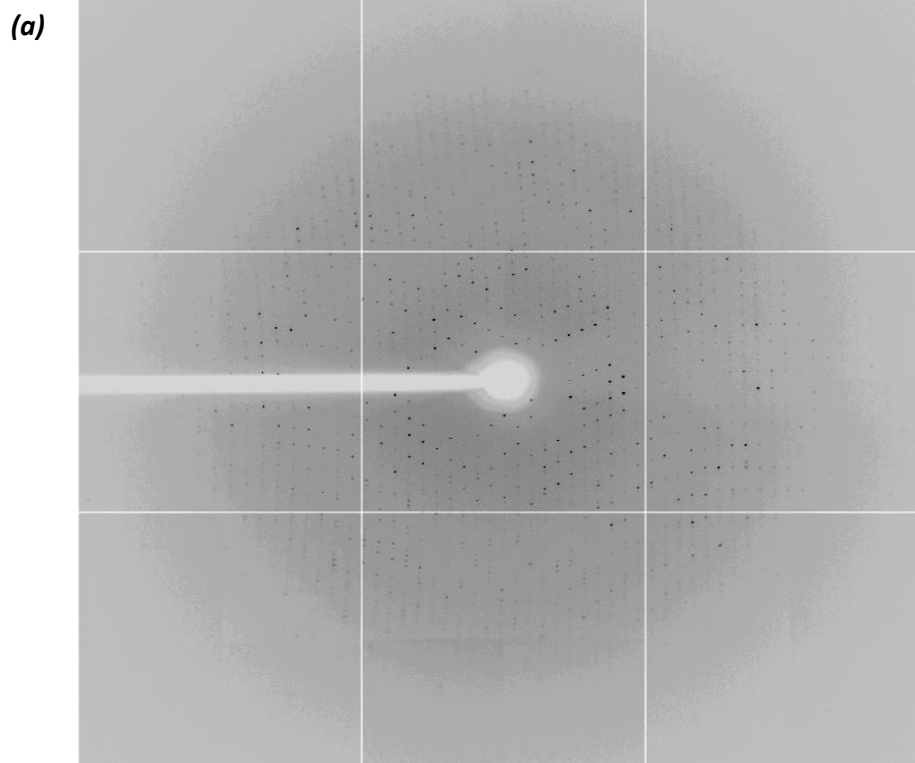


Figure 2.4 Crystals of NeqB and NeqAB The image shows *(a)* the needle shaped crystal of NeqB and *(b)* cuboidal crystals for NeqAB



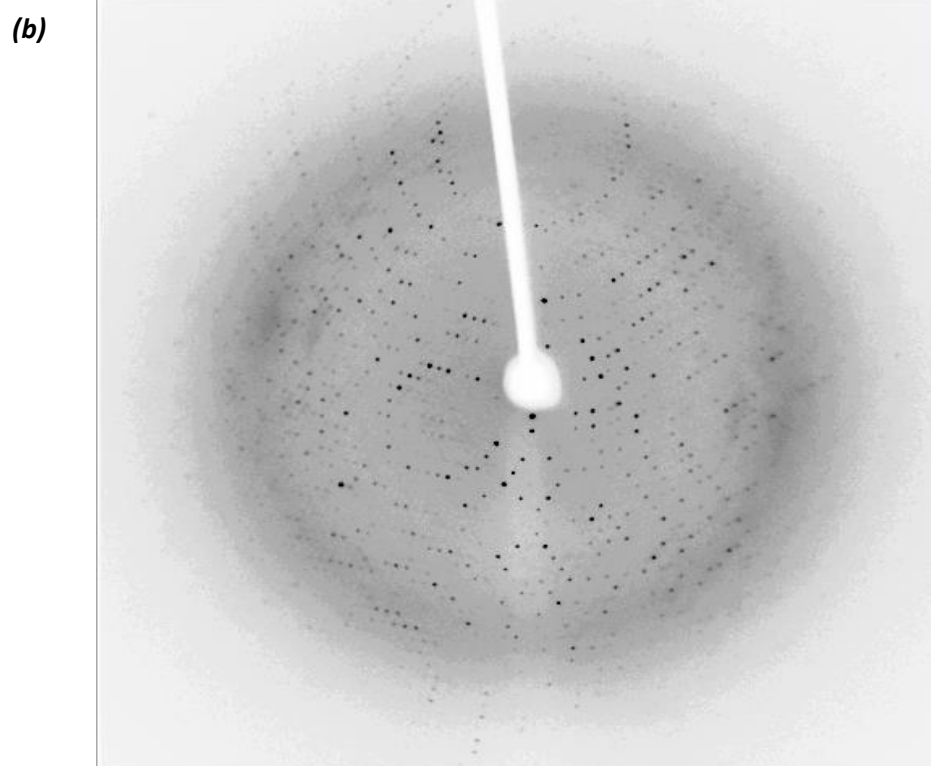


Figure 2.5 Representative diffraction patterns of crystals of NeqB and NeqAB The diffraction pattern for NeqB at 2.8 Å and NeqAB crystals at 2.7 Å shows the data quality.

2.3.4. *Preliminary analysis*

Preliminary analysis of the X-ray diffraction suggests that the crystals belong to space group $P2_12_12_1$ for NeqB and R3 for NeqAB. The Matthews coefficient V_M of $2.88 \text{ \AA}^3\text{Da}^{-1}$ for NeqB and $3.47 \text{ \AA}^3\text{Da}^{-1}$ for NeqAB corresponds to the four molecules of NeqB and one heterodimer of NeqAB in the asymmetric unit with 57.3% and 64.6% solvent content respectively. The structure solutions were obtained by the molecular replacement method using the program, Phaser[91]. The atomic coordinates of the subunit B as well as the A3B3 complex of the *Thermus thermophilus* V1-type ATP synthase were used as the starting search model (PDB: 3GQB) [92]. The structure solution clearly indicates that there are four molecules of NeqB in the asymmetric unit of the crystal. Whereas one heterodimer (NeqA: NeqB in 1:1 ratio) in the asymmetric unit of NeqAB complex crystal.

Table 2.1. Data-collection statistics

| Details | NeqB | Native NeqAB | NeqAB- ADP | NeqAB-AMP- PNP |
|---|---|---|---------------------------------|--|
| X-ray source | NSRRC Beamline 13B | Microfocus rotating anode X- ray generator Rigaku MicroMax(tm)- 007 HF | NSRRC Beamline 13B | Microfocus rotating anode X-ray generator Rigaku MicroMax(tm)- 007 HF |
| Wavelength (Å) | 0.97913 | 1.5418 | 0.97913 | 1.5418 |
| Oscillation angle (°) | 0.5 | 0.5 | 0.5 | 0.5 |
| Unit-cell parameters (Å) | a=77.23 b=155.23 c=177.45 | a = b = 192.61 c = 108.94 | a = b = 192.46 c = 110.24 | a = b = 193.48 c = 108.85 |
| Space group | P2 ₁ 2 ₁ 2 ₁ | R3 | R3 | R3 |
| Matthews coeff (V _M) and | 2.88 | 3.47 | 3.50 | 3.50 |
| Resolution limits (Å) | 50-2.8(2.9- 2.8) | 33.0-3.0(3.05-3.0) | 50-2.0(2.03- 2.0) | 50-2.63(2.68- 2.63) |
| Observed <i>hkl</i> (<i>I</i> > σ <i>I</i>) | 51826 | 32275 | 111905 | 44898 |
| Unique <i>hkl</i> | 3987 | 10086 | 34970 | 7897 |
| Redundancy | 13.0(8.9) | 4.0(2.5) | 5.5(4.5) | 5.7(4.3) |
| Completeness (%) | 98.3(91.8) | 97.6(94.9) | 99.8(98.5) | 99.8(97.3) |
| Overall <i>I</i> / σ (<i>I</i>) | 23(2.0) | 5.3(1.7) | 37.12(2.87) | 22(2.8) |
| R _{sym} | 0.10 (0.56) | 0.23(0.40) | 0.132(0.54) | 0.09(0.51) |

2.4 Discussion

The F_1F_0 ATP synthases and the V_1 -ATPases have been extensively studied and characterized and most of this information comes from crystal structures. On the other hand, the archaeal ATP synthases are yet to be understood in detail due to the dearth of structural information. Archaeal species employ many unique and unusual modes of bioenergetics such as high temperature and salt tolerance and anaerobic modes of respiration [85]. As respiration and ATP synthesis go hand in hand, the archaeal ATP synthases are similarly adapted and hence are interesting subjects for the study of evolution of ATP synthases as well as bioenergetics. *N. equitans* was found to be even more unique due to its highly reduced genome, absence of important metabolism pathway and presence of only a partial set of ATP synthase genes. Hence, structural characterization of the *Nanoarchaeum equitans* ATP synthase complex would be very interesting. In this chapter we have reported the cloning, expression, purification, characterization and crystallization of its regulatory subunit NeqB, and the hexameric core complex, NeqAB.

We have obtained a 2.8Å diffraction data for NeqB. We have also obtained the diffraction data for the 330kD NeqAB hexameric complex with and without nucleotides at resolutions between 2.0Å to 3Å with one heterodimer (subunit A and B) in the asymmetric unit. This complex is the core system of the ATP synthetic machinery. The structure determination of these ATP synthase core hexameric complexes will not only lead to understand the ATP hydrolysis mechanism of this archaeal species *Neq* but also the evolution of ATP synthases. The structural and associated functional studies and analysis were presented in chapter 3.

Chapter 3

**Structural basis for a unique ATP synthase
core complex from *Nanoarchaeum equitans***

3.1 Introduction

As discussed in Chapter 1, there are three major categories of ATP synthases; the F-type, V-type and A-type. To recapitulate, F_1F_0 -ATP synthases are the major ATP synthetic machines and V_1V_0 -ATPases execute ATP hydrolysis. A-type ATP synthases are structurally similar to V-type ATPases but function as ATP generators, which is reminiscent of the function of the F-type; thus, A-type ATP synthases are considered as chimeras of the F-/V-types [64, 93]. They are found in most archaeal organisms and some hyperthermophilic bacteria, such as *Thermus thermophilus*, acquired through horizontal gene transfer [94]. Because V-type ATPases are known to have originated in archaea and given the significant structural resemblance between V- and A-types, these two types are often mutually compared [38]. However, in all of the ATP synthase structures shown to date, the overall morphology of the complex remains similar, with differences usually found only in the stoichiometry of the subunits, particularly those comprising the membrane rotor [45, 95] [96].

Even though archaea are a diverse group of organisms that can live at extreme temperatures, pH and salinity, utilising unique modes of respiration and bioenergetics to derive their energy, they all perform ATP synthesis through the A_1A_0 ATP synthase [85, 97]. The evolution of ATP synthases and the mechanism of cellular energetics under extreme conditions could be uncovered through structural and functional studies; however, difficulties in isolating and culturing these organisms, concomitant with the lack of operons in most of them, has left this particular class of ATP synthases relatively understudied. The most well-known model for archaeal ATP synthases arose from the cryo-EM

studies of the ATP synthase from *Methanosarcina mazei* and *Methanococcus janaschii* [90, 98] where the presence of complete ATP synthase operon provided an opportunity to characterise this nine-subunit complex [43, 99, 100]: subunits A and B form the core hexamer (A₃B₃); E and H form the peripheral stalk that stabilizes rotation; D, C and F are the central stalk required for rotation; and K and I form the ion translocating ring complex [90].

As mentioned in chapter 1, *Nanoarchaeum equitans* is a recently discovered hyperthermophilic archaeal species, an obligatory parasite on *Ignicoccus hospitalis* [85, 101]. Genomic analysis of *N. equitans* has revealed highly primitive characteristics. [101]. Indeed, phylogenetic analyses show that *N. equitans* might have arisen before the divergence of Eukarya and Prokarya [102]. Hence, the study of its systems and processes hold potential insight into the biogenesis and evolution of several vital proteins and complexes.

The ATP synthases/ATPase family of proteins is one of the earliest enzyme systems to arise. Owing to its highly conserved nature and complex organization, the study of its evolution has become of great interest. Given the ancestral reputation of *N. equitans*, understanding how its ATP synthase is organized and functions could answer many questions. Interestingly, the genomic interrogation of *N. equitans* indicates that it has only five representative subunits of the ATP synthase [85]. The simplest ATP synthase to date is that of *E. coli*, which has about eight subunits [28] and, thus, of all the known ATP synthases, *N. equitans* harbours the smallest number of representative subunits known so far. A comparison of the *N. equitans* ATP

synthase subunits with its homolog (*M.mazei* ATP synthase) revealed the presence of representatives of ATP synthase such as the A and B subunits (which form the hexameric core hexamer, A_3B_3), the central stalk subunit D, rotor subunit I subunits and proteolipid subunit c/K which forms the proton ring. However, some of the other central stalk subunits such as subunit F and C and the peripheral stalk (E and the H subunits) seem to be completely absent in *N. equitans*. Moreover, the B subunit is shorter than its known homologues. Therefore, it has been widely speculated whether this organism possesses a rudimentary yet functional ATP synthase [103].

Our objective was to explore the structural and functional aspects of the *N. equitans* hexameric core hexamer (A_3B_3). In this chapter, we report the crystal structures, along with biophysical studies, of the *N. equitans* ATP synthase regulatory subunit B (NeqB), the core subunits in complex (AB), and its complex with ADP and AMP-PNP (a non-hydrolysable analogue of ATP). Comparing it with the homologous V/A/F-ATPase structures revealed key aspects of the evolutionary process of the ATP synthases: Structurally, we show that the core complex (NeqAB) is forms a hexameric ring. However, we observe conformational inflexibility upon nucleotide binding which leads us to speculate that the hexameric core complex might not yet be functional, owing to the primitive or intermediate stage in evolution [35, 104].

3.2 Materials and Methods

3.2.1 Sequence alignment and phylogenetic analysis

Representative V/A/F-type subunit homologues were selected from a BLAST search with NeqA and NeqB and were converted into FASTA format. Sequence alignment was done using the T-coffee software and the figures for sequence alignment were generated using Boxshade. The same sequences were used for phylogenetic analysis and tree building. This was performed using the Phylogeny.fr software platform using the “advanced” mode[105]. In this module, the sequence alignment was done using MUSCLE, curation using G-blocks, phylogeny using PhyML and final tree building using TreeDyn. The bootstrapping value in the phylogeny mode was set to 100 iterations.

3.2.2 Cloning, expression and purification of Neq ATP synthase subunits

The details of the cloning, expression and purification of NeqB and NeqAB complex are given in Chapter 2 (page # 36-38).

The gene for *NeqD* (NEQ166), coding for 198 amino acids was cloned into the p-LIC-His vector using ligation independent cloning. This construct was transformed into BL21-De3 cells and kept at 37°C pre-induction and 16°C post induction. 0.25mM of IPTG was used to induce the construct. NeqD was extracted using BPER phosphate buffer supplemented with 1% Triton X-100. Purification was done using affinity chromatography in the presence of 1% Triton X-100.

3.2.3 Crystallization, data collection and structure determination

Details for crystallization and data collection of NeqB and NeqAB complexes are provided in Chapter 2 (page # 39-40).

All data sets were processed using HKL2000 followed by structure solution using Phenix PHASER [91]. All structures were solved by molecular replacement method using PDB 3GQB as a search model. The required manual model building was done in Coot [106] and the refinement was performed using Phenix refine [107]. The structure-related figures presented in this thesis were prepared using PyMol (The PyMOL Molecular Graphics System, Version 1.3 Schrödinger, LLC).

3.2.4 Blue Native PAGE

Blue Native PAGE experiments were carried out using Native PAGE Novex Bis-Tris 4–16% gradient gels from Life Technologies (Carlsbad, CA, USA). Gels were washed and stained with Simply Blue safe stain (Life Technologies) and the protein bands were compared with the Native Mark protein ladder (Life Technologies).

3.2.5 Isothermal titration calorimetry (ITC)

Isothermal titration calorimetry was used to study the interaction of NeqA and NeqB subunits with and without nucleotides. All ITC experiments were performed using VP-ITC calorimeter (Microcal, LLC, Northampton, MA, USA) at 25°C. For nucleotide binding studies, 10 μ M of protein (NeqA and NeqB) was used in the cell for titration against 300 μ M to 1 mM of Mg-ATP in the injection syringe. For binding studies of NeqA and NeqB, 100 μ M of NeqA or NeqB in the syringe was titrated against 10 μ M NeqB or NeqA in the cell. All samples were dialysed into the same buffer, degassed and centrifuged to remove any precipitates. Volumes of 10 μ L per injection were used for all experiments and consecutive injections were separated by 4 min to allow the

calorimetric signal (thermal power) to return to baseline. For experiments with NeqB, stirring speed was reduced to 220 rpm and spacing between injections was increased to 300 s as the protein is prone to precipitation. ITC data were analysed with a single ligand binding site model using Origin 7.0 software (OriginLab Corp., Northampton, MA, USA).

3.2.6 Dynamic Light Scattering (DLS)

The experimental conditions and details of the dynamic light scattering experiments are provided in the previous chapter (page # 38).

3.2.7 Analytical ultracentrifugation (AUC)

The NeqAB complex was subjected to sedimentation velocity experiments using analytical ultracentrifugation to verify complex formation. The AB complex was purified and dialyzed into PBS buffer. A range of concentrations up to 2 mg/ml were used for conducting trials. Sedimentation velocity profiles were collected by monitoring the absorbance at 280 nm. The samples were sedimented at 40,000 rpm at 24°C for 5 h in a Beckman Optima XL-I centrifuge (Beckman Coulter Inc., Brea, CA, USA) fitted with a four-hole AN-60 rotor and double-sector aluminium centre pieces, and equipped with absorbance optics. A total of 200 scans were collected and analysed using the Sedfit[108].

3.2.8 Reconstitution of NeqABD complex

As the D subunit was found to be unstable on its own, we attempted to stabilize it by adding partially purified AB complex and further purifying the entire NeqABD complex. As a first step, reconstitution was carried out by pooling the AB and D elution fractions after affinity purification and incubating overnight

at 4°C. The reconstituted samples were subjected to detergent removal using Pierce Spin columns and ion-exchange chromatography using a GE MonoQ column. The concentrated protein complex was loaded onto Superdex-S200 and eluted with 50 mM Tris 150 mM NaCl, pH 8.0, and the peaks corresponding to the hexameric state were concentrated and analysed on Novex 4–12% Bis-Tris gels for purity. The proteins were quantified using a Pierce BCA assay.

3.2.9 ATPase assay

ATPase activity was measured using the ATP regenerating system, adopting the microplate photometric assay [109]. Final protein concentrations from 0.5 µM to 2 µM were added to 300 µL of reaction solution containing 50 mM Tris-HCl, pH 8.0, 200 mM KCl, 3 mM phosphoenolpyruvate, 5 U pyruvate kinase, 7 U lactate dehydrogenase, 1 mM ATP-Mg, and 0.5 mM NADH, and a decrease in the absorbance at 340 nm was monitored at 25°C. ADP (100 µM) was used as control to check the sensitivity of the regenerating system. Absorbance measurements were done at different time points using the Tecan system (Tecan Systems, San Jose, CA, USA) and data were plotted using the Tecan Magellan software. Phosphoenolpyruvate (PEP), pyruvate kinase (PK), L-lactate dehydrogenase (LDH), and NADH were purchased from Sigma-Aldrich (St. Louis, MO, USA).

3.3 Results

3.3.1 Sequence homology of *Neq* ATP synthase subunits

PSI-BLAST was performed for the *N. equitans* catalytic subunit NeqA (gi|40068623) and regulatory subunit NeqB (gi|40068781) against the non-

redundant protein database. Both subunits were found to be similar to subunits A and B from the ATP synthase superfamily from eukaryotic, prokaryotic and archaeal species.

NeqA was found to be highly homologous to thermophilic bacteria, such as *Thermus thermophilus*, and archaeal species, such as *Pyrococcus horikoshii*. The specific sequence alignment of NeqA with other subunit A homologues showed approximately 50% sequence identity with A-type from *T. thermophilus*, *P. horikoshii*, and *M. mazei*, and V-type from *Enterococcus hirae*, and approximately 30% sequence identity with F-type from *Saccharomyces cerevisiae* and *E.coli* (Fig. 3.1a). Similarly, NeqB exhibited 45% sequence identity with V/A-type subunit B from hyperthermophilic archaeal *Methanocaldococcus*, *Pyrococcus*, *Thermococcus* species, but 23% and 25% sequence identity, respectively, with F-type *E.coli* and the yeast α -subunit (Fig.1a).

The search for conserved motifs indicated that the ²³³GPFSGGKT²⁴⁰ and ²⁵¹GER²⁵³ region of NeqA is the Walker A motif/P loop and Walker B motif, respectively. These motifs are highly conserved in proteins that bind to and hydrolyse ATP to ADP [30, 76, 110]. The search for conserved motifs indicated that the ¹³⁴SPPGLPHN¹⁴¹ and ¹⁶⁴GVP¹⁶⁶ motifs on NeqB aligned with the SxSGLPHN and GIT motifs on the V/A-type ATPases. The SxSGLPHN motif is known to be the Walker A homologous region in the regulatory subunit B of the V/A-type ATP synthase family (Fig.3.1a) [111]. The Arg326 residue of NeqB was also found to be highly conserved across the homologues. This arginine residue has been reported to be crucial for nucleotide hydrolysis [92, 104].

Chapter 3

Overall, our analysis suggests that the A and B subunits of the *N. equitans* ATP synthase possess most of the conserved features observed in V/A/F-ATP synthase complexes.

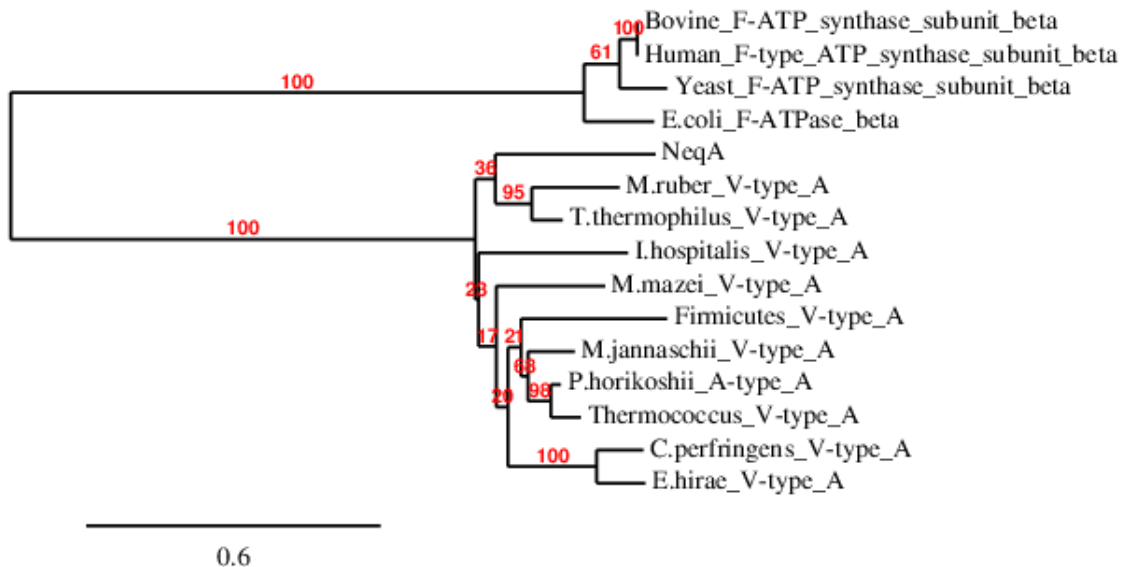
| | | | | | | | |
|--|-----|---------------|---------------|-------------|-------------|------------|---------------|
| NeqA (NEQ103) | 200 | FITGTRVLDIMFP | IAKGGSAAVE | GGPFGSGKTV | LNQQIAKW--- | ADSDIVYIYG | GERGNE |
| <i>E.hirae</i> _V-type_ATPase_A | 209 | MITGQRVIDTFF | FPVTKGGAAAVE | GGPFGAGKTV | VQHQIAKW--- | SDVDLVVYV | GGGERGNE |
| <i>T.thermophilus</i> _V-type_ATPase_A | 204 | FLTGMRILDVLF | FPVAMGGTAAIE | GGPFGSGKTV | TQOQLAKW--- | SNADV VVYV | GGGERGNE |
| <i>M.mazei</i> _V-type_ATPase_A | 182 | LVTGQRILDGLF | FPVAKGGTAAIE | GGPFGSGKTV | TQQQLSKW--- | SDTEIVVYI | GGGERGNE |
| <i>M.jannaschii</i> _V-type_ATPase_A | 218 | LITGQRVEDTFF | TFLAKGGTAAIE | GGPFGSGKTV | TQHQLAKW--- | SDADV VVYI | GGGERGNE |
| <i>E.coli</i> _F-type_A | 127 | LETGIKVIDLM | CPFAKGGKVGLE | GGAGVGKTV | NMELIRNIAIE | HSGYSVFAGV | GERTRE |
| Yeast_F-type_A | 167 | LETGIKVVDLL | LAPYARGGKIGLE | GGAGVGKTV | FIQELINNI | AKAHGGFSV | FVTGVERTRE |
| <i>Bos taurus</i> _F-type_beta | 180 | LVTGIKVVDLL | LAPYAKGGKIGLE | GGAGVGKTV | LIMELINNV | AKAHGGYSV | FVAGVERTRE |
| Human_F-type_beta | 180 | LVTGIKVVDLL | LAPYAKGGKIGLE | GGAGVGKTV | LIMELINNV | AKAHGGYSV | FVAGVERTRE |
| | | | | Walker A | | Walker B | * |
| | | | | | | | |
| NeqB (NEQ263) | 125 | LKGQKIAIEF | SPPGLPMER | LALQIARNVAK | ----- | DKTIIFAAI | GVPSDIYK |
| <i>E.hirae</i> _V-type_ATPase_B | 142 | VRGQKLPVFS | SGSGLPHKE | LAAQIARQATV | LD----- | SSDDFAVV | FVAAGITFEEAE |
| <i>T.thermophilus</i> _V-type_ATPase_B | 145 | VRGQKLPVFS | SGSGLPANE | LAAQIARQATV | RPDLSGE | GEKEEPFAV | VFAAMGITORELS |
| <i>M.mazei</i> _V-type_ATPase_B | 141 | VRGQKLPVFS | SASGLPHNE | LALQIARQASV | PG----- | SESAFAVV | FVAAMGITNEEAQ |
| <i>M.jannaschii</i> _V-type_ATPase_B | 147 | VRGQKLPVFS | SGSGLPHNQ | LAAQIARQAKV | RG----- | EGEKFAVV | FVAAMGITSEAN |
| <i>E.coli</i> _F-type_beta | 141 | AKGGKVGLE | GGAGVGKTV | NMELIRNIAIE | ----- | HSGYSVFAGV | GERTREGN |
| Yeast_F-type_beta | 180 | ARGGKIGLE | GGAGVGKTV | FIQELINNI | AKA----- | HGGFSVFTG | VVERTREGN |
| <i>Bos taurus</i> _F-type_beta | 197 | AKGGKIGLE | GGAGVGKTV | LIMELINNV | AKA----- | HGGYSVFAGV | GERTREGN |
| Human_F-type_beta | 197 | AKGGKIGLE | GGAGVGKTV | LIMELINNV | AKA----- | HGGYSVFAGV | GERTREGN |
| | | | Homologous | Walker A | | Homologous | Walker B |

Figure 3.1 Conserved sequences on NeqA and Neq B This figure shows the sequence alignment of the conserved regions of NeqA (NEQ103) and NeqB (NEQ263) with A/V and F-type ATP synthase subunits A and B. The regions highlighted on A subunits are the Walker A and B motifs and the conserved Glu256 residue (*). The homologous Walker regions are highlighted on subunit B

3.3.2 Phylogenetic analysis

A phylogenetic analysis was performed for NeqA and NeqB to understand the evolutionary path of the *N. equitans* ATP synthase subunits. It is well known that the ATP synthase family arose from a common ancestor and subsequently diverged into the F- and V/A-types [64] [62]. Our phylogenetic analysis shows that *N. equitans* appears after the divergence of the F- and the V/A-types and belongs to the V/A family of ATP synthases (Fig.3.2b and 3.2c). *N. equitans* subunits arose early during evolution of the ATP synthases and share a common ancestor with the rest of its archaeal and prokaryotic homologs. It can be deduced from the branch lengths of NeqA and NeqB in their respective phylogenetic trees that these sequences have undergone significant evolutionary remodeling (Fig.3.2b and 3.2c). This can be an effect of the early association of *N.equitans* and *I.hospitalis* and subsequent evolution of *N.equitans* as an energetically dependent parasite, leading to loss of catalytic function of its ATP synthase [88, 112]. The absence of several subunits of the *N. equitans* ATP synthase can also be attributed to genomic loss due to parasitism, a trait seen in many obligatory bacterial endoparasites [113, 114].

a.



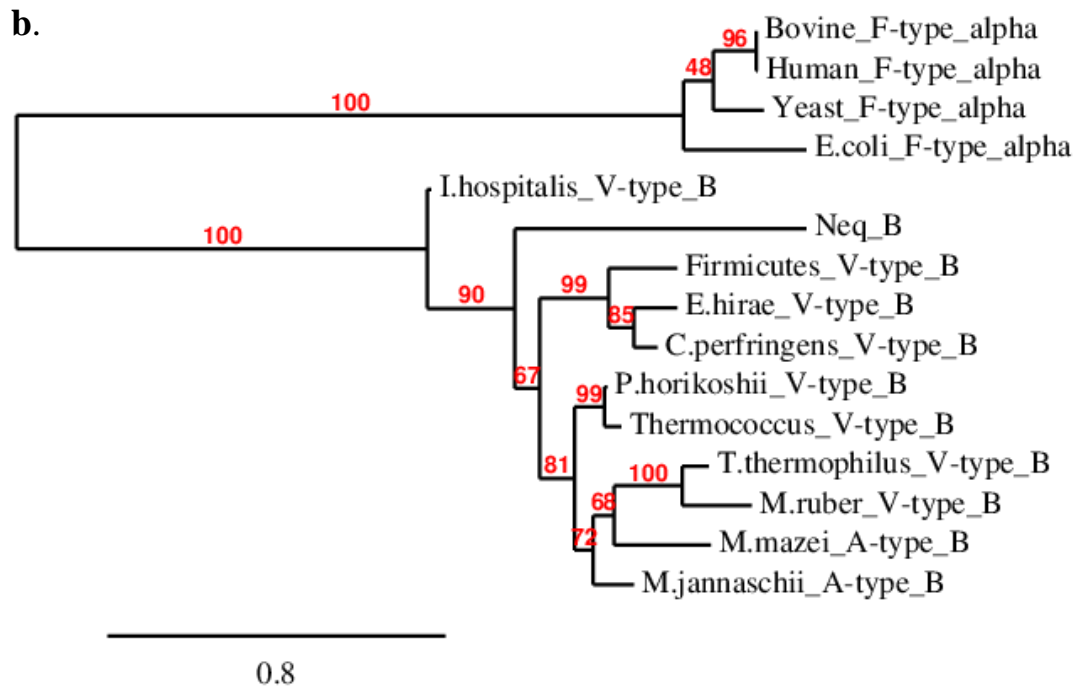


Figure 3.2 Phylogenetic analysis of NeqA and NeqB Phylogenetic tree shows the evolutionary distance between (a) NeqA and (b) NeqB and their homologs. The numbers in red indicate the confidence levels obtained from bootstrapping for that particular node.

3.3.3 Structure of the regulatory subunit NeqB

The NeqB structure was determined at 2.8 Å resolution. There are four molecules in the asymmetric unit. We did not observe electron density for the first five N-terminal residues, or for Glu50–Ile54 and Ile98–Tyr103, and hence these stretches of amino acids are not included in the model. The model was well refined with good stereo chemical parameters (Table 3.1). The structure of NeqB consists of an N-terminal β barrel (Pro6–Ile115) region, a central αβ region (Ser116–Leu327), and a C-terminal α-helical region (Ala328–Leu410) comprising three helices (Fig.3.3a and b). All four molecules in the asymmetric unit were similar (RMSD is 0.38 Å for all Cα atoms). A structural homology search with DALI revealed that NeqB bears significant structural similarity with the subunit B from the V1 complex structure of *E. hirae* (PDB 3VR3) and *T. thermophilus* (PDB 3GQB) as well as of the independent A-type subunit B from *M.mazei* (PDB 2C61) (Table 3.2). Moreover, despite of its low sequence identity (24%), NeqB was found to be equally similar to the α-subunit of mitochondrial F-type ATPase, suggesting that the NeqB subunit adopts the overall structure of the regulatory subunit B/α, even with the evolutionary distance (Table 3.2). NeqB was found to be shorter at the C-terminus by approximately 20 residues as compared with its close homologues from *T.thermophilus* and *E.hirae*. However, this did not affect the overall tertiary structural features of NeqB.

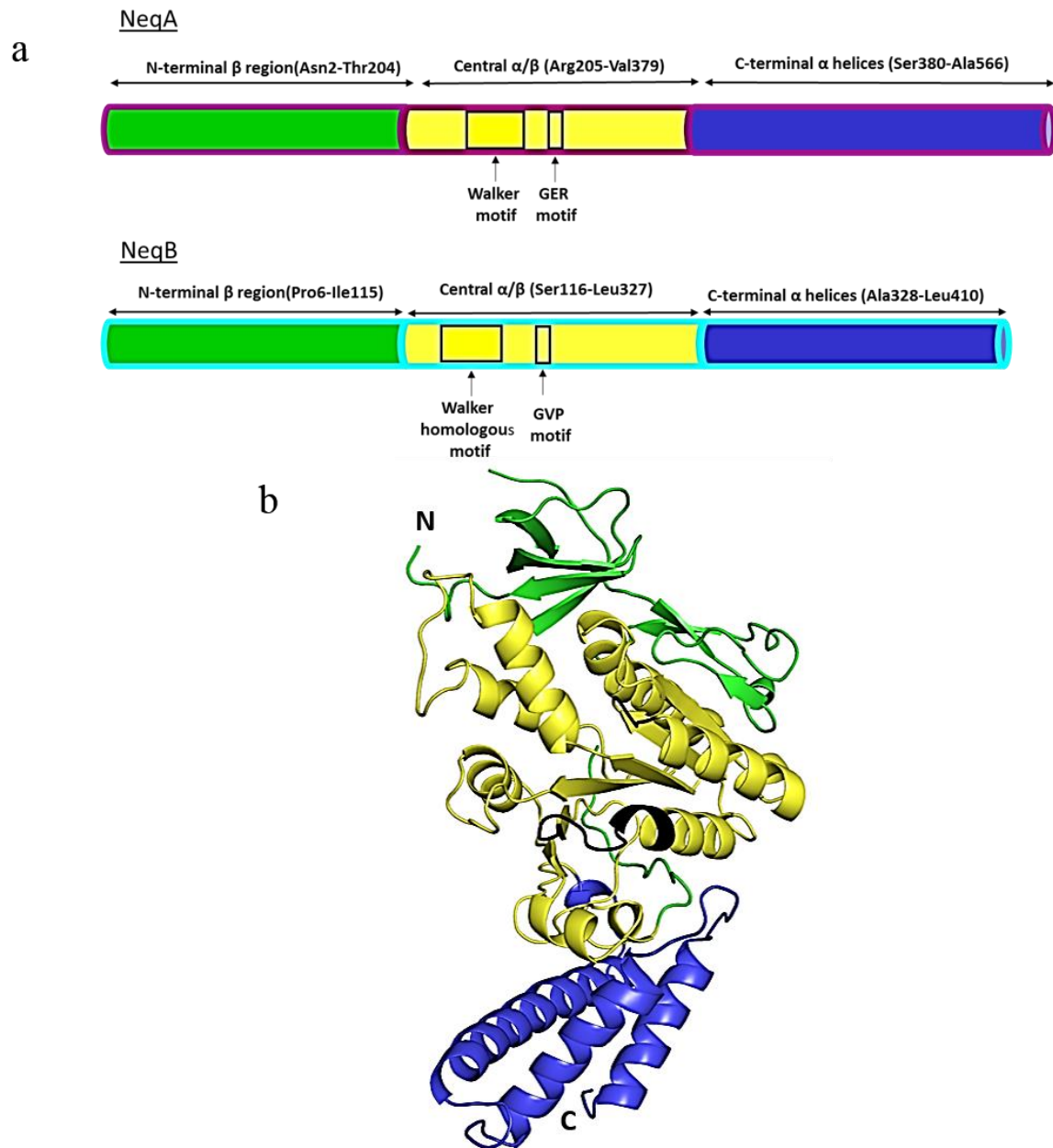


Figure 3.3. Structure of Neq subunits. a. Bar diagram representing conserved motifs on the NeqA and NeqB subunits. b. Crystal structure of NeqB (in corresponding colors). The Walker homologous and GVP motif are labelled. The N terminal and C terminals are marked for reference.

Table 3.1. Crystallographic refinement details

| | NeqB | NeqAB_apo | NeqAB_ADP | NeqAB_ANP |
|--|---|------------------------------|------------------------------|------------------------------|
| Data collection | | | | |
| Space group | P2 ₁ 2 ₁ 2 ₁ | R3 | R3 | R3 |
| Molecules in asymmetric unit | Four monomers | One heterodimer | One heterodimer | One heterodimer |
| Cell dimensions <i>a</i> , <i>b</i> , <i>c</i> (Å) | a=77.23 b=155.23 c=177.45 | a = b = 192.61 c = 108.94 | a = b = 192.46 c = 110.24 | a = b = 193.48 c = 108.85 |
| Wavelength (Å) | 0.97913 | 1.5418 | 0.97913 | 1.5418 |
| Resolution (Å) [*] | 50-2.8(2.9-2.8) | 33.0-3.0(3.05-3.0) | 50-2.0(2.03-2.0) | 50-2.63(2.68-2.63) |
| <i>R</i> _{sym} ^a | 0.10 (0.56) | 0.23(0.39) | 0.132(0.54) | 0.09(0.51) |
| <i>I</i> / σI | 23(2.0) | 5.6(2.6) | 37.12(2.87) | 22(2.8) |
| Completeness (%) | 98.3(91.8) | 96.9(87) | 99.8(98.5) | 99.8(97.3) |
| Redundancy | 13.0(8.9) | 4(2.5) | 5.5(4.5) | 5.7(4.3) |
| Refinement ^b | | | | |
| Resolution (Å) | 29.78-2.8 | 32.10-3.0 | 30.65-2.0 | 27.37-2.7 |
| <i>R</i> _{work} ^c (no. of reflections) | 0.2161(50654) | 0.2167(29083) | 0.1827(102518) | 0.2154(39977) |
| <i>R</i> _{free} ^d (no. of reflections) | 0.2568(1944) | 0.2526(2039) | 0.2067(1767) | 0.2617(2090) |
| B-factors | | | | |
| Protein (no. of atoms) | 52.95 (12003) | 43.42 (7566) | 50.64(7583) | 55.32 (7674) |
| Water (no. of atoms) | 0 | 0 | 57.635 (428) | 46.91 (325) |
| No. of nucleotide atoms | - | - | 27 | 31 |
| R.m.s deviations | | | | |
| Bond lengths (Å) | 0.009 | 0.002 | 0.010 | 0.003 |
| Bond angles (°) | 1.262 | 0.540 | 0.927 | 0.675 |
| Ramachandran plot | | | | |
| Most favored regions (%) | 93.79 | 94.11 | 96.96 | 94.98 |
| Allowed regions (%) | 4.96 | 5.57 | 2.51 | 4.71 |
| Disallowed regions (%) | 1.26 | 0.32 | 0.52 | 0.31 |

^a $R_{\text{sym}} = \sum |I_i - \langle I \rangle| / I_i$ where I_i is the intensity of the i^{th} measurement, and $\langle I \rangle$ is the mean intensity for that reflection.

^bReflections with $I > \sigma$ was used in the refinement.

^c $R_{\text{work}} = |F_{\text{obs}} - F_{\text{calc}}| / |F_{\text{obs}}|$ where F_{calc} and F_{obs} are the calculated and observed structure factor amplitudes, respectively.

^d $R_{\text{free}} =$ as for R_{work} , but for 5–7% of the total reflections chosen at random and omitted from refinement.

*The high resolution bin details are in the parentheses

Table 3.2. Comparison independent NeqB structure with its homologs

| PDB/Protein name | PDB Chain ID | Subunit | Type | Organism | Ligand | RMSD | Cα atoms | DALI Z score |
|-------------------------|---------------------|----------------|----------------|-----------------------------|---------------|-------------|-----------------------------------|---------------------|
| 2C61 | A | B | A ₁ | <i>Methanosarcina mazei</i> | None | 0.764 | 272 | 48.5 |
| 3W3A | L | B | V ₁ | <i>Thermus thermophilus</i> | None | 1.298 | 314 | 41 |
| 3W3A | M | B | V ₁ | <i>Thermus thermophilus</i> | ADP | 2.010 | 323 | 38.3 |
| 3VR3 | D | B | V ₁ | <i>Enterococcus hirae</i> | None | 1.132 | 304 | 47.4 |
| 3VR3 | E | B | V ₁ | <i>Enterococcus hirae</i> | ANP | 0.836 | 293 | 47.7 |
| 3GQB | B | B | V ₁ | <i>Thermus thermophilus</i> | None | 0.758 | 290 | 47.7 |
| 1BMF | A | α | F ₁ | <i>Bos taurus</i> | AMPPNP | 2.140 | 273 | 41 |
| NeqB_apo | B | B | V/A | <i>Nanoarcheum equitans</i> | None | 1.432 | 323 | - |
| NeqB_ADP | B | B | V/A | <i>Nanoarcheum equitans</i> | ADP | 1.466 | 326 | - |
| NeqB_ANP | B | B | V/A | <i>Nanoarcheum equitans</i> | ANP | 1.365 | 329 | - |

*Total number of amino acids in NeqB monomer is 397.

The ¹⁵⁰SASGLPHN¹⁵⁷ and ¹⁸⁴GIT¹⁸⁶ motifs of subunit B of A-type *M. mazei* are known as the P-loop consensus regions and previous crystallographic data indicates that Ser150 and Ala151 make contact with the phosphate group of the bound nucleotide [111]. The K_d for the binding between wild-type *M. mazei* subunit B and Mg-ATP was shown to be 22 μ M [111]. From our sequence alignment, we observed that the equivalent regions in NeqB are ¹³⁴SPPGLPME¹⁴¹ and the ¹⁶⁴GVP¹⁶⁶ and we found these regions to be structurally similar to that of the *M. mazei* subunit B. Using ITC, we observed a K_d of 62 μ M for NeqB interacting with Mg-ATP, which corresponds to a binding affinity three-fold lower to that of the *M. mazei* subunit B (Fig 3.4b). The K_d of NeqA with Mg-ATP under similar conditions was 5.2 μ M (Fig.3.4a). However, our attempts to briefly co-crystallize NeqB with the nucleotide did not yield any complex crystals.

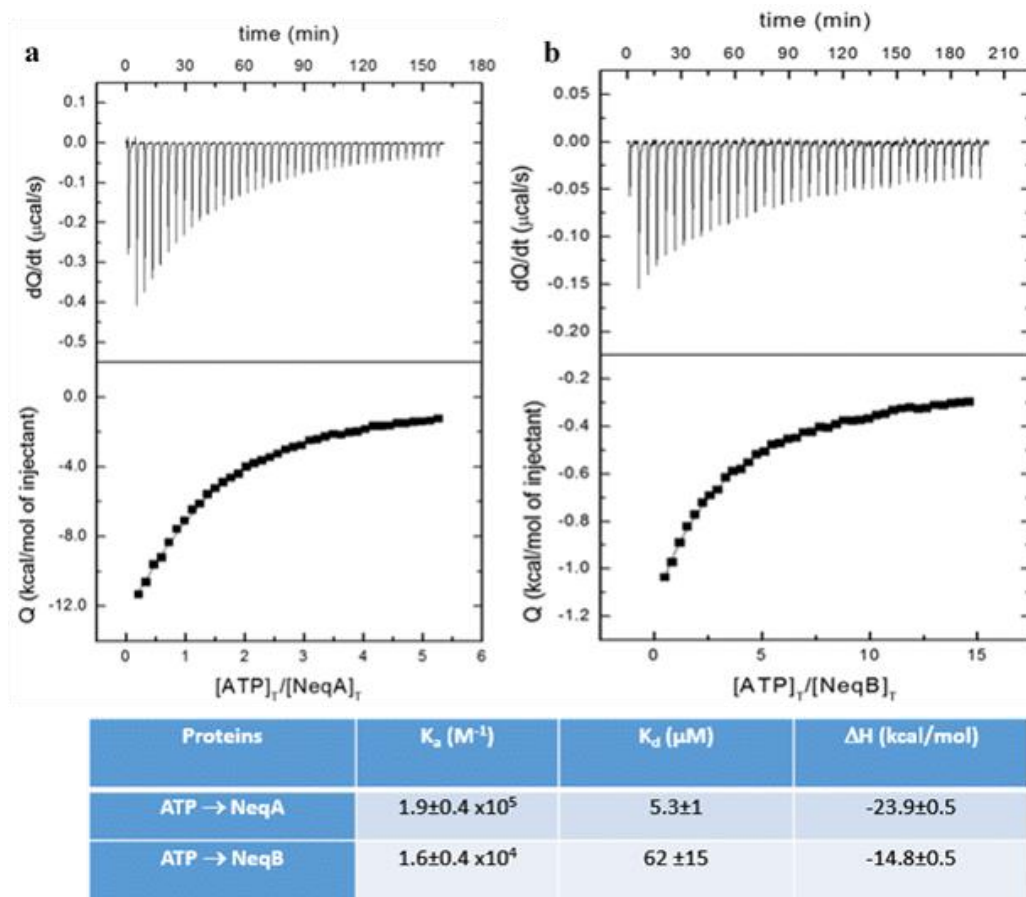


Figure 3.4 Interactions of NeqA and NeqB with nucleotides: The binding affinity of NeqA and NeqB were determined using Isothermal Titration Calorimetry (ITC) experiments. Representative ITC profiles are shown. The upper part of each panel shows the thermogram (thermal power versus time) after baseline correction and the bottom part of each panel shows the binding isotherm (normalized heat versus molar ratio of reactants for each injection). The solid lines in the bottom part of each panel show the fit of the data to a model considering a single class of binding sites. ITC profile representing (a) single site, moderate affinity, 1:1 binding between Mg-ATP (300 μM) and NeqA (10 μM). The c-value is 1.9. (b) single site, low affinity, 1:1 binding between Mg-ATP (1 mM) and NeqB (10 μM). The c-value is 0.16. The table below shows the thermodynamic parameters obtained for above experiments.

Further, we studied the interactions between the NeqA and the NeqB subunits through pull-down assays, Native-PAGE, analytical ultracentrifugation (AUC) and ITC experiments. We had seen in chapter 2 that NeqAB elutes as a possible hexamer (Fig 2.3). The results from each assay clearly indicated complex formation between NeqA and NeqB (Fig. 3.5). Moreover, it was seen that the

interaction between NeqA and NeqB is strengthened (100-fold decrease in the complex dissociation constant) in the presence of ADP as shown by the ITC data (Fig.3.6b). Mg-ADP pre-bound to the subunits promotes a stronger interaction by slightly accommodating the subunits into a high-affinity conformation and lowering an energetic penalty of entropic nature (3 kcal/mol, approximately), since the binding enthalpy for NeqA interacting with NeqB is hardly affected by the presence of Mg-ADP.

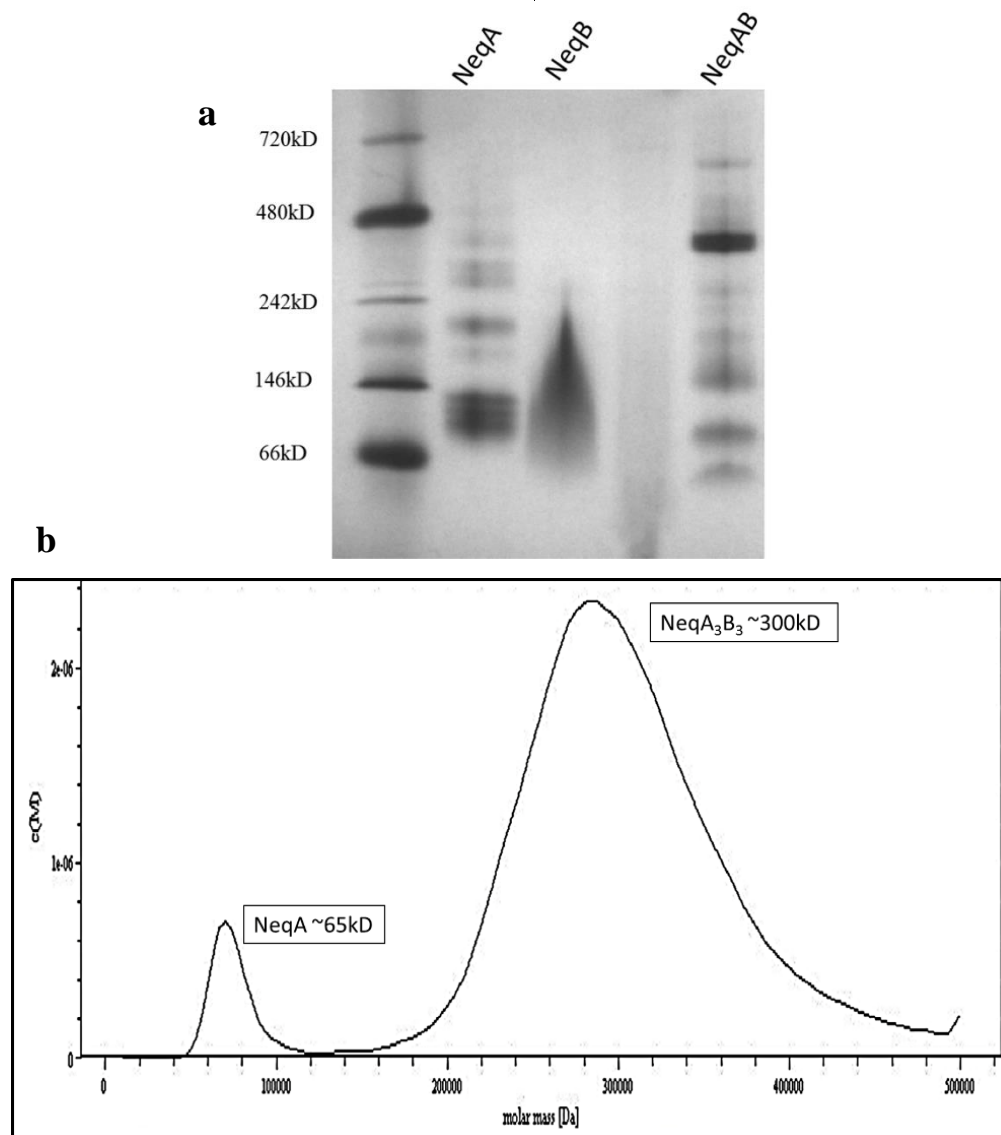


Figure 3.5. Oligomeric states of NeqA and NeqB: (a) NeqAB complex was compared with monomeric NeqA and NeqB using Blue Native gel to show formation of a ~300 kD hexamer in case of NeqAB (b) Analytical ultracentrifugation experiments to show the interactions between NeqA and

NeqB subunits and the formation of the hexameric core (A_3B_3) hexamer (~350kD)

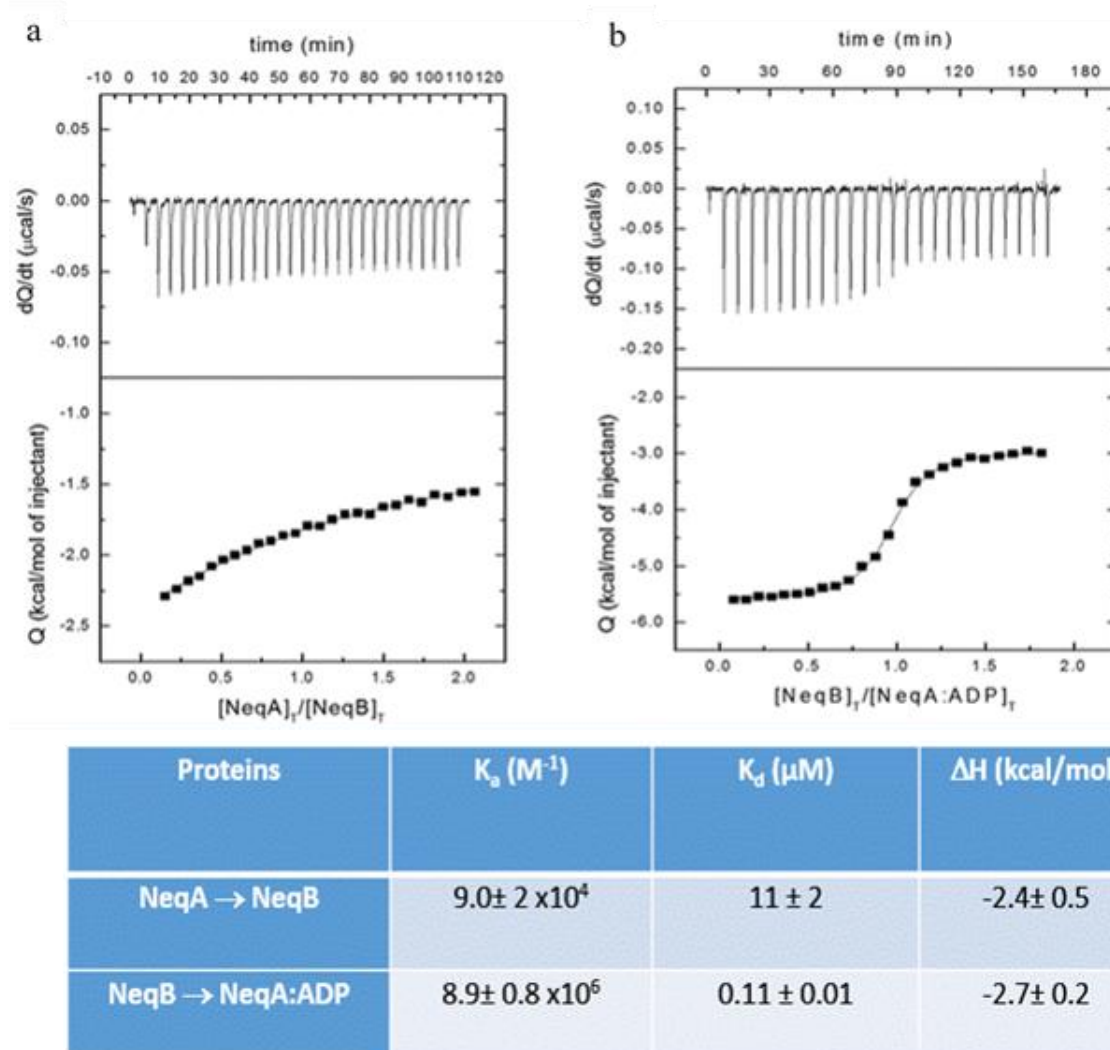


Figure 3.6. Interactions between NeqA and NeqB Calorimetric titrations corresponding to the interaction between NeqA and NeqB (a) in the absence of nucleotide (100 μM NeqA titrated into 10 μM NeqB). The c -value is 0.9 (b) in the presence of nucleotide (Mg-ADP) (100 μM NeqB titrated into 10 μM NeqA). The c -value is 89. An increase in binding affinity between NeqA and NeqB is observed due to the presence of nucleotide Mg-ADP (100-fold decrease in K_d), as indicated by the sigmoidal profile for the nucleotide-bound NeqA.

3.3.4 Structure of nucleotide-free NeqAB complex

Next, we solved the structure of the hexameric core complex of the Neq ATP synthase to gain a better understanding of its catalytic mechanism. The

nucleotide-free form of the NeqAB complex was determined at 3.0 Å (Table 3.1). The asymmetric unit consisted of a single NeqAB heterodimer.

NeqA in the NeqAB complex comprised an N-terminal β -barrel region (Asn2-Thr204) followed by the central $\alpha\beta$ region (Arg205-Val379) consisting of the P-loop and α helical C-terminal region (Ser380-Ala566) of six helices (Fig.3.3a and 3.8). A DALI structural homology search showed that NeqA resembled the subunit A of *T. thermophilus* and *E.hirae* V₁ ATPase (Table 3.3). Moreover, the NeqA β -barrel region (Asp109-Tyr179) appears as a peripheral bulge, compared to the β -subunit of bovine mitochondrial F₁ ATP synthase (PDB 1BMF) (Fig. 3.7); this bulge region and a part of the C-terminal α -helical region (Asp492-Ala566) of NeqA did not superimpose well. These features are characteristic signatures in V/A-types and structurally distinct from the F-types [92, 115]. We observed a sulphate ion in the nucleotide binding site of NeqA and it also interacts with Arg326 of NeqB. Previously, sulphate ion was reported in *P. horikoshii* subunit A, in which the P-loop region interacts with the sulphate ion [116] consistent with our observation in NeqA. The comparison of the *P. horikoshii* subunit A structures with (PDB 3I72) and without the sulphate ion (PDB 1VDZ) shows no significant conformational changes (Table 3.3).

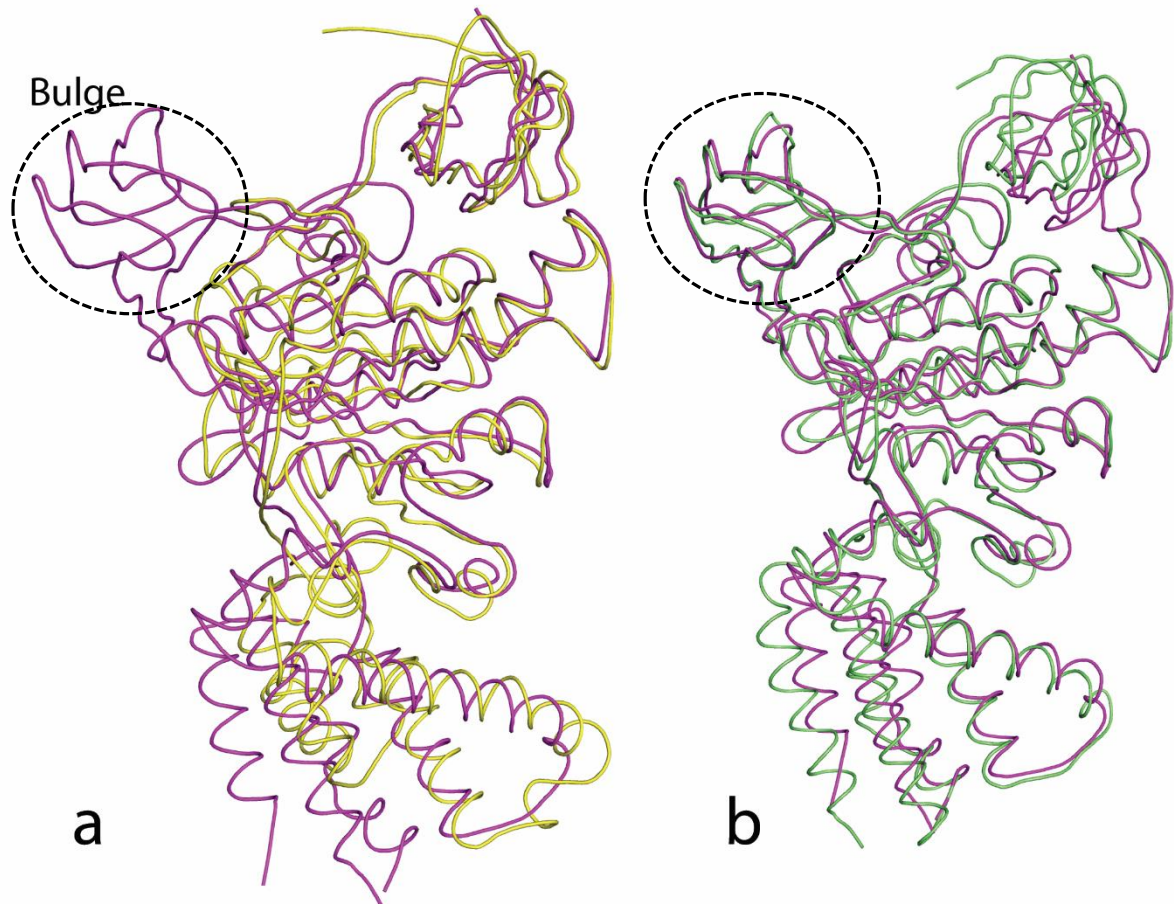


Fig 3.7. $C\alpha$ trace representation of bulge region on NeqA NeqA (magenta) overlaid with (a) F-type beta (yellow) and (b) V-type A subunit (green) shows the “bulge” region which is typical of the V/A-type ATPase subunit A. The bulge region is demarcated in dotted circles in both the structures.

The overall structure of NeqA resembles NeqB, despite the low sequence identity (RMSD is 2.252 Å for 276 $C\alpha$ atoms; sequence identity 30%) (Fig.3.8).

This is consistent with the previous suggestions that the catalytic A and the regulatory B subunits are from a common ancestor through a gene duplication event [64].

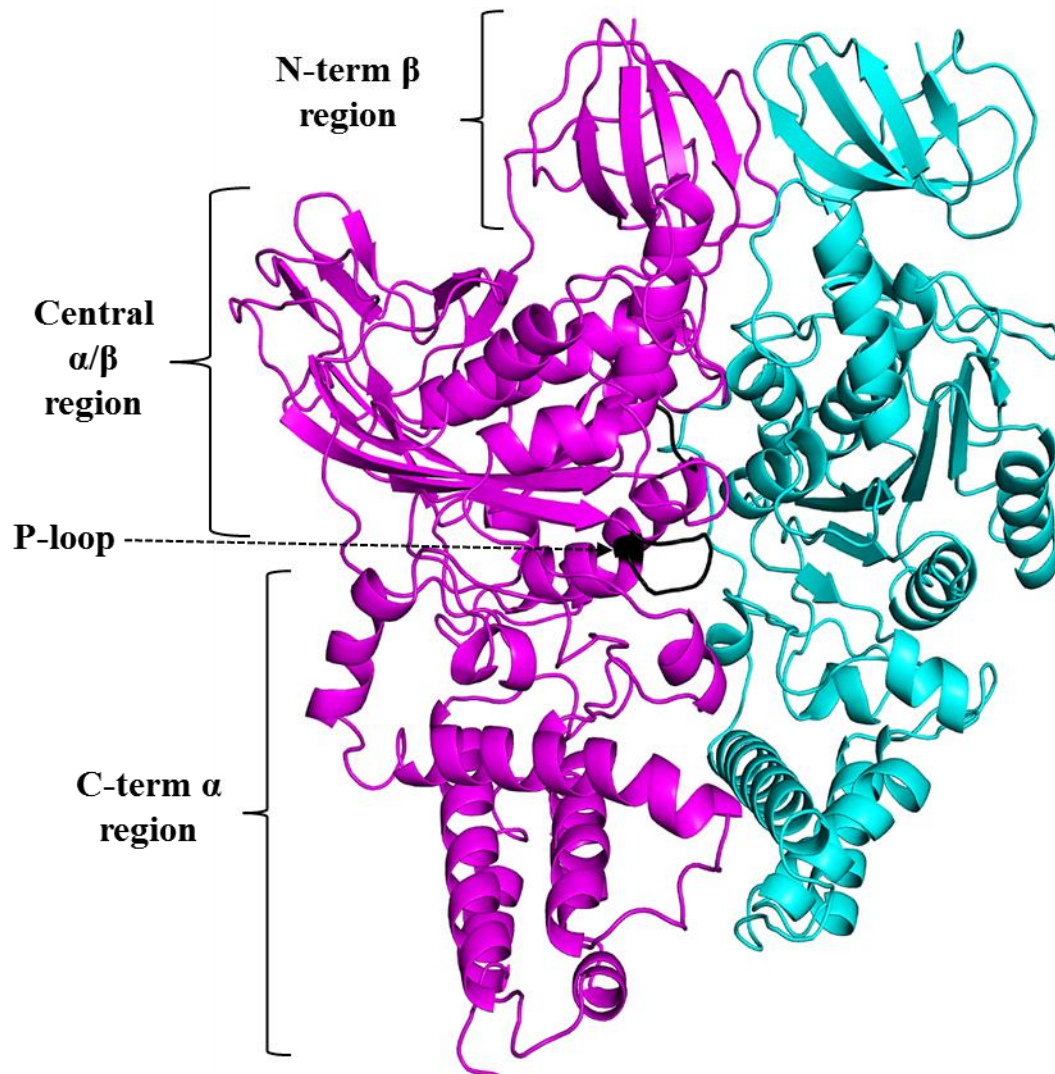


Fig 3.8. Structure of *NeqAB* dimer This figure shows the structure of nucleotide free or native *NeqAB*. *NeqA* is in magenta and *NeqB* is in cyan. The three main secondary structural regions are labelled. The P loop or the nucleotide binding loop on *NeqA* is denoted in black. The structural similarities between *NeqA* and *NeqB* can be seen in this figure.

Table 3.3. Comparison of NeqA with its homologs

| PDB | PDB Chain ID | Subunit | Type | Organism | Ligand | RMSD | Cα atoms | DALI Z score |
|----------------|---------------------|----------------|----------------|------------------------------|-----------------|-------------|-----------------------------------|---------------------|
| *NeqA_AMNP-PNP | A | A | V/A | <i>Nanoarcheum equitans</i> | AMP-PNP | 0.429 | 563 | - |
| *NeqA_ADP | A | A | V/A | <i>Nanoarcheum equitans</i> | ADP | 0.468 | 562 | - |
| 3VR3 | B | A | V ₁ | <i>Enterococcus hirae</i> | AMP-PNP | 0.966 | 473 | 47.6 |
| 3GQB | A | A | V ₁ | <i>Thermus thermophilus</i> | None | 1.761 | 452 | 46.9 |
| 3VR3 | A | A | V ₁ | <i>Enterococcus hirae</i> | None | 1.787 | 457 | 44.7 |
| 3W3A | J | A | V ₁ | <i>Thermus thermophilus</i> | None | 1.711 | 456 | 42.3 |
| 3W3A | I | A | V ₁ | <i>Thermus thermophilus</i> | ADP | 1.714 | 497 | 40.2 |
| 1VDZ | A | A | A ₁ | <i>Pyrococcus horikoshii</i> | None | 1.713 | 382 | 40.1 |
| 3W3A | K | A | V ₁ | <i>Thermus thermophilus</i> | ADP | 1.669 | 504 | 40.1 |
| 3I72 | A | A | A ₁ | <i>Pyrococcus horikoshii</i> | SO ₄ | 1.714 | 383 | 40 |
| 3I73 | A | A | A ₁ | <i>Pyrococcus horikoshii</i> | ADP | 1.702 | 380 | 39.8 |
| 3I4L | A | A | A ₁ | <i>Pyrococcus horikoshii</i> | AMP-PNP | 1.676 | 381 | 39.6 |
| 1BMF | D | β | F ₁ | <i>Bos taurus</i> | ADP | 2.080 | 313 | 32.1 |
| 1BMF | F | β | F ₁ | <i>Bos taurus</i> | AMP-PNP | 2.148 | 314 | 32.1 |
| 1BMF | E | β | F ₁ | <i>Bos taurus</i> | None | 3.285 | 328 | 30.1 |

Total number of C α atoms for NeqA_apo are 563 atoms. *NeqA from the NeqAB apo structure was compared with NeqA from the AB_ADP and AB_AMPPNP bound structures. †DALI Z scores have been calculated using chain A from NeqAB_apo model

The nucleotide-free NeqAB heterodimer was superimposed with nucleotide-bound and nucleotide-free AB heterodimers from V-type *E.hirae* and *T. thermophilus* ATPase (Table 3.5). In the homologue nucleotide-free structures, hydrophobic interactions were observed mostly at the N-terminal region, which left the C-terminal regions of the A and B subunits wide apart in an “open” conformation; a “closed” conformation occurs upon binding of a nucleotide in a pocket formed at the interface of A and B subunits [104]. Superimposition of the NeqAB structure, however, showed that the nucleotide-free NeqAB heterodimer was most similar to the nucleotide-bound rather than nucleotide-free forms of these homologous V-type complexes in a more closed conformation (Fig.3.13, Table.3.5). Furthermore, unlike its homologs, the NeqA and NeqB interface comprised 26 hydrogen bonding contacts and several hydrophobic interactions. The interface area between NeqA and NeqB was determined to be 2768 Å², which is higher than that of the nucleotide-free form of the AB dimers of *E. hirae* (2380 Å²; PDB 3VR3) and *T. thermophilus* (2340Å²; PDB 3W3A) [104].

Table 3.4. Comparison of NeqAB_native with its nucleotide free and nucleotide bound homologs from V₁/F₁ complexes

| PDB code | PDB Chain ID | Complex | Type | Organism | Ligand | State | RMSD (Å) | C α -atoms aligned | Ref |
|----------|--------------|-------------------------------|--------|-----------------------|---------|--------|----------|---------------------------|-------|
| 3W3A | J,L | V ₁ | V-type | <i>T.thermophilus</i> | Empty | Open | 3.705 | 888 | [104] |
| 3W3A | I,N | V ₁ | V-type | <i>T.thermophilus</i> | ADP | Closed | 1.727 | 870 | [104] |
| 3W3A | K,M | V ₁ | V-type | <i>T.thermophilus</i> | ADP | Closed | 1.680 | 856 | [104] |
| 3VR3 | A,D | V ₁ | V-type | <i>E.hirae</i> | Empty | Open | 2.832 | 790 | [35] |
| 3VR3 | B,E | V ₁ | V-type | <i>E.hirae</i> | AMP-PNP | Closed | 1.302 | 813 | [35] |
| 3VR3 | C,F | V ₁ | V-type | <i>E.hirae</i> | AMP-PNP | Closed | 1.213 | 802 | [35] |
| 3GQB | A,B | A ₃ B ₃ | V-type | <i>T.thermophilus</i> | Empty | Open | 2.263 | 768 | [92] |
| 1BMF | A,E | F ₁ | F-type | <i>Bos taurus</i> | Empty | Open | 2.26 | 664 | [30] |
| 1BMF | B,F | F ₁ | F-type | <i>Bos taurus</i> | AMP-PNP | Closed | 2.22 | 709 | [30] |
| 1BMF | C,D | F ₁ | F-type | <i>Bos taurus</i> | ADP | Closed | 2.15 | 766 | [30] |

*Superimposition of NeqAB_apo with NeqAB_ADP and NeqAB_AMPPNP shows high similarity. Total number of C α atoms of NeqAB_apo is 967.

Superimposition of the independent NeqB and NeqB from native NeqAB complex (RMSD of 1.319 Å for all C α atoms) showed subtle differences at the N-terminal region (Fig.3.9). A similar N-terminal conformational difference was observed between NeqB and its homologous B subunit from V1 complexes from *T. thermophilus* and *E. hirae* (Fig 3.10b). On the other hand, the N-terminal conformation of NeqB and the independent *M. mazei* A-type subunit B were similar (Fig 3.10a). This result suggests that the N-terminus of NeqB becomes more ordered upon binding with NeqA. This is further supported by the observation that there are 28 hydrogen bonding contacts between N-terminal regions of NeqA and NeqB.

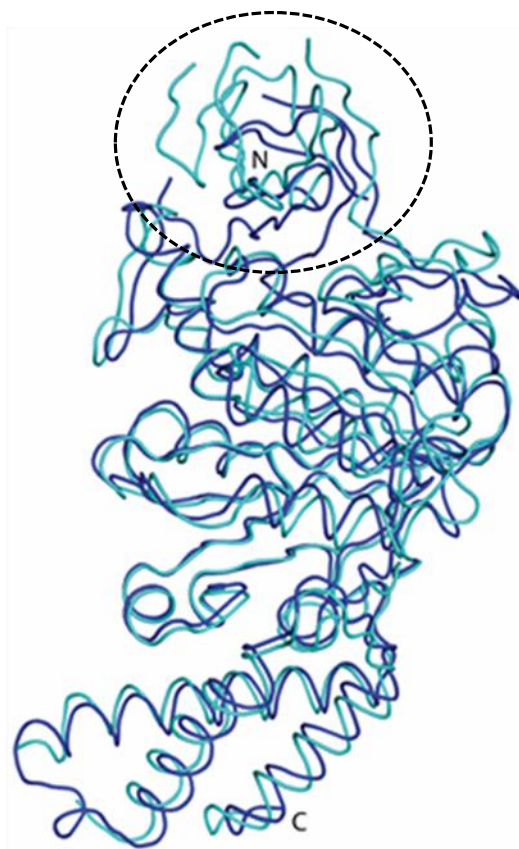


Figure 3.9. Superimposition of NeqB subunits C α trace representation of superimposition of NeqB (cyan) from native NeqAB complex and independent NeqB (blue) showing the conformational differences in the N terminal regions (marked by the dotted circle). The N and C terminals are labelled for reference.

Overall, NeqB, NeqA and the NeqAB complex possess all of the important, conserved structural features of a V/A-type ATP synthase, consistent with our sequence analysis.

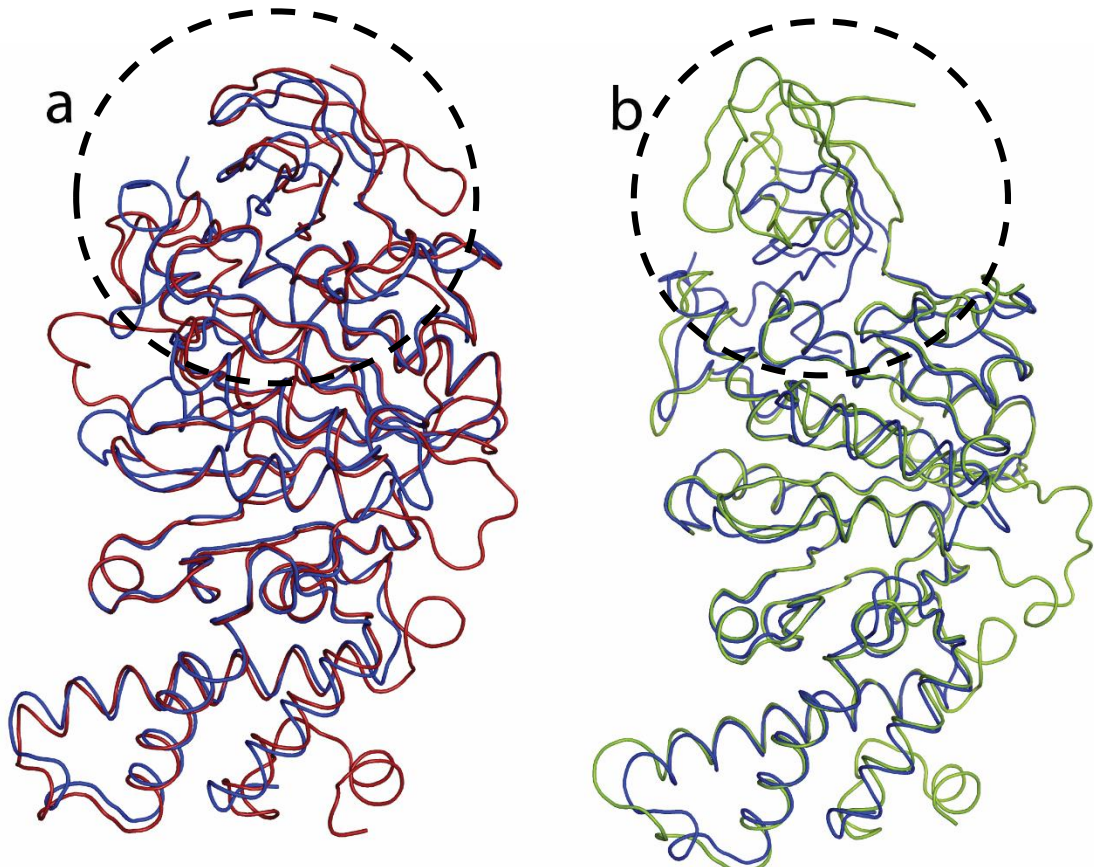


Fig 3.10. Superimposition of Ca trace representation of independent NeqB (marine blue) with homologs such as (a) independent *M.mazei* subunit B (2C61)(dark red) (b) subunit B from *T.thermophilus* V1 complex (3GQB)(green) showing the conformational change taking place in the N terminal due to binding of subunit A (shown in the dotted black circles).

3.3.5 Structure of nucleotide-bound NeqAB complex

We next solved the structures of the ADP- and the AMP-PNP- (a non-hydrolysable analogue of ATP) bound NeqAB complexes and refined them up to 2.0 Å and 2.7 Å, respectively. In both complexes, the asymmetric unit consisted of a NeqAB heterodimer, similar to that observed in the nucleotide-free structure.

Our structures showed that the nucleotide binding pocket is located at the interface of the NeqAB heterodimer mainly composed of residues from NeqA (Fig 3.12). This pocket formed between the central α/β region of NeqA (encompassing the Walker A and Walker B (²⁵¹GER²⁵³ loop) motifs) and a Ser260–Gly330 stretch, including the conserved Arg326, from NeqB (Fig.3.12a and b). In the ADP complex, there were 21 hydrogen bonding contacts (<3.4 Å) between NeqAB and the ADP, in which 16 of them form with NeqA (Table 3.6): the phosphate groups interacted with Gly226, Gly228, Lys229, Thr230 and Val231 from the Walker A motif whereas the adenine head group made contact with Gln491 and Ala493 of NeqA (Fig.3.12a). Arg326 from NeqB made five hydrogen bonding contacts (<3.4 Å) with the β phosphate of ADP. Superimposition of the ADP-bound NeqAB and V₁-ATPase from *T. thermophilus* (PDB 3W3A) showed similarity between them (RMSD, 1.727 Å for 870 Ca atoms) as well as similar nucleotide binding positions. In the ADP-bound NeqAB, the interface area is 2729 Å², which is similar to the interface area calculated for the nucleotide-free NeqAB structure [104].

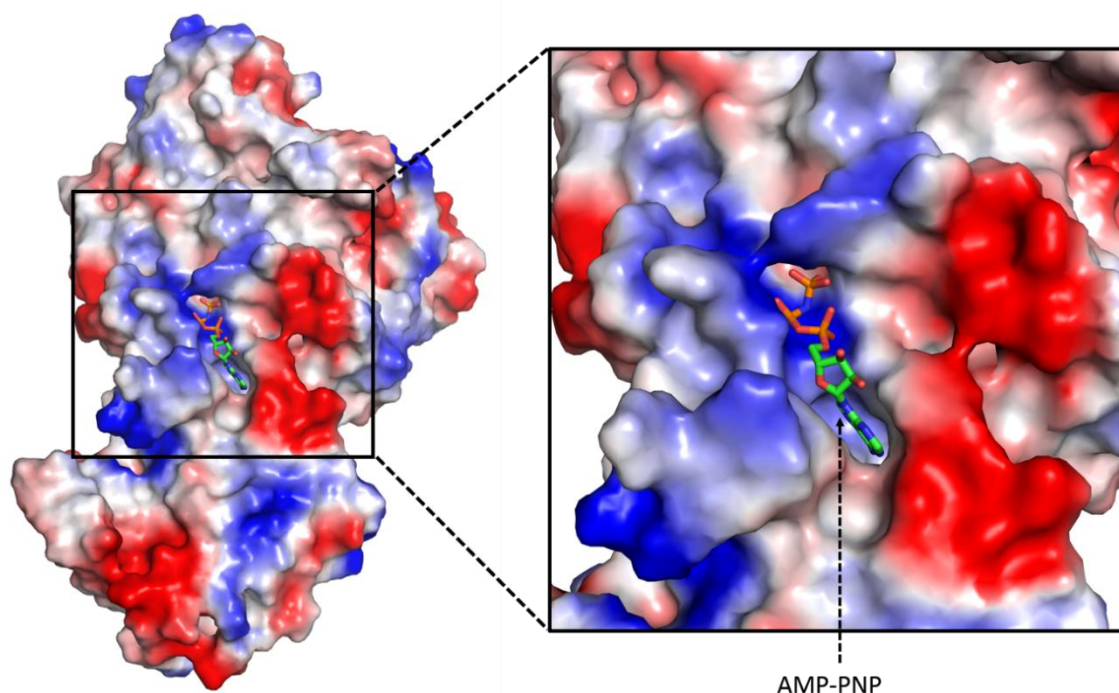


Figure 3.11. Surface representation of nucleotide binding pocket on NeqA. NeqA is represented in electrostatic surface representation and AMP-PNP is shown in the stick representation. The inset shows the orientation of AMP-PNP on the surface of NeqA. For clarity, we did not show the NeqB for this figure.

In the AMP-PNP-bound complex, 26 hydrogen bonding contacts ($<3.4 \text{ \AA}$) were observed between AMP-PNP (ANP) ligand and NeqA and NeqB out of which 21 were with NeqA (Table 3.7). The phosphate groups of the AMP-PNP were in contact with the P-loop residues (Gly226-Val231) of NeqA, with two additional contacts made between the Arg253 of the $^{251}\text{GER}^{253}$ loop and Glu256 of NeqA with the γ -phosphate of the ANP moiety (Fig.3.12b). This shows tight binding of NeqA with nucleotide which is confirmed by our ITC data (Fig.3.4.a). However, interestingly, the buried area between NeqA and NeqB with AMP-PNP was 286 \AA^2 less than that observed for the ADP-bound complex. This difference might be due to the tighter packing in the presence of ADP.

In *T. thermophilus*, the ADP-bound form of the V1 ATPase is an inhibitory state to avoid unnecessary hydrolysis of ATP upon the loss of proton transport [117-119]. The asymmetric state in the crystal structure of *T. thermophilus* at 3.9 Å demonstrated two distinct conformations of the AB complex in the presence of a nucleotide: one “intermediate” and one “tight” [104]. It has been suggested that the compactness of the nucleotide binding pocket in the “tight” form is one of the factors contributing to the molecular mechanism of ADP inhibition [117]. We analysed the buried area between the A and B subunits of *T. thermophilus* in these two states and we found that the “tight” form has a higher buried area of approximately 200 Å². After superimposing all of the C α atoms of the ADP-bound NeqAB complex with these tight and intermediate forms, we found that the NeqAB-ADP complex was marginally more similar to the tight form (RMSD: 1.6 Å for 849 C α atoms) than the intermediate form (RMSD: 1.65 Å for 860 C α atoms), and we therefore speculate that the ADP-bound NeqAB complex possibly represents the inhibited form of the AB core complex.

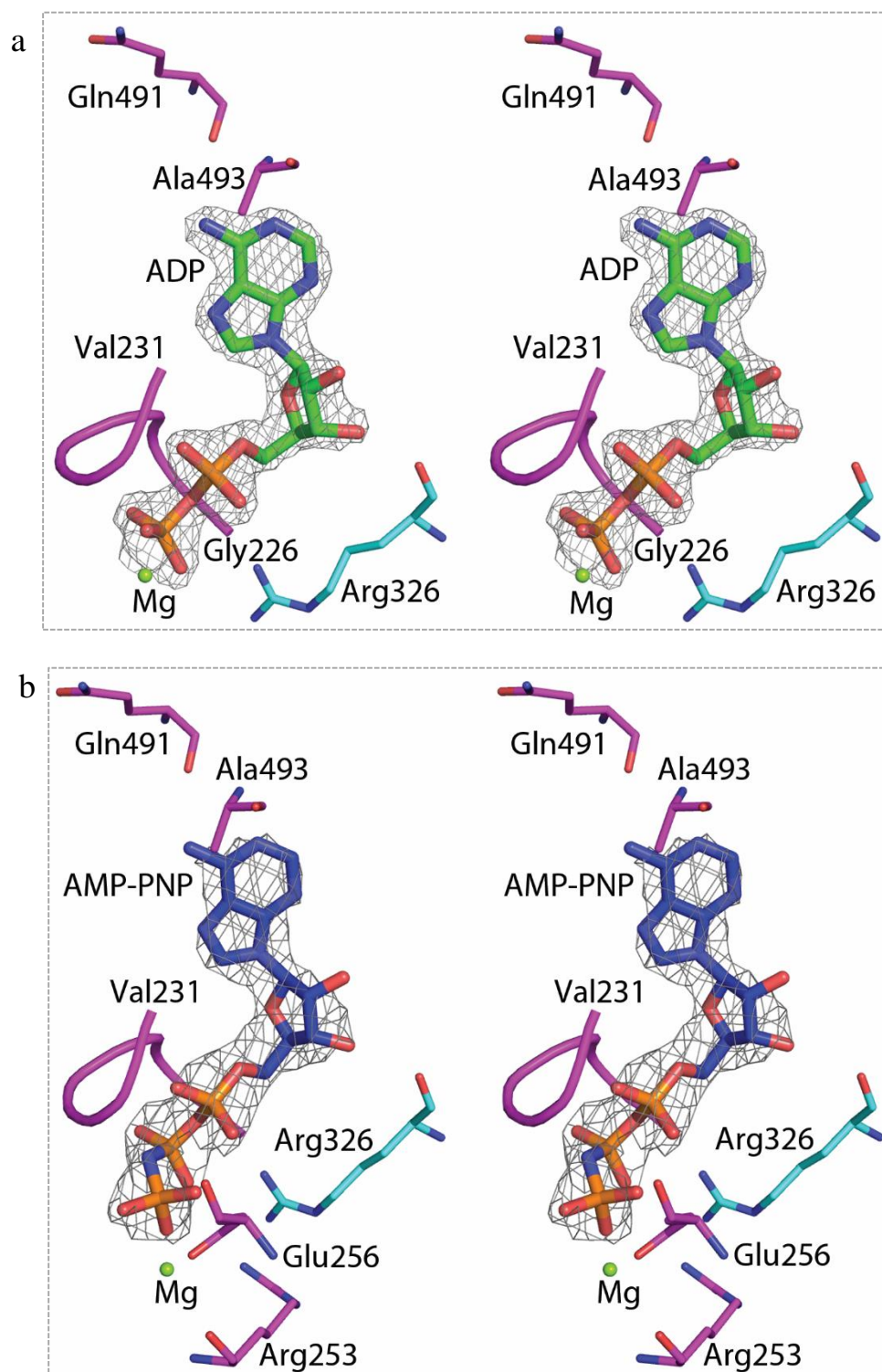


Figure 3.12. Interacting residues of the NeqA and NeqB with nucleotides. The P-loop motif residues of NeqA interacting with ligand are shown in cartoon loop representation; the side chains of interacting residues from NeqA and NeqB and the ligands, ADP (green) and AMPPNP (blue) are in stick representation. (a) Shows the side chains of NeqA and NeqB interacting with Mg-ADP. (b) Shows the side chains of NeqA and NeqB interacting with Mg-AMPPNP. The final electron density map ($2F_o - F_c$ map, contoured at 1.0σ) is shown for both ADP and AMPPNP.

Table 3.5. Hydrogen bonding contacts between ADP and NeqAB (<3.4Å)

| Subunit | Residue (atom) | Ligand (atom) | Bond length (Å ²) |
|---------|----------------|---------------|-------------------------------|
| A | Thr230(N) | ADP(O1B) | 3.00 |
| A | Thr230(OG1) | ADP(O1B) | 2.93 |
| A | Lys229(N) | ADP(O2B) | 2.85 |
| A | Lys229(NZ) | ADP(O2B) | 2.73 |
| A | Ser227(N) | ADP(O2B) | 3.33 |
| A | Gly228(N) | ADP(O2B) | 2.80 |
| A | Gly226(N) | ADP(O3B) | 2.75 |
| A | Gly226(N) | ADP(O1A) | 3.28 |
| A | Gly228(N) | ADP(O1A) | 3.17 |
| A | Thr230(N) | ADP(O1A) | 3.07 |
| A | Val231(N) | ADP(O1A) | 2.68 |
| A | Gly228(N) | ADP(O3A) | 3.07 |
| A | Gln491(O) | ADP(N6) | 3.12 |
| A | Ala493(N) | ADP(N1) | 2.93 |
| B | Arg326(NH1) | ADP(O3B) | 2.78 |
| B | Arg326(NH2) | ADP(O3B) | 3.26 |
| B | Arg326(NH1) | ADP(O2A) | 2.98 |
| B | Arg326(NH1) | ADP(O3A) | 3.37 |
| B | Arg326(O) | ADP(O3A) | 3.32 |

Overall, the ADP- and AMP-PNP-bound forms were highly similar (RMSD of 0.278Å for 870 C α atoms) and superimposition of the nucleotide-bound and nucleotide-free forms did not show any conformational changes (Table 3.5). In the recently reported *E. hirae* A₃B₃ complex structure with AMP-PNP (PDB: 3VR3), three AB heterodimers were present in the asymmetric unit, two of which were in an AMP-PNP-bound (closed) state but the third in an open or unbound state [35]. Similar open/closed differences have been shown for *T. thermophilus*, as described above [104]. These closed and open forms have also been observed in the bovine mitochondrial F₁-ATP synthase [30] as well as other V-type ATPases from *T. thermophilus* [73]. Furthermore, transition states of ADP capture have been shown for *M. mazei* subunit B, indicating this C-terminal entry route for the nucleotide [111, 120, 121] and the nucleotide binding-induced conformational change required for its catalytic mechanism [35, 104]. However, in our NeqAB complexes, we do not observe any conformational transitions as a result of from nucleotide binding (Fig.3.13). The transition from an “open” to a “closed” state has been shown to be the basis of the “binding change” mechanism of catalysis of the F-type ATP synthase, where the AB dimers have different binding affinities for the nucleotide.

Table 3.6. Hydrogen bonding contacts between AMPPNP (ANP) and NeqAB (<3.4Å)

| Subunit | Residue (atom) | Ligand (atom) | Bond length (Å ²) |
|---------|----------------|---------------|-------------------------------|
| A | Thr230 (OG1) | ANP(PG) | 3.02 |
| A | Asp320 (OD1) | ANP (O2G) | 3.31 |
| A | Thr230 (OG1) | ANP(O3G) | 2.96 |
| A | Arg253 (NH1) | ANP(O3G) | 3.16 |
| A | Glu256 (OE2) | ANP(O3G) | 3.03 |
| A | Glu256 (OE2) | ANP(O3G) | 3.03 |
| A | Gly226 (N) | ANP (O1B) | 2.61 |
| A | Lys229 (N) | ANP(O2B) | 2.85 |
| A | Ser227 (N) | ANP(O2B) | 3.02 |
| A | Lys229 (OG) | ANP(O2B) | 2.88 |
| A | Ser227 (N) | ANP(O2B) | 3.14 |
| A | Gly228 (N) | ANP(O2B) | 2.70 |
| A | Lys229 (N) | ANP(N3B) | 3.39 |
| A | Thr230 (N) | ANP(N3B) | 3.05 |
| A | Lys229 (N) | ANP(O1A) | 3.22 |
| A | Thr230 (N) | ANP(O1A) | 2.87 |
| A | Val231 (N) | ANP(O1A) | 3.04 |
| A | Gly228 (N) | ANP(O3A) | 3.07 |
| A | Gln491 (O) | ANP(N6) | 2.84 |
| A | Ala493 (N) | ANP(N6) | 3.39 |
| A | Ala493 (N) | ANP (N1) | 2.99 |
| B | Arg326 (NH1) | ANP(O1B) | 3.13 |
| B | Arg326 (NH2) | ANP(O1B) | 3.31 |
| B | Arg326 (NH1) | ANP(PA) | 3.35 |
| B | Arg326 (NH1) | ANP(O2A) | 2.62 |
| B | Arg326 (NH1) | ANP(O3A) | 3.17 |

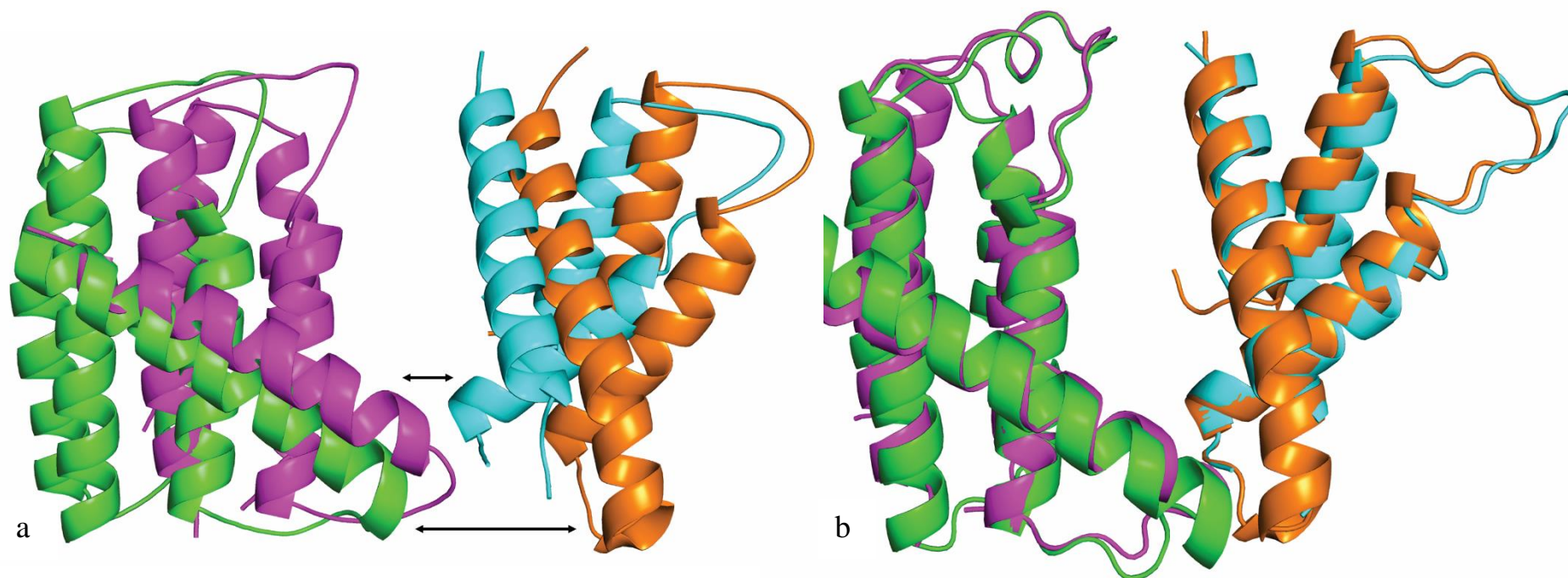


Figure 3.13. Cartoon representation of “closed” conformation of NeqAB complexes: The nucleotide free NeqAB complex was overlaid with (a) open or nucleotide free form and (b) nucleotide bound form of asymmetric AB dimers from *T.thermophilus* V1 complex. This shows the lack of displacement between the C-terminal helices of NeqA and NeqB. The displacement of the helices is indicated by black arrows. This figure shows only the C-terminal regions of the structures compared.

3.3.6 Structure of hexameric ring of NeqAB complexes (A_3B_3) and comparison with homologues

Our gel filtration, AUC and Native PAGE data indicate that the NeqAB complex forms a hexamer (Fig.2.3, Fig3.6). The hexameric ring of NeqAB complex (A_3B_3) was generated using symmetry-related molecules and this was compared with the homologous structures of several nucleotide-free and nucleotide-bound hexamers (A_3B_3). Most of the well-characterized F_1 and V_1 complexes have an A_3B_3 hexamer in their structural asymmetric states in one asymmetric unit of the crystal, which enables direct visualization of the entire A_3B_3 core complex and the central cavity. We also generated hexamers using symmetry-related AB dimers for selected ATP synthase crystal structures that do not have a hexamer in the asymmetric unit, similar to that of our case [71, 122, 123]. We then compared the central cavities in all of these cases. We found that the central cavity of the nucleotide free NeqAB complex was cylindrical while the nucleotide bound structures appeared to be tapered and closed at the bottom of the hexameric ring (Fig.3.14). In the NeqAB nucleotide complex, our analysis showed that the tapering of the cavity was caused by the second α -helix (Asp440-Ser463) of NeqA and first α -helix of NeqB (residues Lys334-Ala355) in the C-terminal region running transversely toward the centre of the cylinder, hence occluding the opening.

Following this, we identified the NeqAB complex (A_3B_3) “closed cavity” feature in F_1 ATPase from rat liver (PDB: 1MAB, 2F43) and spinach chloroplast F_1 ATPase (PDB: 1FX0). These structures were bound with nucleotides or had subunits of the central stalk, and the β -subunits adopted a “closed conformation”. Based on our analysis of these symmetric and asymmetric structures, it can be proposed that the “closed cavity” conformation either depends on the presence of the central stalk or the nucleotide.

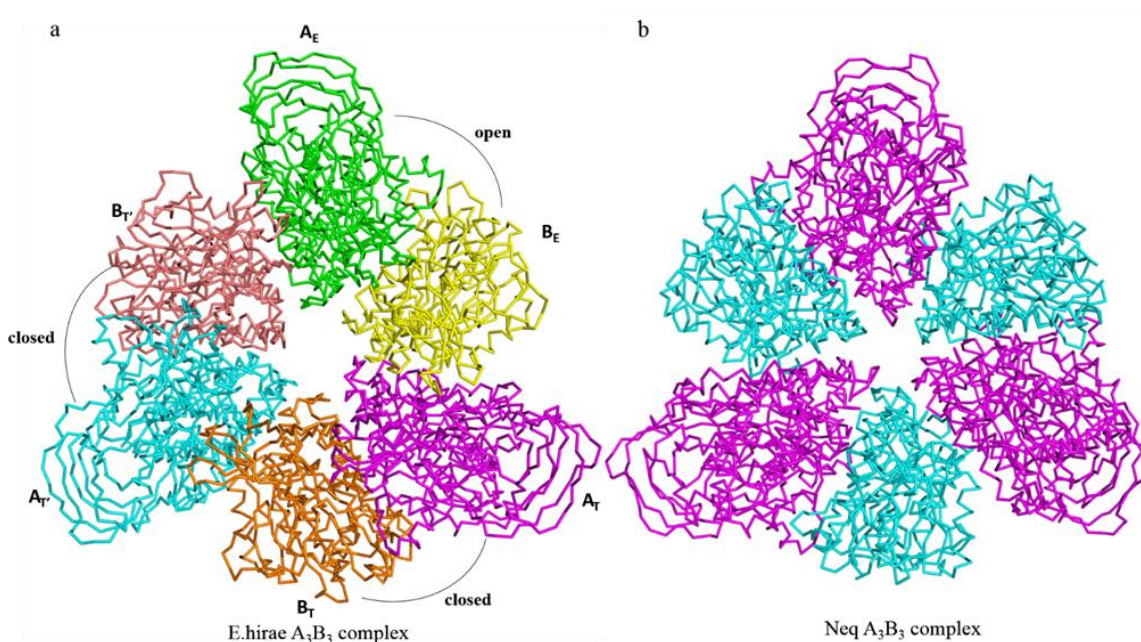


Figure 3.14. Comparison of hexameric core complex (A_3B_3 hexamer) These figures show the ribbon representation of NeqAB hexameric core complex (A_3B_3) generated using the symmetry related molecules displaying a top-down view of the central cavity. (a) the top view of the central cavity of *E. hirae* A_3B_3 hexamer (b) the top view of the central cavity of NeqAB_AMP-PNP complex.

Table 3.7. Comparison of Neq A₃B₃ (hexamer) with its homologs

| PDB code | Organism | State | Asymmetric unit | Bottom aperture of hexamer | Nucleotide binding | Reference |
|-----------------|-------------------------|--------------|----------------------------------|-----------------------------------|---------------------------|------------------|
| 5BN5 | <i>N.equitans</i> | Symmetric | AB | Narrow | Empty | Present study |
| 5BN3 | <i>N.equitans</i> | Symmetric | AB | Narrow | ADP | Present study |
| 5BN4 | <i>N.equitans</i> | Symmetric | AB | Narrow | AMP-PNP | Present study |
| 3GQB | <i>T.thermophilus</i> | Symmetric | (AB) ₂ | Wide | Empty | [92] |
| 3VR2 | <i>E.hirae</i> | Asymmteric | A ₃ B ₃ | Wide | Empty | [35] |
| 3VR3 | <i>E.hirae</i> | Asymmteric | A ₃ B ₃ | Wide | AMP-PNP | [35] |
| 3VR4 | <i>E.hirae</i> | Asymmteric | A ₃ B ₃ DG | Wide | Empty | [35] |
| 3VR6 | <i>E.hirae</i> | Asymmteric | A ₃ B ₃ DG | Wide | AMP-PNP | [35] |
| 3W3A | <i>T.thermophilus</i> | Asymmteric | A ₃ B ₃ DF | Wide | ADP | [104] |
| 1BMF | Bovine | Asymmteric | $\alpha_3\beta_3\gamma$ | Wide | ADP, AMP-PNP | [30] |
| 1MAB | Rat | Symmetric | $\alpha\beta\gamma_{1/3}$ | Narrow | ADP,ATP | [71] |
| 2F43 | Rat | Symmetric | $\alpha\beta\gamma_{1/3}$ | Narrow | ADP,ATP | [122] |
| 1FX0 | Spinach | Symmetric | $\alpha\beta$ | Narrow | Empty | [124] |
| 1SKY | <i>Bacillus PS3</i> | Symmetric | $\alpha\beta$ | Wide | Empty | [125] |
| 2QE7 | <i>Bacillus Sp. TA2</i> | Symmetric | $\alpha_3\beta_3\gamma\epsilon$ | Wide | Empty | [126] |

3.3.7 ATP hydrolysis assay

To further ascertain the catalytic capability of NeqAB core complex, ATP hydrolysis of the A_3B_3 complex was studied using an ATP regeneration system. First, we sought to study the independent hydrolytic capacity of the AB complex similar to those reported for its homologues [127]. The sensitivity of the assay was assessed by adding 100 μM ADP to the regenerating system which leads to a sudden drop in absorbance. The assay was done with a range of protein concentrations up to 2 μM (Fig 3.15). We did not observe any hydrolytic activity for Neq A_3B_3 . The central stalk subunits, D has been shown to be important for hydrolysis [128]. We reconstituted the A_3B_3D complex and conducted the assay with concentrations of the A_3B_3D complex up to 0.5 μM . Again, we observed negligible hydrolytic activity even with increasing durations (10 to 80 min). As mentioned in the previous section, we suspected that ADP inhibition might be occurring in the NeqAB complex. To rule out the possibility of ADP inhibition, we performed a Pi-EDTA nucleotide removal treatment, as described by Nakano et al. [127]. While we did notice marginal levels of activity in the case of the A_3B_3D complex as compared to the NeqAB complex (Fig.3.15). Based on these observations, we suggest that the Neq A_3B_3 complex is possibly functionally inactive (Fig.3.16).

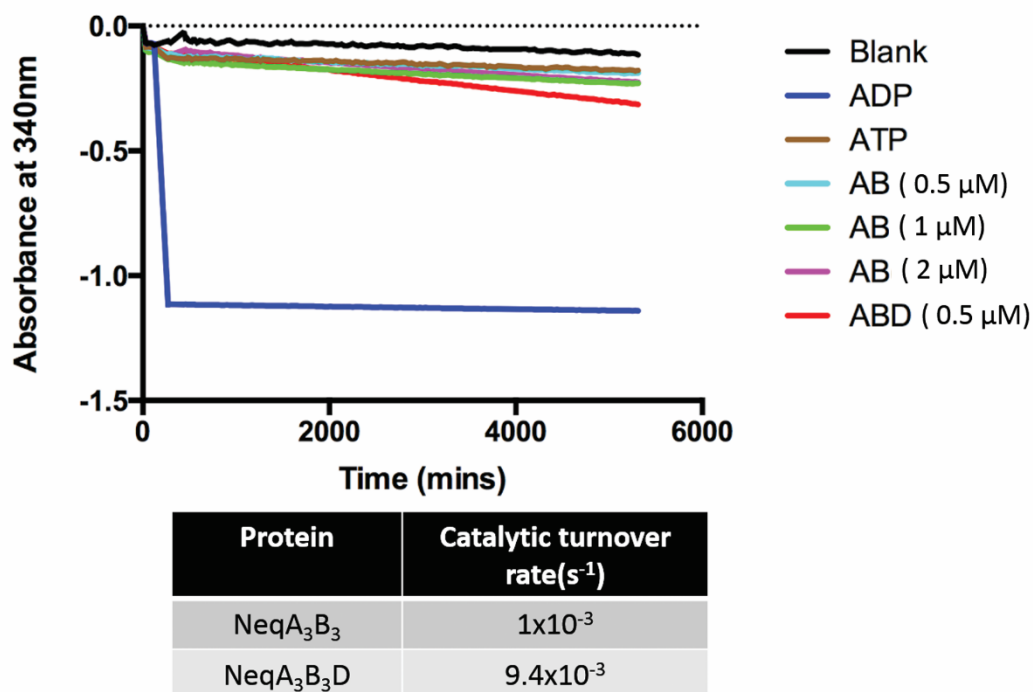


Figure 3.15. ATP hydrolytic activity of NeqA₃B₃ and NeqA₃B₃D complex: The conversion of ATP to ADP by of NeqA₃B₃ and NeqA₃B₃D is associated by simultaneous conversion of NADH to NAD⁺ which leads to a decrease of absorbance at 340 nm. The blue line represents the drop in the absorbance in the presence of 100 μM of Mg-ADP displaying the sensitivity of the ATP regeneration system. The cyan, green and magenta lines represent activity of 0.5, 1 and 2 μM of Neq A₃B₃ post nucleotide removal and no significant activity is seen. The red line shows the activity of NeqA₃B₃D after nucleotide removal treatment. The table at the bottom shows the turnover rate for the NeqA₃B₃ and NeqA₃B₃D complexes.

3.4 Discussion

The core ATP synthase subunits (subunits A and B) from eukaryotic and bacterial F-type and bacterial V-type are well characterized, while limited structural details of ATP synthases from archaea are available [35, 92]. Among the ATP synthases reported from archaea species, the *M. mazei* and *Pyrococcus sp.* ATP synthases are

the most studied, however the information is limited to low resolution cryo-EM data and structures of individual subunits [43, 49, 116, 120, 129, 130]. To date, there is no crystal structure available for the hexameric core complex of ATP synthases from archaea species. The present study reports the crystal structure of the regulatory subunit B (NeqB) and hexameric core complex subunits AB (NeqAB) in its nucleotide bound and unbound forms of the *N. equitans* ATP synthase. It has been widely accepted that the A-type, F-type and V-type arose from a common ancestor [62], with the catalytic sector of the ATP synthase family probably the first to arise [131]. Archaeal organisms are believed to be amongst the pioneering life forms on earth, in particular the hyperthermophilic ones, and therefore, the structural and functional studies of *N. equitans* ATP synthase offer an evolutionary perspective of the diverse class of ATP synthases.

There are several crystal and cryo-EM structures available for the F/V-type ATPase complexes which have revealed asymmetric states of the AB heterodimers in the A_3B_3 headpiece of the hexameric core [30, 43, 73, 104]; these studies are in support of the binding–change model of catalysis. Although initially attributed to the interaction of the A_3B_3 headpiece with the central stalk (D and F subunits in V-type and γ , δ , ϵ subunits in the F-type), recent studies have shown that the A_3B_3 headpiece, even in the absence of nucleotide, exhibits asymmetric states [35]. Furthermore, the $\alpha_3\beta_3$ headpiece of the F-type ATP synthase, which is devoid of a central stalk, can rotate in the presence of nucleotides, which confirms the importance of the conformational transition from an open to a close state [132, 133]. Here, we have shown that, although the Neq A_3B_3 complex retains its nucleotide

binding traits, the lack of a conformational change (open/closed), coupled with negligible hydrolytic activity, suggest that the NeqAB hexameric core is possibly functionally inactive reduced form of the enzyme complex that has lost its subunits as well as activity through the course of evolution due to its parasitic energetic dependency on *I.hospitalis* (Fig.3.17). This is supported by recent evidence that shows that *I.hospitalis* ATP synthase machinery faces the periplasmic space and its membrane is in close contact with *N. equitans* cells [87]. This unusual location was attributed to the possible transmission of ATP into the *N. equitans* cells. Others have also noted an active efflux of proteins and lipids from the host into *N. equitans*, which lacks the synthetic machinery required [112]. Moreover, the lack of the subunit F (central stalk) in the *N. equitans* genome, which has been shown to be essential for hydrolytic activity [128], also corroborates this possibility that *N. equitans* might not possess a fully functional ATP synthase complex.

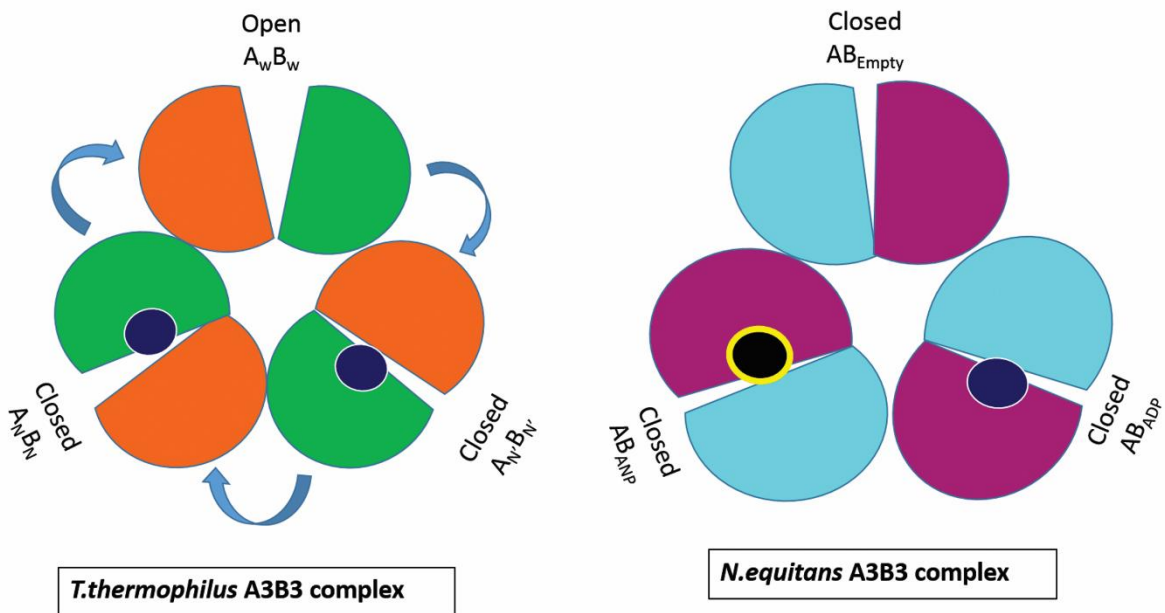


Figure 3.16. Schematic model of the inactive mechanism of the Neq core complex system: The nucleotide induced conformational changes as seen in the

asymmetric states of the active *T. thermophilus* A₃B₃ complex (PDB 3W3A) are represented in the left panel. The ADP bound to the AB dimers is shown as dark blue solid circles. In the right panel, shows the lack of conformational changes in Neq AB dimer in the presence of nucleotide, AMP-PNP (black-yellow circle) and ADP (blue circle).

It is well established that *N. equitans* relies on its host, *I. hospitalis* for several physiological functions as well as essential metabolites [112, 134]. *N. equitans* has been shown to be unable to survive when detached from its host, *I. hospitalis* [114]. It has been seen that there is a dynamic transport of lipids and amino acids from *I. hospitalis* into *N. equitans* [112, 135] and transmission electron microscopy studies of *I. hospitalis* have shown vesicles blebbing out from the inner plasma membrane into the periplasmic space [136]. A recent study has shown that the *I. hospitalis* ATP synthase is located on the inner plasma membrane with its catalytic head facing the periplasmic space instead of the cytoplasmic space [87]. This unique and uncommon feature coupled with the inherent lack of several ATP synthase subunits from *N. equitans* hints at potential parasitic dependence of *N. equitans* on *I. hospitalis* for energy. This is supported by the lack of the gene that codes for subunit F (central stalk), essential for hydrolytic activity, in the *N. equitans* genome [128]. All of these studies suggest that *N. equitans* relies on *I. hospitalis* for its bioenergetics and the lack of subunits in the *N. equitans* ATP synthase might result from a reductive evolution linked to its parasitic lifestyle, leading to a functionally inactive ATP synthase.

While our results as well as previous studies strongly indicate that *N. equitans* ATP synthase might be inactive, it also needs to be considered that, given the right

physiological conditions, this rigid ATP synthase might possess some *in vivo* activity. Despite its parasitic nature, *N. equitans* demonstrates self-sufficiency in various other processes, such as DNA replication and repair, RNA transcription and recombination, and protein transportation, to name a few [114]. An analysis of the proteome of *N. equitans* also shows the presence of the ATP synthase subunits from *I. hospitalis* [137]. Therefore, it is possible that the *N. equitans* ATP synthase can assemble into a functional form by borrowing the missing subunits from *I. hospitalis*. Future projects will be aimed at deriving an understanding of the bioenergetics of this unique organism.

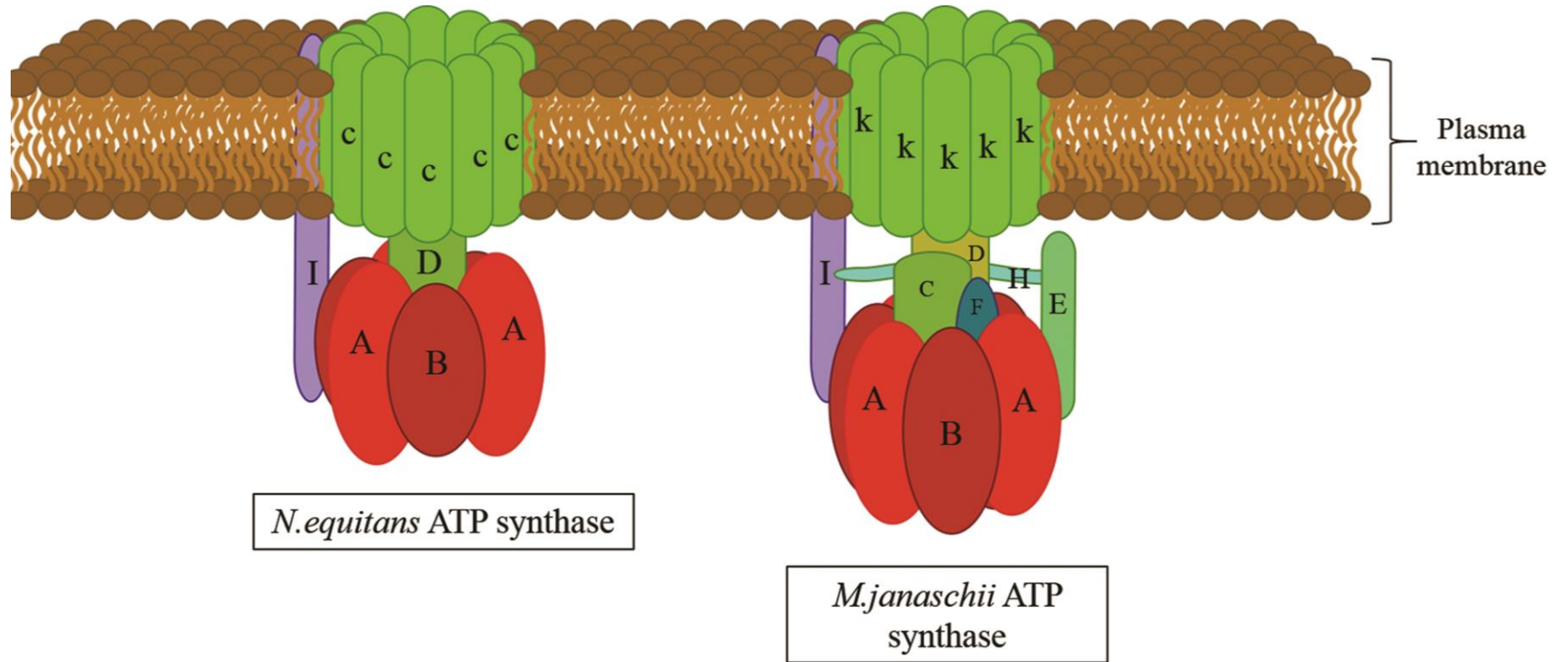


Figure 3.17. Representation of the putative partially formed Neq ATP synthase : The Neq ATP synthase is made up of five subunits – A,B,D, I and c (proteolipid) were put together based on the model of A_1A_0 ATP synthase of *Methanococcus janaschii* (right panel). The Neq ATP synthase represents a reduced form of the ATP synthase complex.

Chapter 4

Conclusion and future directions

4.1 Conclusion

There has been a lot of speculation about the architecture of *Nanoarchaeum equitans* ATP synthase ever since the genome of the organism has been known. In spite of that, there is no structural or functional data available for the *N.equitans* ATP synthase. In this thesis, we have reported the structures of the regulatory B subunit of this ATP synthase as well as that of the hexameric A_3B_3 complex, its nucleotide complexes along with their ATP assays and functional analysis.

In addition to this, we have also reported the sequence and phylogenetic analysis as well as biophysical characterization of these subunits. Overall, we showed that the B subunit bears significant resemblance with the V-type or A-type subunit B in terms of the general structural architecture. We have also observed that the tertiary structure of subunit B is similar to that of subunit A. Moreover, we have shown that subunit B has much lower affinity for nucleotide binding than the catalytic subunit, A, as it lacks the consensus Walker A motif.

Initial reports of the genes coding for *N.equitans* stated that the B subunit is about 5kD or about 20 residues shorter than its homologs and it was hypothesized that it might not be able to form a stable complex with the A subunit. Through our work, we showed that, in spite of this difference, A and B subunits form a stable hexameric complex which is further enhanced by nucleotide binding.

We have also determined the crystal structure for the nucleotide free and bound forms of A_3B_3 complex. Unlike the earlier A_3B_3 structures, no asymmetry was observed upon nucleotide binding. Interestingly, no open to closed transition

was observed upon nucleotide binding which is the central feature of all functional ATP synthase complexes and forms the basis for rotational catalysis.

Further, the subunit D was purified and reconstitutes the A₃B₃D complex which we used to analyse the ATPase activity of the complex. No significant ATPase activity was observed with this complex.

Based on our observations and analysis, we hypothesize that the *N.equitans* ATP synthase complex is a rudimentary form which has possibly lost its function due to its obligatory dependency on *Ignicoccus hospitalis* to meet its energetic requirements. Further studies need to be done with this hexameric core complex to unravel more intricate details of this reduced ATP synthase.

4.2 Future directions

Although the structure and function of the ATP synthase complex has been studied exhaustively both in the eukaryotic and prokaryotic systems, there are still some unanswered questions on the evolution of this catalytic complex. While the concept of modular evolution has been widely accepted, experimental models of an evolutionary intermediate of ATP synthases are have not been observed yet in spite of the diversity of organisms in which these complexes have been studied. The biological makeup of *Nanoarchaeum equitans* presents the ideal situation for the study of the evolution of ATP synthases due to its archaic genetic and incomplete proteomic composition. Hence, the ATP synthase ensemble in *Nanoarchaeum equitans* might also incompletely formed, representing a primitive evolutionary stage.

As a next step to further understand the *Nanoarchaeum equitans* ATP synthase complex is to obtain the stable A₃B₃D complex and structurally characterize the

complex. Our experiments have shown that the NeqD subunit is highly insoluble and unstable and all efforts made to co-purify it with the A₃B₃ complex did not yield any stable complex yet. However, methods like creating an artificial operon with all three genes and expressing it in a strain lacking intrinsic ATP synthase such as the *E.coli* DK8 can be explored. This complex can be used for crystallization trials, cryo-EM experiments as well as functional studies such as ATPase assays. Another exciting aspect that can be potentially explored is the visualization of the ATP hydrolysis induced rotation of the catalytic head using atomic force microscopy. The study of this putative complete A₁ complex will give us invaluable insight into how this curious machine functions.

Further, we would like to explore the possible interactions between the subunits of *N.equitans* ATP synthase complex with the subunits from the ATP synthase of the host, *Ignicoccus hospitalis* (*Ih*). The interaction between NeqD and IhF (Ih Subunit F) would be the most likely candidate for this study.

Collectively, these studies will bring out a wider picture of the structure and mechanism of action of Neq ATP synthase. This will, in turn, add invaluable information about the biogenesis and evolutionary pathway of the ATP synthase family of proteins. This will be highly significant in the area of ATP synthase research.

References

1. Gest, H., M.D. Kamen, and H.M. Bregoff, *Studies on the metabolism of photosynthetic bacteria vs photoproduction of hydrogen and nitrogen fixation by Rhodospirillum rubrum*. Journal of Biological Chemistry, 1950. **182**(1): p. 153-170.
2. Favinger, J., R. Stadtwald, and H. Gest, *Rhodospirillum centenum, sp. nov., a thermotolerant cyst-forming anoxygenic photosynthetic bacterium*. Antonie van Leeuwenhoek, 1989. **55**(3): p. 291-296.
3. M Kalckar, H., *The function of phosphate in cellular assimilations*. Biological Reviews, 1942. **17**(1): p. 28-45.
4. Kalckar, H., *The function of phosphate in enzymatic syntheses*. Annals of the New York Academy of Sciences, 1944. **45**(9): p. 395-408.
5. Lipmann, F., *Metabolic generation and utilization of phosphate bond energy*. Adv. Enzymol. Relat. Areas Mol. Biol, 1941. **1**: p. 99-162.
6. Chance, B. and G. Williams, *The respiratory chain and oxidative phosphorylation*. Adv Enzymol Relat Areas Mol Biol, 1956. **17**: p. 65-134.
7. Koumandou, V.L. and S. Kossida, *Evolution of the FOF1 ATP Synthase Complex in Light of the Patchy Distribution of Different Bioenergetic Pathways across Prokaryotes*. PLoS computational biology, 2014. **10**(9): p. e1003821.
8. Hicks, D.B., et al., *F1FO-ATP synthases of alkaliphilic bacteria: lessons from their adaptations*. Biochim Biophys Acta, 2010. **1797**(8): p. 1362-77.
9. Muller, V., C. Ruppert, and T. Lemker, *Structure and function of the A1A0-ATPases from methanogenic Archaea*. J. Bioener. Biomemb. , 1999. **31**(1): p. 15-27.
10. Boyer, P.D., *The binding change mechanism for ATP synthase—some probabilities and possibilities*. Biochimica et Biophysica Acta (BBA)-Bioenergetics, 1993. **1140**(3): p. 215-250.
11. Boyer, P.D. *A perspective of the binding change mechanism for ATP synthesis*. in *The FASEB Journal*. 1989.
12. Boyer, P.D., *Energy, Life, and ATP (Nobel Lecture)*. Angewandte Chemie International Edition, 1998. **37**(17): p. 2296-2307.
13. Walker, J.E., *ATP Synthesis by Rotary Catalysis (Nobel lecture)*. Angewandte Chemie International Edition, 1998. **37**(17): p. 2308-2319.
14. Boyer, P.D., *The ATP synthase—a splendid molecular machine*. Annu Rev Biochem, 1997. **66**(1): p. 717-49.
15. Gay, N.J. and J.E. Walker, *The atp operon: nucleotide sequence of the promoter and the genes for the membrane proteins, and the δ subunit of Escherichia coli ATP-synthase*. Nucleic acids research, 1981. **9**(16): p. 3919-3926.
16. Saraste, M., et al., *The atp operon: nucleotide sequence of the genes for the γ , β , and ϵ subunits of Escherichia coli ATP synthase*. Nucleic acids research, 1981. **9**(20): p. 5287-5296.
17. Yoshida, M., E. Muneyuki, and T. Hisabori, *ATP synthase—a marvellous rotary engine of the cell*. Nature Reviews Molecular Cell Biology, 2001. **2**(9): p. 669-677.
18. Kojima, S. and D.F. Blair, *The bacterial flagellar motor: structure and function of a complex molecular machine*. Int Rev Cytol, 2004. **233**: p. 93-134.
19. Pallen, M.J., C.M. Bailey, and S.A. Beatson, *Evolutionary links between FliH/YscL-like proteins from bacterial type III secretion systems and second-*

References

- stalk components of the FoF1 and vacuolar ATPases*. Protein Sci, 2006. **15**(4): p. 935-41.
20. Pullman, M.E., et al., *Partial resolution of the enzymes catalyzing oxidative phosphorylation. I. Purification and properties of soluble dinitrophenol-stimulated adenosine triphosphatase*. J Biol Chem, 1960. **235**: p. 3322-9.
 21. Muller, V. and G. Gruber, *ATP synthases: structure, function and evolution of unique energy converters*. Cell Mol Life Sci, 2003. **60**(3): p. 474-94.
 22. Senior, A.E., *Two ATPases*. Journal of Biological Chemistry, 2012. **287**(36): p. 30049-30062.
 23. von Ballmoos, C., G.M. Cook, and P. Dimroth, *Unique Rotary ATP Synthase and Its Biological Diversity*. Annual Review of Biophysics, 2008. **37**(1): p. 43-64.
 24. Mitchel, P., *Coupling of phosphorylation to electron and hydrogen transfer by a chemi-osmotic type mechanism*. Nature, 1962. **191**(4784).
 25. Hennig, J. and R.G. Herrmann, *Chloroplast ATP synthase of spinach contains nine nonidentical subunit species, six of which are encoded by plastid chromosomes in two operons in a phylogenetically conserved arrangement*. Molecular and General Genetics MGG, 1986. **203**(1): p. 117-128.
 26. Daum, B., et al., *Arrangement of photosystem II and ATP synthase in chloroplast membranes of spinach and pea*. The Plant Cell Online, 2010. **22**(4): p. 1299-1312.
 27. Maloney, P.C., E. Kashket, and T.H. Wilson, *A protonmotive force drives ATP synthesis in bacteria*. Proceedings of the National Academy of Sciences, 1974. **71**(10): p. 3896-3900.
 28. Capaldi, R.A., et al., *Cross-linking and electron microscopy studies of the structure and functioning of the Escherichia coli ATP synthase*. J Exp Biol, 2000. **203**(Pt 1): p. 29-33.
 29. Walker, J.E., et al., *Identification of the subunits of F1FO-ATPase from bovine heart mitochondria*. Biochemistry, 1991. **30**(22): p. 5369-5378.
 30. Abrahams, J.P., et al., *Structure at 2.8 Å resolution of F1-ATPase from bovine heart mitochondria*. Nature, 1994. **370**(6491): p. 621-628.
 31. Löbau, S., J. Weber, and A.E. Senior, *Catalytic Site Nucleotide Binding and Hydrolysis in F1Fo-ATP Synthase*. Biochemistry, 1998. **37**(30): p. 10846-10853.
 32. Beyenbach, K.W. and H. Wiczorek, *The V-type H⁺ ATPase: molecular structure and function, physiological roles and regulation*. J Exp Biol, 2006. **209**(4): p. 577-89.
 33. Drory, O. and N. Nelson, *The emerging structure of vacuolar ATPases*. Physiology, 2006. **21**(5): p. 317-325.
 34. Saroussi, S. and N. Nelson, *The little we know on the structure and machinery of V-ATPase*. J Exp Biol, 2009. **212**(Pt 11): p. 1604-10.
 35. Arai, S., et al., *Rotation mechanism of Enterococcus hirae V1-ATPase based on asymmetric crystal structures*. Nature, 2013. **493**(7434): p. 703-7.
 36. Kane, P.M. and T.H. Stevens, *Subunit composition, biosynthesis, and assembly of the yeast vacuolar proton-translocating ATPase*. Journal of bioenergetics and biomembranes, 1992. **24**(4): p. 383-393.
 37. Lolkema, J.S., Y. Chaban, and E.J. Boekema, *Subunit composition, structure, and distribution of bacterial V-type ATPases*. Journal of bioenergetics and biomembranes, 2003. **35**(4): p. 323-335.
 38. Nelson, N., *Evolution of organellar proton-ATPases*. Biochim Biophys Acta, 1992. **1100**(2): p. 109-24.

References

39. Nishi, T. and M. Forgac, *The vacuolar (H⁺)-ATPases — nature's most versatile proton pumps*. Nat Rev Mol Cell Biol, 2002. **3**(2): p. 94-103.
40. DeLong, E., *Archaeal means and extremes*. Science, 1998. **280**(5363): p. 542-543.
41. Forterre, P., C. Brochier, and H. Philippe, *Evolution of the Archaea*. Theoretical population biology, 2002. **61**(4): p. 409-422.
42. Bult, C.J., et al., *Complete genome sequence of the methanogenic archaeon, Methanococcus jannaschii*. Science, 1996. **273**(5278): p. 1058-1073.
43. Coskun, U., et al., *Three-dimensional organization of the archaeal A1-ATPase from Methanosarcina mazei Go1*. J. Biol. Chem., 2004. **279**(21): p. 22759-64.
44. *Structure and subunit arrangement of the A-type ATP synthase complex from the archaeon Methanococcus jannaschii visualized by electron microscopy*.
45. Müller, V., *An Exceptional Variability in the Motor of Archaeal A1A0ATPases: From Multimeric to Monomeric Rotors Comprising 6–13 Ion Binding Sites*. J. Bioener. Biomem., 2004. **36**(1): p. 115-125.
46. Pogoryelov, D., et al., *High-resolution structure of the rotor ring of a proton-dependent ATP synthase*. Nat Struct Mol Biol, 2009. **16**(10): p. 1068-73.
47. McMillan, D.G., et al., *A1Ao-ATP synthase of Methanobrevibacter ruminantium couples sodium ions for ATP synthesis under physiological conditions*. Journal of Biological Chemistry, 2011. **286**(46): p. 39882-39892.
48. Schlegel, K., et al., *Promiscuous archaeal ATP synthase concurrently coupled to Na⁺ and H⁺ translocation*. Proc Natl Acad Sci U S A, 2012. **109**(3): p. 947-52.
49. Pisa, K.Y., et al., *A sodium ion-dependent A1AO ATP synthase from the hyperthermophilic archaeon Pyrococcus furiosus*. FEBS J, 2007. **274**(15): p. 3928-38.
50. Mulkidjanian, A.Y., P. Dibrov, and M.Y. Galperin, *The past and present of sodium energetics: May the sodium-motive force be with you*. Biochimica et Biophysica Acta (BBA) - Bioenergetics, 2008. **1777**(7–8): p. 985-992.
51. Birkenhäger, R., et al., *The FO Complex of the Escherichia Coli ATP Synthase*. European Journal of Biochemistry, 1995. **230**(1): p. 58-67.
52. Kish-Trier, E. and S. Wilkens, *Domain architecture of the stator complex of the A1A0-ATP synthase from Thermoplasma acidophilum*. J Biol Chem, 2009. **284**(18): p. 12031-40.
53. Walker, J.E., et al., *Primary structure and subunit stoichiometry of F1-ATPase from bovine mitochondria*. J. Mol Bio., 1985. **184**(4): p. 677-701.
54. Fenchel, T. and B.J. Finlay, *The evolution of life without oxygen*. American Scientist, 1994: p. 22-29.
55. Nelson, N., et al., *Cell Biology and Evolution of Proton Pumps*. Cellular Physiology and Biochemistry, 1992. **2**(3-4): p. 150-158.
56. Cross, R.L. and L. Taiz, *Gene duplication as a means for altering H⁺/ATP ratios during the evolution of F1FO ATPases and synthases*. FEBS letters, 1990. **259**(2): p. 227-229.
57. Hilario, E. and J.P. Gogarten, *The prokaryote-to-eukaryote transition reflected in the evolution of the V/F/A-ATPase catalytic and proteolipid subunits*. Journal of molecular evolution, 1998. **46**(6): p. 703-715.
58. <Prokaryote to Eu transition and evolution of ATPases.pdf>.
59. Dyall, S.D., M.T. Brown, and P.J. Johnson, *Ancient invasions: from endosymbionts to organelles*. Science, 2004. **304**(5668): p. 253-257.

References

60. Cavalier-Smith, T., *The simultaneous symbiotic origin of mitochondria, chloroplasts, and microbodies*. Annals of the New York Academy of Sciences, 1987. **503**(1): p. 55-71.
61. Mulkidjanian, A.Y., M.Y. Galperin, and E.V. Koonin, *Co-evolution of primordial membranes and membrane proteins*. Trends Biochem Sci, 2009. **34**(4): p. 206-15.
62. Mulkidjanian, A.Y., et al., *Inventing the dynamo machine: the evolution of the F-type and V-type ATPases*. Nat. Rev. Microbiol. , 2007. **5**(11): p. 892-899.
63. Hingorani, M.M., et al., *The dTTPase mechanism of T7 DNA helicase resembles the binding change mechanism of the F(1)-ATPase*. Proceedings of the National Academy of Sciences of the United States of America, 1997. **94**(10): p. 5012-5017.
64. Cross, R.L. and V. Muller, *The evolution of A-, F-, and V-type ATP synthases and ATPases: reversals in function and changes in the H⁺/ATP coupling ratio*. FEBS Lett, 2004. **576**(1-2): p. 1-4.
65. Walker, J. and A. Cozens, *Evolution of ATP synthase*. Chem Scr B, 1986. **26**: p. 263-272.
66. Noji, H., et al., *Direct observation of the rotation of F1-ATPase*. Nature, 1997. **386**(6622): p. 299-302.
67. Slater, E.C., *Mechanism of phosphorylation in the respiratory chain*. 1953.
68. Kayalar, C., J. Rosing, and P.D. Boyer, *An alternating site sequence for oxidative phosphorylation suggested by measurement of substrate binding patterns and exchange reaction inhibitions*. Journal of Biological Chemistry, 1977. **252**(8): p. 2486-2491.
69. Hackney, D.D. and P.D. Boyer, *Subunit interaction during catalysis. Implications of concentration dependency of oxygen exchanges accompanying oxidative phosphorylation for alternating site cooperativity*. Journal of Biological Chemistry, 1978. **253**(9): p. 3164-3170.
70. Gresser, M.J., J.A. Myers, and P.D. Boyer, *Catalytic site cooperativity of beef heart mitochondrial F1 adenosine triphosphatase. Correlations of initial velocity, bound intermediate, and oxygen exchange measurements with an alternating three-site model*. Journal of Biological Chemistry, 1982. **257**(20): p. 12030-12038.
71. Bianchet, M.A., et al., *The 2.8-Å structure of rat liver F1-ATPase: configuration of a critical intermediate in ATP synthesis/hydrolysis*. Proc Natl Acad Sci U S A, 1998. **95**(19): p. 11065-11070.
72. Hutton, R. and P. Boyer, *Subunit interaction during catalysis. Alternating site cooperativity of mitochondrial adenosine triphosphatase*. Journal of Biological Chemistry, 1979. **254**(20): p. 9990-9993.
73. Numoto, N., et al., *Inter-subunit interaction and quaternary rearrangement defined by the central stalk of prokaryotic V1-ATPase*. EMBO Rep, 2009. **10**(11): p. 1228-34.
74. Muller, V., et al., *ATP synthases with novel rotor subunits: new insights into structure, function and evolution of ATPases*. J Bioenerg Biomembr, 2005. **37**(6): p. 455-60.
75. Saraste, M., P.R. Sibbald, and A. Wittinghofer, *The P-loop—a common motif in ATP- and GTP-binding proteins*. Trends in biochemical sciences, 1990. **15**(11): p. 430-434.

References

76. Walker, J.E., et al., *Distantly related sequences in the alpha-and beta-subunits of ATP synthase, myosin, kinases and other ATP-requiring enzymes and a common nucleotide binding fold*. EMBO J, 1982. **1**(8): p. 945.
77. Gibbons, C., et al., *The structure of the central stalk in bovine F1-ATPase at 2.4 Å resolution*. Nat. Struct. Mol. Bio., 2000. **7**(11): p. 1055-1061.
78. Aggeler, R., M.A. Haughton, and R.A. Capaldi, *Disulfide bond formation between the COOH-terminal domain of the beta subunits and the gamma and epsilon subunits of the Escherichia coli F1-ATPase. Structural implications and functional consequences*. J Biol Chem, 1995. **270**(16): p. 9185-91.
79. Gogol, E.P., et al., *Ligand-dependent structural variations in Escherichia coli F1 ATPase revealed by cryoelectron microscopy*. Proceedings of the National Academy of Sciences, 1990. **87**(24): p. 9585-9589.
80. Itoh, H., et al., *Mechanically driven ATP synthesis by F1-ATPase*. Nature, 2004. **427**(6973): p. 465-468.
81. Yasuda, R., et al., *F1-ATPase Is a Highly Efficient Molecular Motor that Rotates with Discrete 120° Steps*. Cell, 1998. **93**(7): p. 1117-1124.
82. Yasuda, R., et al., *Resolution of distinct rotational substeps by submillisecond kinetic analysis of F1-ATPase*. Nature, 2001. **410**(6831): p. 898-904.
83. Imamura, H., et al., *Evidence for rotation of V1-ATPase*. Proc Natl Acad Sci U S A, 2003. **100**(5): p. 2312-5.
84. Huber, H., et al., *A new phylum of Archaea represented by a nanosized hyperthermophilic symbiont*. Nature, 2002. **417**(6884): p. 63-67.
85. Lewalter, K. and V. Muller, *Bioenergetics of archaea: ancient energy conserving mechanisms developed in the early history of life*. Biochim Biophys Acta, 2006. **1757**(5-6): p. 437-45.
86. Junglas, B., et al., *Ignicoccus hospitalis and Nanoarchaeum equitans: ultrastructure, cell-cell interaction, and 3D reconstruction from serial sections of freeze-substituted cells and by electron cryotomography*. Arch Microbiol, 2008. **190**(3): p. 395-408.
87. Kuper, U., et al., *Energized outer membrane and spatial separation of metabolic processes in the hyperthermophilic Archaeon Ignicoccus hospitalis*. Proc Natl Acad Sci U S A, 2010. **107**(7): p. 3152-6.
88. Podar, M., et al., *A genomic analysis of the archaeal system Ignicoccus hospitalis-Nanoarchaeum equitans*. Genome Biol, 2008. **9**(11): p. R158.
89. Erik Kish-Trier, L.-A.K.B., Stanley D. Dunn, and Stephan Wilkens, *The Stator Complex of the A1A0-ATP synthase — Structural Characterization of the E and H Subunits*. J Mol Biol, 2008. **375**(3): p. 673–685.
90. Lingl, A., et al., *Isolation of a complete A1A0 ATP synthase comprising nine subunits from the hyperthermophile Methanococcus jannaschii*. Extremophiles, 2003. **7**(3): p. 249-57.
91. McCoy, A.J., *Solving structures of protein complexes by molecular replacement with Phaser*. Acta Crystallogr D Biol Crystallogr, 2007. **63**(Pt 1): p. 32-41.
92. Maher, M.J., et al., *Crystal structure of A3B3 complex of V-ATPase from Thermus thermophilus*. EMBO J 2009. **28**(23): p. 3771-9.
93. Meyering-Vos, G.S.a.M., *F-type or V-type? The chimeric nature of the archaeobacterial ATP synthase*. Biochimica et Biophysica Acta., 1992. **1101**: p. 232-235.
94. Hilario, E. and J.P. Gogarten, *Horizontal transfer of ATPase genes—the tree of life becomes a net of life*. Biosystems, 1993. **31**(2): p. 111-119.

References

95. Stock, D., *Molecular architecture of the rotary motor in ATP synthase*. Science, 1999. **286**(5445): p. 1700-1705.
96. Gruber, G. and V. Marshansky, *New insights into structure-function relationships between archeal ATP synthase (A1A0) and vacuolar type ATPase (V1V0)*. Bioessays, 2008. **30**(11-12): p. 1096-109.
97. Deppenmeier, U. and V. Müller, *Life close to the thermodynamic limit: how methanogenic archaea conserve energy*, in *Bioenergetics*, G. Schäfer and H. Penefsky, Editors. 2008, Springer Berlin Heidelberg. p. 123-152.
98. Grüber, G., et al., *Structural Insights into the A1 ATPase from the Archaeon, Methanosarcina mazei Gö1†*. Biochemistry, 2001. **40**(7): p. 1890-1896.
99. Thorsten Lemker, C.R., Heidi Stoeger, Soenke Wimmers and Volker Mueller, *Overproduction of a functional A1 ATPase from the archaeon Methanosarcina mazei Gö1 in Escherichia coli*. Eur. J. Biochem., 2001. **268**: p. 3744-3750.
100. Lemker, T., et al., *Defined subcomplexes of the A1 ATPase from the archaeon Methanosarcina mazei Gö1: biochemical properties and redox regulation*. FEBS Letters, 2003. **544**(1-3): p. 206-209.
101. Waters, E., et al., *The genome of Nanoarchaeum equitans: insights into early archaeal evolution and derived parasitism*. Proc. Natl. Acad. Sci. U.S.A. 2003. **100**(22): p. 12984-8.
102. Di Giulio, M., *The tree of life might be rooted in the branch leading to Nanoarchaeota*. Gene, 2007. **401**(1-2): p. 108-13.
103. Mayer, F. and V. Müller, *ATP Synthases from Archaea: Structure and Function*, in *Encyclopedia of Biophysics*, G.K. Roberts, Editor. 2013, Springer Berlin Heidelberg. p. 122-129.
104. Nagamatsu, Y., et al., *Origin of asymmetry at the intersubunit interfaces of V1-ATPase from Thermus thermophilus*. J Mol Biol, 2013. **425**(15): p. 2699-708.
105. Dereeper, A., et al., *Phylogeny.fr: robust phylogenetic analysis for the non-specialist*. Nucleic Acids Res, 2008. **36**(Web Server issue): p. W465-9.
106. Emsley, P. and K. Cowtan, *Coot: model-building tools for molecular graphics*. Acta Crystallographica Section D: Biological Crystallography, 2004. **60**(12): p. 2126-2132.
107. Adams, P.D., et al., *PHENIX: a comprehensive Python-based system for macromolecular structure solution*. Acta Crystallogr D Biol Crystallogr, 2010. **66**(Pt 2): p. 213-21.
108. Brown, P.H. and P. Schuck, *Macromolecular size-and-shape distributions by sedimentation velocity analytical ultracentrifugation*. Biophysical journal, 2006. **90**(12): p. 4651-4661.
109. Kiiianitsa, K., J.A. Solinger, and W.D. Heyer, *NADH-coupled microplate photometric assay for kinetic studies of ATP-hydrolyzing enzymes with low and high specific activities*. Analytical biochemistry, 2003. **321**(2): p. 266-271.
110. Ramakrishnan, C., V. Dani, and T. Ramasarma, *A conformational analysis of Walker motif A [GXXXXGKT (S)] in nucleotide-binding and other proteins*. Protein engineering, 2002. **15**(10): p. 783-798.
111. Kumar, A., et al., *Spectroscopic and crystallographic studies of the mutant R416W give insight into the nucleotide binding traits of subunit B of the A1A0 ATP synthase*. Proteins, 2009. **75**(4): p. 807-19.

References

112. Jahn, U., et al., *Nanoarchaeum equitans* and *Ignicoccus hospitalis*: new insights into a unique, intimate association of two archaea. *J Bacteriol*, 2008. **190**(5): p. 1743-50.
113. Das, S., et al., *Analysis of Nanoarchaeum equitans genome and proteome composition: indications for hyperthermophilic and parasitic adaptation*. *BMC Genomics*, 2006. **7**: p. 186.
114. Waters, E., et al., *The genome of Nanoarchaeum equitans: insights into early archaeal evolution and derived parasitism*. *Proc Natl Acad Sci U S A*, 2003. **100**(22): p. 12984-12988.
115. Shao, E., et al., *Mutational analysis of the non-homologous region of subunit A of the yeast V-ATPase*. *J Biol Chem*, 2003. **278**(15): p. 12985-91.
116. Kumar, A., et al., *Nucleotide binding states of subunit A of the A-ATP synthase and the implication of P-loop switch in evolution*. *J Mol Biol*, 2010. **396**(2): p. 301-20.
117. Kishikawa, J., et al., *Molecular basis of ADP inhibition of vacuolar (V)-type ATPase/synthase*. *J Biol Chem*, 2014. **289**(1): p. 403-12.
118. Yokoyama, K., et al., *V-ATPase of Thermus thermophilus is inactivated during ATP hydrolysis but can synthesize ATP*. *J Biol Chem*, 1998. **273**(32): p. 20504-20510.
119. Nakano, M., et al., *ATP hydrolysis and synthesis of a rotary motor V-ATPase from Thermus thermophilus*. *Journal of Biological Chemistry*, 2008. **283**(30): p. 20789-20796.
120. Kumar, A., M.S. Manimekalai, and G. Gruber, *Structure of the nucleotide-binding subunit B of the energy producer A1A0 ATP synthase in complex with adenosine diphosphate*. *Acta Crystallogr D Biol Crystallogr*, 2008. **64**(Pt 11): p. 1110-5.
121. Manimekalai, M.S.S., et al., *A second transient position of ATP on its trail to the nucleotide-binding site of subunit B of the motor protein A1A0 ATP synthase*. *Journal of structural biology*, 2009. **166**(1): p. 38-45.
122. Chen, C., et al., *Mitochondrial ATP synthase. Crystal structure of the catalytic F1 unit in a vanadate-induced transition-like state and implications for mechanism*. *J Biol Chem*, 2006. **281**(19): p. 13777-83.
123. Shirakihara, Y., et al., *The crystal structure of the nucleotide-free alpha 3 beta 3 subcomplex of F1-ATPase from the thermophilic Bacillus PS3 is a symmetric trimer*. *Structure*, 1997. **5**(6): p. 825-36.
124. Groth, G. and E. Pohl, *The structure of the chloroplast F1-ATPase at 3.2 Å resolution*. *J Biol Chem*, 2001. **276**(2): p. 1345-1352.
125. Shirakihara, Y., et al., *The crystal structure of the nucleotide-free alpha3beta3 subcomplex of F1-ATPase from the thermophilic Bacillus PS3 is a symmetric trimer*. *Structure*, 1997. **5**(6): p. 825-836.
126. Stocker, A., et al., *The structural basis for unidirectional rotation of thermoalkaliphilic F1-ATPase*. *Structure*, 2007. **15**(8): p. 904-914.
127. Nakano, M., et al., *ATP hydrolysis and synthesis of a rotary motor V-ATPase from Thermus thermophilus*. *The Journal of biological chemistry*, 2008. **283**(30): p. 20789-96.
128. Alam, M.J., et al., *Loose binding of the DF axis with the A3B3 complex stimulates the initial activity of Enterococcus hirae V1-ATPase*. *PLoS One*, 2013. **8**(9): p. e74291.
129. Vonck, J., et al., *Three-dimensional structure of A1A0 ATP synthase from the hyperthermophilic archaeon Pyrococcus furiosus by electron microscopy*. *J Biol Chem*, 2009. **284**(15): p. 10110-9.

References

130. Manimekalai, M.S., et al., *The transition-like state and Pi entrance into the catalytic a subunit of the biological engine A-ATP synthase*. J Mol Biol, 2011. **408**(4): p. 736-54.
131. Nelson, N., *Structure, molecular genetics, and evolution of vacuolar H⁺-ATPases*. Journal of Bioenergetics and Biomembranes, 1989. **21**(5): p. 553-571.
132. Uchihashi, T., et al., *High-speed atomic force microscopy reveals rotary catalysis of rotorless F1-ATPase*. Science, 2011. **333**(6043): p. 755-758.
133. Ariga, T., E. Muneyuki, and M. Yoshida, *F1-ATPase rotates by an asymmetric, sequential mechanism using all three catalytic subunits*. Nat Struct Mol Biol, 2007. **14**(9): p. 841-846.
134. Burghardt, T., et al., *The interaction of Nanoarchaeum equitans with Ignicoccus hospitalis: proteins in the contact site between two cells*. Biochem Soc Trans, 2009. **37**(Pt 1): p. 127-32.
135. Jahn, U., et al., *Composition of the lipids of Nanoarchaeum equitans and their origin from its host Ignicoccus sp. strain KIN4/I*. Archives of microbiology, 2004. **182**(5): p. 404-413.
136. Rachel, R., et al., *The ultrastructure of Ignicoccus: evidence for a novel outer membrane and for intracellular vesicle budding in an archaeon*. Archaea, 2002. **1**(1): p. 9-18.
137. Giannone, R.J., et al., *Proteomic characterization of cellular and molecular processes that enable the Nanoarchaeum equitans-Ignicoccus hospitalis relationship*. PLoS One, 2011. **6**(8): p. e22942.